Gezamenlijke opleiding UHasselt en KU Leuven

2018•2019

Faculteit Industriële ingenieurswetenschappen

master in de industriële wetenschappen: chemie

Masterthesis

Microwave assisted roasting of sulphidic tailings

PROMOTOR :
Prof. dr. ir. Leen BRAEKEN

PROMOTOR :
dr. Jeroen SPOOREN

COPROMOTOR :
dr. ir. Maarten EVERAERT

BEGELEIDER :
dr. Thomas ABO ATIA

Vincent Lemmens

Scriptie ingediend tot het behalen van de graad van master in de industriële wetenschappen: chemie

2018•2019
Faculteit Industriële ingenieurswetenschappen
master in de industriële wetenschappen: chemie

Masterthesis

Microwave assisted roasting of sulphidic tailings

PROMOTOR :
Prof. dr. ir. Leen BRAEKEN

PROMOTOR :
dr. Jeroen SPOOREN

COPROMOTOR :
dr. ir. Maarten EVERAERT

BEGELEIDER :
dr. Thomas ABO ATIA

Vincent Lemmens

Scriptie ingediend tot het behalen van de graad van master in de industriële wetenschappen: chemie

Acknowledgements

During 15 weeks, I was a part of the Sustainable Materials Management unit focused on recycling technologies at VITO in Mol. The subject of pyrometallurgy was new for me. I improved my laboratory skills, learned new methods and new analytical techniques. As a last year student Master of Chemical Engineering Technology, this internship was a perfect choice to round up my education program with an excellent learning experience in the R&D sector at VITO.

I am thankful for the opportunity that I got to step into the study/project of "Microwave-assisted roasting of sulphidic tailings". First of all, I want to thank Dr. Ir. Maarten Everaert who is a researcher in the Sustainable Materials Management unit and my external promotor. He helped me on a daily basis in the lab as well as for writing and correcting my thesis, presentation and poster. His way of looking at data, gave me new insight in raw data processing.

I also want to thank my external promotor Dr. Jeroen Spooren, who is one of the main researchers at the Sustainable Materials Management unit, for reading and correcting my thesis, presentation and poster. His experience and knowledge really helped during difficult choices that were to be made between experiment setups as well as during data processing.

Thirdly, I wish to thank Dr. Thomas Abo Atia, who is a postdoc and my third external promotor, for his help and experienced guidance with microwave roasting.

I would also like to thank my internal school promotor Prof. Dr. Ir. Leen Braeken who gave me feedback on my thesis, presentation and poster and excellent tips for my final defense.

It was a pleasure to be a part of the Sustainable Materials Management unit during these 15 weeks. I want to thank everyone for creating such a good work environment with positive energy. Especially I would like to thank the following persons. Myrjam Mertens for measuring all the XRD samples, characterizing the data peaks and performing Rietveld analysis on the data. Warre Van Dun for his technical support and measurements regarding the ICP-OES. Bo Peeraer for his technical support and explanation of the handheld XRF. Anne-Marie De Wilde for the TGA analysis.

Last but not least I want to thank my family, girlfriend and friends who supported me during this internship. I would like to thank everyone else who helped me in a way to realize this thesis.

Vincent Lemmens
Student Master of Chemical Engineering Technology
UHasselt – KU Leuven
June 2019

Table of contents

Acknowledgements 1

List of tables 7

List of figures 9

Glossary 11

Abstract 13

Abstract in Dutch 15

1 Introduction 17

- 1.1 Context 17
- 1.2 Problem statement 17
- 1.3 Objectives 20
- 1.4 Strategy 20

2 Literature 21

- 2.1 Acid mine drainage 21
  - 2.1.1 Effects of AMD 21
  - 2.1.2 Treatment and prevention of AMD 21
- 2.2 Chemistry of roasting 22
  - 2.2.1 Oxidative roasting 22
  - 2.2.2 Sulphation roasting 22
  - 2.2.3 Sulphide roasting reactions 23
- 2.3 Roasting kinetics 24
  - 2.3.1 The shrinking core model 24
- 2.4 Thermodynamics of roasting 25
  - 2.4.1 The Cu-S-O system 27
- 2.5 Influence of temperature on conventional roasting 29
- 2.6 Introducing carbonates to the roasting process 34
- 2.7 Microwave-assisted roasting 36
  - 2.7.1 Mineralogy and temperature 38
  - 2.7.2 Influence of power, sample mass, time and ratio 39
  - 2.7.3 Influence of particle size 41
  - 2.7.4 Phase changes of $CuFeS_2$-$CaCO_3$ roasting 41

2.8 Chemical Leaching ... 42
  2.8.1 Acid leaching ... 42
  2.8.2 Alkaline leaching ... 43

3 Materials and methods ... 45
  3.1 Materials ... 45
  3.2 Experiments ... 46
    3.2.1 Roasting ... 46
    3.2.2 Ammoniacal leaching ... 51
    3.2.3 Leaching kinetics ... 52
  3.3 Analyses ... 53
    3.3.1 X-ray fluorescence (XRF) ... 53
    3.3.2 X-ray diffraction (XRD) ... 54
    3.3.3 Thermogravimetric analysis (TGA) ... 55
    3.3.4 Inductively coupled plasma optical emission spectroscopy (ICP-OES) ... 56

4 Results and discussion ... 57
  4.1 Composition of the sulphidic tailing and the marl ... 57
  4.2 Conventional roasting ... 58
    4.2.1 Mass loss ... 58
    4.2.2 Sulphur fixation ... 61
    4.2.3 Mineral phase analysis ... 62
    4.2.4 Molar amount of sulphide, sulphate and carbonate ... 66
    4.2.5 Sulphate formation relative to sulphide and carbonate consumption ... 68
    4.2.6 Mass loss based on Rietveld refinement ... 69
  4.3 Microwave roasting ... 70
    4.3.1 Mass loss ... 70
    4.3.2 Sulphur fixation ... 72
    4.3.3 Mineral phase analysis ... 72
  4.4 Leaching ... 76
    4.4.1 Conventional roasted samples ... 76
    4.4.2 Microwave roasted samples ... 79
    4.4.3 Leaching kinetics ... 82

5 Conclusion ... 85

Bibliography 87

Annex 91
  Annex A: Elemental composition via X-ray fluorescence (XRF) and ICP-OES 93

List of tables

Table 1: Main classes of reactions regarding sulphide roasting 23
Table 2: Thermodynamic data used for calculating the Cu-S-O system 28
Table 3: Overview of phases during roasting at different temperatures 32
Table 4: Heating results of different products during microwave irradiation 38
Table 5: Mineralogy effect on microwave heating 39
Table 6: Phases present in chalcopyrite-calcite microwave and conventional roasted products 42
Table 7: Copper leaching studies performed in the past decade with ammonium/ammonium carbonates lixivent 44
Table 8: List of used chemical agents 45
Table 9: Theoretical sample ratios, prepared for one batch of conventional roasting 46
Table 10: Theoretical sample ratios, prepared for one batch of microwave roasting 48
Table 11: Microwave settings 49
Table 12: Theoretical sample ratios, prepared for TGA analysis 55
Table 13: Composition of sulphidic tailing and marl, determined with XRF and ICP-OES 57
Table 14: Comparison of weight loss after heating to 800 °C with TGA and in a conventional furnace 61
Table 15: Overview of Rietveld refinement on conventional roasted samples 63
Table 16: Mass loss comparison between conventional roasting and microwave-assisted roasting 71
Table 17: Overview of Rietveld refinement on microwave roasted samples 74

List of figures

Figure 1: Schematic representation of problem statement 18
Figure 2: Model for the oxidation of pyrite 21
Figure 3: Visual representation of the shrinking core model 24
Figure 4: General Kellogg diagram of a Me-S-O system for a given temperature 26
Figure 5: The predominance diagram of the Cu-S-O system 28
Figure 6: Roaster diagram for the Cu-S-O system at a total pressure of 0.25 atm 29
Figure 7: Kinetic curve of the desulphurization of fluxed Sokolovsk-sarbaisk pellets 34
Figure 8: Sulfur content in Kostomuksha pellets relative to the roasting temperature and basicity 35
Figure 9: Dipole realignment in an electromagnetic field 36
Figure 10: Interactions to a microwave field 37
Figure 11: The influence of microwave power and sample mass on the absorbed microwave power 40
Figure 12: The influence of particle size for various power densities on the temperature 41
Figure 13: Retsch® Disc Mill DM 200, used for grinding the marl 45
Figure 14: Conventional roasting setup with corresponding temperatures for each batch, unroasted samples, oven setup and roasted samples 47
Figure 15: Theoretical temperature profile of the conventional roasting 48
Figure 16: Internal microwave furnace setup 49
Figure 17: External microwave furnace setup 50
Figure 18: Temperature profile of microwave furnace 50
Figure 19: Setup for adding leaching solution 51
Figure 20: Grant GLS 400, linear shaking water bath setup 51
Figure 21: Setup for leachate recovery 52
Figure 22: XRF sample preparation and handheld stand setup 53
Figure 23: XRD sample preparation, sample rack and diffractometer 54
Figure 24: Primary dilution of filtered leachates setup 56
Figure 25: Diffractograms of the original sulphidic tailing and the marl 58
Figure 26: Mass loss during conventional roasting 59
Figure 27: TGA analysis of the starting materials and three tailing/marl mixtures 60
Figure 28: The relative amount of sulphur retained during conventional roasting in relation to the marl content 62
Figure 29: Representation of the Rietveld data from mixed conventional roasted samples 65
Figure 30: The molar amount of sulphide, sulphate and carbonate in the conventional roasted samples, represented as the amount per gram material (mmol/g material) or as the total amount in each sample (mmol) 67
Figure 31: The sulphate formation, the sulphate formation to sulphide consumed and the sulphate formation to carbonate consumed, all presented as a function of the marl content 69
Figure 32: Mass loss based on Rietveld refinement and crucible weight for conventional roasted samples 70
Figure 33: Mass loss during microwave roasting 71
Figure 34: Relative retained sulphur in relation to the marl content (microwave roasting) 72

Figure 35: X-ray diffractogram of microwave roasted samples at different temperatures for 60 min 73
Figure 36: X-ray diffractogram of microwave roasted samples at 500 °C with different dwell times 73
Figure 37: The molar content of sulphide, sulphate and carbonate in the microwave-assisted roasted samples, represented as the amount per gram material (mmol/g) 75
Figure 38: Filtered leachates of conventional roasted pure tailing 76
Figure 39: Elemental recovery from conventionally roasted samples using ammoniacal leaching 78
Figure 40: Filtered leachates of microwave roasted pure tailing 79
Figure 41: Elemental recovery during leaching of microwave roasted samples using ammoniacal leaching 81
Figure 42: Filtered leachates of conventional roasted samples conducted at different leaching times 82
Figure 43: Elemental recovery in function of the leaching time 83

Glossary

Abbreviation/chemical formula	Description	Units
AMD	Acid mine drainage	-
Gangue material	Material surrounding or mixed with a mineral ore of interest. It is seen as being economically worthless.	-
ICP-OES	Inductively Coupled Plasma Optical Emission Spectroscopy	-
Q-XRD	Quantitative X-ray diffraction	-
TGA	Thermogravimetric Analysis	-
wt%	Weight percentage	%
XRD	X-ray diffraction	-
XRF	X-ray fluorescence	-

Abstract

Microwave assisted roasting of sulphidic tailings

By: Vincent Lemmens

Promotors:
Dr. Jeroen Spooren - VITO
Dr. ir. Maarten Everaert - VITO
Dr. Thomas Abo Atia - VITO
Prof. dr. ir. Leen Braeken - KU Leuven

Mining practices produce large amounts of waste. For example, sulphidic tailings are stored in large ponds and still contain low levels of valuable metals, such as copper (Cu). Sulphidic tailings are an environmental concern as they are prone to form acid mine drainage waters.

This work aimed to combine two mining wastes, *i.e.* sulphidic tailing and carbonate rich waste rock, in a roasting step to simultaneously oxidize sulphide minerals and fixate the formed SO_2 gas as sulphates. Subsequently, the influence of this treatment on the Cu leachability in an ammoniacal solution was tested.

Firstly, the roasting procedure was optimized using a conventional furnace (CF). Later the optimized conditions were tested with a microwave furnace (MW). The MW provides a faster and more selective heating and is less energy consuming. Solid samples were examined using XRF and Q-XRD. A subsequent ammoniacal leaching step was performed and the Cu extraction was examined by ICP-OES.

The sulphate formation (SO_2 fixation) is the highest for samples roasted at 500 °C in the CF. MW roasting at 500 °C performs slightly worse, as FeS_2 is not fully oxidized. Cu recovery is the highest for samples roasted at 500 °C, with leaching for 3 h at 60 °C being optimal. This study shows that addition of waste rock during the roasting step increases SO_2 fixation and that Cu recovery increases after MW roasting, but decreases after CF roasting with increasing waste rock content.

Abstract in Dutch

Microwave assisted roasting of sulphidic tailings

By: Vincent Lemmens

Promotors: Dr. Jeroen Spooren - VITO
Dr. ir. Maarten Everaert - VITO
Dr. Thomas Abo Atia - VITO
Prof. dr. ir. Leen Braeken - KU Leuven

Mijnbouw produceert grote hoeveelheden afval. Bijvoorbeeld sulfidische *tailings*, deze bevatten nog steeds waardevolle metalen zoals koper (Cu). Sulfidische *tailings* zijn een probleem voor het milieu omdat ze zure mijneffluenten afgeven die uitloging van metalen veroorzaken.

Deze thesis trachtte twee afvalstromen uit de mijnbouw te combineren, nl. sulfidische *tailing* en carbonaat-rijk afvalgesteente, in een rooststap waarbij simultaan sulfidische mineralen geoxideerd werden en SO_2 gas gefixeerd werd als sulfaten. Vervolgens werd de invloed van deze rooststap getest op de Cu uitloogbaarheid in een ammonia-oplossing.

Als eerste werd de rooststap geoptimaliseerd in een conventionele oven (CF). Hierna werden de geoptimaliseerde condities getest in een microgolfoven (MW). De MW biedt een snellere en meer selectieve opwarming, en is bovendien energiezuiniger. Vaste stalen werden geanalyseerd via XRF en Q-XRD. Vervolgens werd er met ammonium uitgeloogd en de Cu extractie bepaald via ICP-OES.

De gevormde hoeveelheid sulfaat (gefixeerde SO_2) is het hoogst voor gerooste stalen op 500 °C in de CF. MW roosten bij 500 °C vertoont lagere sulfaatvorming, omdat FeS_2 niet volledig geoxideerd is. Het meeste Cu is uitgeloogd voor stalen geroost op 500 °C, waarbij uitloging gedurende 3 h op 60 °C optimaal is. Deze studie toont aan dat toevoeging van afvalgesteente tijdens de rooststap de SO_2 fixatie doet toenemen en dat de Cu recovery na MW roosten toeneemt, maar daalt na CF roosten met toenemend gehalte aan afvalgesteente.

1 Introduction

1.1 Context

VITO (Flemish Institute for Technological Research) is an independent Flemish research organization in the area of cleantech and sustainable development. Its headquarters are situated in Mol, Belgium. They are also active in China, India and the Middle East. The main research areas of VITO are sustainable chemistry, materials, land use and health and energy. This research project took place in the Sustainable Materials Management unit. The main objectives of this research unit are: 1) circular economy strategies; 2) product & process innovations; and 3) waste and recycling technologies. This study pertains to the last category [1].

Closing material cycles and avoiding wastages are of key importance to sustainable usage of raw material. These raw materials include low-value residual streams and waste streams like mine tailings. Valuable elements such as metals, *e.g.* copper, can be recovered. VITO has specialized experience with physical separation techniques and advanced leaching methods that are utilized for these recoveries. As such, VITO contributes to the transition to a circular economy [1].

1.2 Problem statement

Demand for main commodity metals such as lead, zinc, cadmium, cobalt, nickel and especially copper has increased tremendously over the last couple of decades [2]. As observed by Krausmannc *et al.* an 8-factor increase from 1900 to 2005 occurred [3]. More recently from 1998 to 2014 extraction of the commodity metals globally increased by a 1.7-fold and since the start of recording data, one quarter of the copper production was produced in just the past 10 years. This means that global copper production doubled every 25 years. Due to high demand, the average copper ore grade decreased with approximately 25% in just ten years when the energy consumption progressed more than the production, with 46% and 30% respectively [4].

Current procedure of extraction and its high energy consumption endangers the environment. It leads to the generation of large quantities of waste streams, greenhouse gas emissions, water demand and social costs. Continuation results in two options to maintain the metal demand: 1) opening new mines with lower ore grades but higher environmental impact, with high restrictions by law; and 2) continuing extractions from older mines which as mentioned, increases environmental and energy costs. Therefore, studies investigating recycling options and sustainable use of resources should be of high priority. Because, raw materials are getting scarce and current processing has a negative impact on the environment and the energy consumption [4].

The investigated material, in this study, originates from the Cobre las Cruces mine in Spain. The method for mining the ore from the mineral deposit is open pit mining, a surface mining technique. To reach the ore deposit the upper layer must be removed, which is waste rock, as it contains no valuable metals (Figure 1). The ore is mined and send to a processing plant where the ore is ground and concentrated. Subsequently, the concentrate is smelted and cast in copper anodes which reach a purity of about 98%. These anodes are used in an electrowinning process in which copper cathodes are generated which contain 99.99% pure metal copper. Further processing includes creating final products from the cathodes like copper wires and heat conducting components.

This study focusses on the sustainable recycling option by utilizing low-grade sulphidic mine tailing (waste stream, that mainly consists of pyrite FeS_2) to recover commodity metals. More specifically, the focus is on the recovery of copper from the sulphidic tailings.

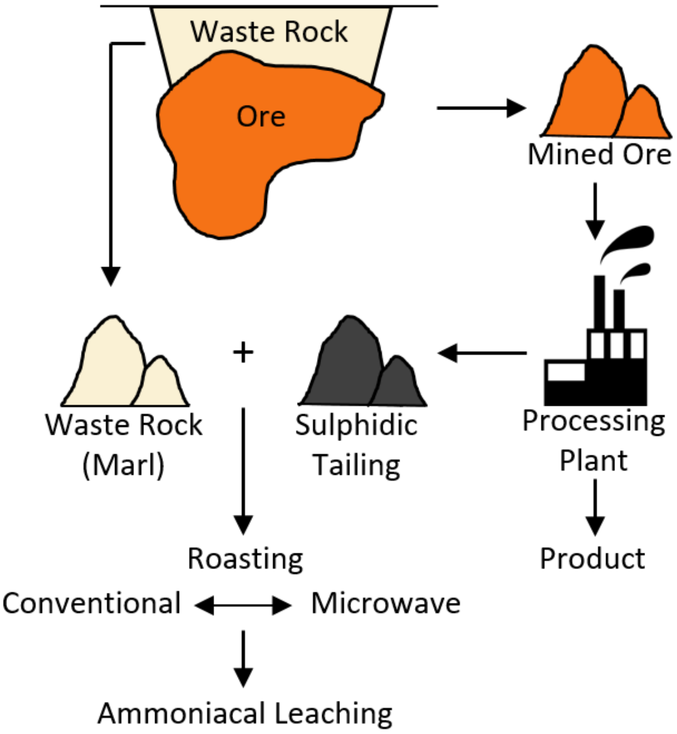

Figure 1: Schematic representation of problem statement

Roasting of pyrite, a main constituent of sulphide ores, yields metal oxides (Equation 1). During this process SO_2 gas is set free, which can react with moisture in the atmosphere to form corrosive sulphuric acid. This could result in acid rain and corrosive mist. Therefore, it is obliged to reduce or eliminate the formation of SO_2 gas in processes. To neutralize SO_2 gasses, carbonates such as $CaCO_3$, CaO and Na_2CO_3 can be used. This results in the formation of Na_2SO_4 or $CaSO_4$ [5]. The waste rock from the Cobre Las Cruces mine also contained a large amount of $CaCO_3$. Therefore, this study investigated if both the waste rock and the sulphidic tailing could be combined during the roasting step to capture sulphur, *i.e.* reduce SO_2 release.

$$4\ FeS_2\ (s) + 11\ O_2\ (g) \rightarrow 2\ Fe_2O_3\ (s) + 8\ SO_2\ (g) \qquad (1)$$

Roasting can be performed by various techniques. However, for sulphide minerals oxidative and sulphation roasting is mainly applied. Generally, the oxidative roasting reaction is presented by Equation 2 [6].

$$\mathrm{MeS} + 1.5\ \mathrm{O_2(g)} \rightarrow \mathrm{MeO} + \mathrm{SO_2(g)} \qquad (2)$$

Sulphide minerals are often found in iron ores and thus, as Equation 2 shows, iron sulphides oxidize to iron oxides, releasing sulphur as SO_2. This results in a desulphurization of the ore. Many reactions can take place, depending on the sulphur content and roasting conditions [7].
Sulphation roasting is performed when metal sulphates are desired. The general sulphation roasting reactions are shown in Equations 3 and 4 [6].

$$\mathrm{MeO} + \mathrm{SO_2(g)} + \tfrac{1}{2}\ \mathrm{O_2(g)} \rightarrow \mathrm{MeSO_4} \qquad (3)$$
$$\mathrm{MeO} + \mathrm{SO_3(g)} \rightarrow \mathrm{MeSO_4} \qquad (4)$$

However, the roasting process is very complex and there are plenty of reactions involving sulphides [8]. The chemical and mineralogical composition of the material, as well as parameters such as particle size, reaction time and temperature also have an impact on the formation of the end products [5], [8].
In roasting processes, copper is desired to be in the sulphate form, while iron is expected to remain in the oxide form (Equations 5 and 6) [2].

$$\mathrm{4CuFeS_2} + 15\ \mathrm{O_2(g)} \rightarrow \mathrm{4CuSO_4} + \mathrm{2Fe_2O_3} + \mathrm{4SO_2} \qquad (5)$$
$$\mathrm{2CuFeS_2} + 7\ \mathrm{O_2(g)} \rightarrow \mathrm{2(CuO.CuSO_4)} + \mathrm{Fe_2O_3} + \mathrm{3SO_2} \qquad (6)$$

Subsequently leaching is performed to selectively leach copper from the roasted product. Acid leaching is not used because of high acid consumption due to carbonates present in the gangue material. Therefore, in this study, leaching will be performed in a combined NH_3 and $(NH_4)_2CO_3$ solution (ammoniacal leaching), which eliminates this problem. Hence, copper is be transformed to a copper(II) ammonia complex [9]. These leaching agents were chosen based on Hua *et al.* and are used as the standard leaching method throughout this study [10].

1.3 Objectives

The main objective is to capture the SO_2 during the roasting process of sulphidic tailings, and to recover copper from the obtained roasting products. By adding a carbonate-rich tailing (marl), SO_2 released during oxidation of sulphide minerals is captured as sulphates. This process is optimized, by varying the roasting temperature and the tailing to marl ratio. Subsequently, the optimized conditions are tested with a microwave furnace. Thirdly, an optimization of the operating conditions (microwave temperature and time) is performed. Finally, the copper leaching potential of the obtained roasted samples is investigated. In sum, the research objectives are:

1) Optimization of the roasting process by varying the sulphidic tailing to marl ratio and the roasting temperature to promote the capture of SO_2.
2) Comparison of microwave-assisted roasting to conventional roasting at the optimized condition of conventional roasting.
3) Optimization of the microwave-assisted roasting with respect to temperature and roasting time.
4) Assess the copper leachability from the various materials obtained after roasting in varying conditions.

1.4 Strategy

The sulphidic tailing and the marl are ground separately to a particle size of <1 mm with a disc mill (*Retsch® Disc Mill DM 200*). Subsequently, the prepared batches are ground with a mortar and pestle to a particle size of about 100 µm and roasted in a conventional furnace [11]. These batches include different mass ratios of the sulphidic tailing and the marl and differ in temperatures they are roasted at.

Firstly, experiments in the conventional furnace are performed. The roasting temperature is varied between 400 °C, 500 °C, 600 °C, 700 °C and 800 °C. Secondly, roasting experiments are performed in a microwave furnace, using roasting conditions determined from the results of the conventional roasting. To evaluate the amount of sulphur that is released or captured during roasting, XRF measurements are performed on the roasted samples and compared with the original tailings. Later on, also Q-XRD measurements are performed to accurately determine the phases (and relative quantity of these phases) in which sulphur and copper are present.

A standard alkaline leaching method is selected, based on the work done by Hua *et al.* [10]. The method performs the leaching with a combined solution of NH_3 and $(NH_4)_2CO_3$. After leaching, the solid and liquid phase are separated by filtration after waiting until the participate settles. Samples from the liquid phase are prepared to be measured with ICP-OES. Results show the amount of copper dissolved from each sample. From this, the effect of the roasting pretreatment on the copper leachability is determined.

2 Literature

2.1 Acid mine drainage

One of the major problems of sulphidic tailings is that they are prone to form acid mine drainage (AMD) waters. The main cause of AMD is the oxidation of sulphide minerals due to the exposure to both oxygen and water or microorganisms [12], [13]. Pyrite is considered the main mineral responsible for AMD, because its ease of oxidation when in contact with oxygen and water. Figure 2 presents the different interactions of pyrite with oxygen and water. Severe pollution occurs due to the release of dissolved metals, metalloids and sulphates as well as the low pH which is introduced. It should be noted that acidophilic bacteria can accelerate reaction (2) and (4), represented in Figure 2. These mechanism are not further described but are discussed in Simate *et al.* [13] .

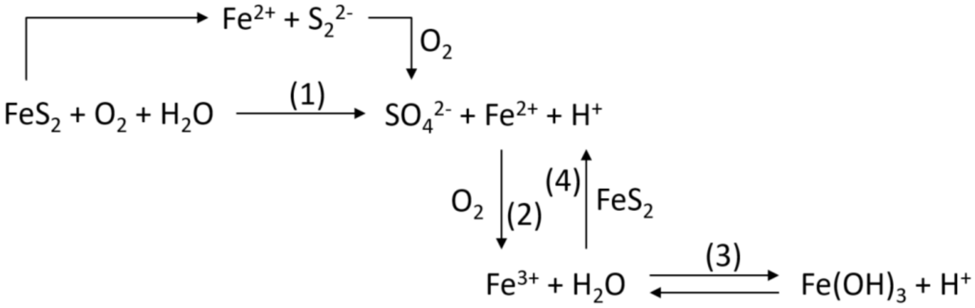

Figure 2: Model for the oxidation of pyrite [13, p. 1787]

2.1.1 Effects of AMD

Acid mine drainage causes the release of H_2SO_4, which promotes the dissolution and release of heavy metals. This mix of toxic elements flows into groundwater and rivers and leads to destruction of aquatic life, ecosystems and infrastructures. Many of the pollutants present in AMD are dangerous for human health, plant, and animal or aquatic life as they include heavy metals such as: As, Cd, Pb, Mn, Hg, Zn, Cr and Cu which introduce acute and long-term toxicity. Heavy metals persist for an extended period in ecosystems and have the ability to accumulate in the biological chain. This causes diseases for humans, cellular damage to plants and dead or long-term effects on animal and aquatic life [13].

2.1.2 Treatment and prevention of AMD

AMD clean-up can be done actively or passively. Active applications include alkaline chemicals to precipitate metals, adsorption, ion exchange and membrane technology. While passive applications include biological treatment and sulphate reducing bioreactors. The neutralization of AMD using $Ca(OH)_2$ or $CaCO_3$ is a common active method for removing metals as metal hydroxides and sulphates such as $CaSO_4.H_2O$ (gypsum). Kefeni *et al.*, lists these and more treatment solutions for AMD clean-up [12].

However, no reliable method for treatment of AMD exists. Therefore, leaching prevention should be aimed for. A possible solution for AMD prevention could be the implementation of mine tailings as raw materials (*e.g.* production of concrete, building materials). Reuse, recycling and reprocessing of the mine tailings is also an option as valuable metals can be extracted in the process [12]. Desulphurization is of importance in these processes to prevent the waste containing the same sulphide minerals, *e.g.* pyrite, being a component for AMD. Desulphurization of sulphide minerals can be achieved by thermal decomposition in air, known as roasting [7]. However, roasting is strongly dependent on temperature and sample mineralogy. Therefore, optimizing the temperature is important for the achieved goal. Subsequently the roasted product can be leached to recover valuable metals and ideally the leftover residue used as raw material.

2.2 Chemistry of roasting

Roasting is considered as a pre-treatment which converts stable metal sulphides in metal ores, *e.g.* Cu_2S or ZnS, to more easily soluble oxides. Such ores, mostly are rich in FeS_2 (pyrite) and other ferrous minerals which are oxidized to Fe_2O_3 (hematite) [2]. Many individual reactions can take place during roasting, depending on temperature, sulphur content, carbonate content, presence and content of an oxidant, etc. During roasting, two parameters are particularly of interest, namely the roasting temperature and the oxidant type. Oxygen (air) is often present as an oxidant as it is cheap and widely available. The influence of the temperature is discussed in detail in section 2.5. It can be stated that desulphurization start from 100 °C and increases with increasing temperature [7]. There are various types of roasting, but for sulphide minerals oxidative and sulphation roasting are mainly of interest.

2.2.1 Oxidative roasting

The general equation for an oxidative roasting reaction is shown in equation 7, in which an oxide product is obtained by burning out sulphur, from sulphide minerals [6], [8], [14], [15].

$$\mathrm{MeS} + 1.5\ \mathrm{O_2(g)} \rightarrow \mathrm{MeO} + \mathrm{SO_2(g)} \qquad (7)$$

Sulphide minerals are often found in iron ores. From Equation 7 it can be derived that iron sulphides oxidize to iron oxides and sulphur is released as SO_2. This results in the desulphurization of the ores. [7], [15].

2.2.2 Sulphation roasting

Sulphation roasting converts metal sulphides or oxides to sulphates. Sulphate formation and thus general sulphation roasting reactions are shown in equations 8 to 10 and are performed to generate sulphate products [6], [8], [14], [16]. Sulphation roasting is introduced because it roasts materials more selectively to their sulphates and thus emits less SO_2 along the way.

$$\mathrm{MeS} + 2\mathrm{O_2(g)} \rightarrow \mathrm{MeSO_4} \qquad (8)$$

$$\mathrm{SO_2(g)} + \frac{1}{2}\mathrm{O_2(g)} \rightarrow \mathrm{SO_3(g)} \qquad (9)$$

$$\mathrm{MeO} + \mathrm{SO_3(g)} \rightarrow \mathrm{MeSO_4} \qquad (10)$$

2.2.3 Sulphide roasting reactions

In reality, the roasting process is complex and cannot be described by only the previous general reaction equations of oxidative or sulphation roasting. An overview (Table 1) of the main classes of reactions involving sulphides are reported by M. Shamsuddin [8]:

Table 1: Main classes of reactions regarding sulphide roasting [8, pp. 42-43]

Class description	Example reactions
Decompostion of higher to lower sulphides	$\mathrm{MeS_2} \rightleftarrows \mathrm{MeS} + 0.5\ \mathrm{S_2}$ $2\ \mathrm{MeS_2} \rightleftarrows \mathrm{Me_2S_3} + 0.5\ \mathrm{S_2}$
Oxidation of sulphide to oxides or sulphates	$2\ \mathrm{MeS} + 3\ \mathrm{O_2} \rightleftarrows 2\ \mathrm{MeO} + 2\ \mathrm{SO_2}$ $\mathrm{MeS} + 2\ \mathrm{O_2} \rightleftarrows \mathrm{MeSO_4}$
Burn-up of sulphur to oxides	$\mathrm{S_2} + 2\ \mathrm{O_2} \rightleftarrows 2\ \mathrm{SO_2}$ $2\ \mathrm{SO_2} + \mathrm{O_2} \rightleftarrows 2\ \mathrm{SO_3}$
Sulphation of metaloxides	$\mathrm{MeO} + \mathrm{SO_3} \rightleftarrows \mathrm{MeSO_4}$ $2\ \mathrm{MeO} + 2\ \mathrm{SO_2} + \mathrm{O_2} \rightleftarrows 2\ \mathrm{MeSO_4}$
Decompostion of sulphates to basic (oxy)sulphates	$2\ \mathrm{MeSO_4} \rightleftarrows \mathrm{MeO.MeSO_4} + \mathrm{SO_3}$ $\mathrm{MeO.MeSO_4} \rightleftarrows 2\ \mathrm{MeO} + \mathrm{SO_3}$ $\mathrm{MeSO_4} \rightleftarrows \mathrm{MeO.ySO_3} + (1-\mathrm{y})\ \mathrm{SO_3}$
Sulphide - sulphate interaction	$\mathrm{MeS} + 3\ \mathrm{MeSO_4} \rightleftarrows 4\ \mathrm{MeO} + 4\ \mathrm{SO_2}$
Sulphide oxide interaction	$\mathrm{MeS} + 2\ \mathrm{MeO} \rightleftarrows 3\ \mathrm{Me} + \mathrm{SO_2}$
Reaction between oxide product and impurity oxides to complex compounds	$2\ \mathrm{MeO} + 2\ \mathrm{FeO} \rightleftarrows 2\ \mathrm{MeFeO_2}$ $2\ \mathrm{MeO} + \mathrm{SiO_2} \rightleftarrows \mathrm{Me_2SiO_4}$
Formation sub- or higher-oxides	$2\ \mathrm{MeO} \rightleftarrows \mathrm{Me_2O} + 0.5\ \mathrm{O_2}$ $2\ \mathrm{MeO} + 0.5\ \mathrm{O_2} \rightleftarrows \mathrm{Me_2O_3}$
Other reduction or oxidation reactions	$3\ \mathrm{Me_3O_4} + \mathrm{MeS} \rightleftarrows 10\ \mathrm{MeO} + \mathrm{SO_2}$ $\mathrm{M} + \mathrm{SO_2} \rightleftarrows \mathrm{MeS} + \mathrm{O_2}$

The formation of certain reaction products does not only depend on the material properties, *i.e.* chemical and mineralogical composition, but is also determined by the operating conditions. The particle size of the material, the reaction time, the temperature and mixing conditions are important parameters to take into account. Also, particularly for roasting, the partial pressures of O_2 and SO_2 influence the formation of the end products [5], [8]. In the following paragraphs the relevant kinetics and thermodynamics with focus on the Kellogg diagram (stability regions) of a M-S-O system are discussed. [14].

2.3 Roasting kinetics

2.3.1 The shrinking core model

The roasting process is basically a fluid-particle reaction, with the fluid being a gas. To evaluate the chemical kinetics, *i.e.* derive the chemical reaction rates, a model must be described. The chemical kinetics depend on the transport rate of the gas to the unreacted solid as well as the reaction between the solid and gas at the solid interface. Factors such as temperature, particle size, particle porosity, particle shape, chemical composition and mineralogy influence these rates [2], [5], [6].

The model that is valid for the prediction of these non-catalytical solid-gas interactions in case of sulphidic mineral roasting is the shrinking core model. A visual representation of the shrinking core model is given in Figure 3. The model describes a reaction during which the unreacted particles shrink in size during the reaction. Here, a flaking ash, gaseous products or a flaking product material is formed. This operation refers to the shrinking core model. The reaction starts at the particle surface and moves inwards, thereby consuming the solid along the way. This leaves inert solid and fully converted material, referred to as ash [5], [6].

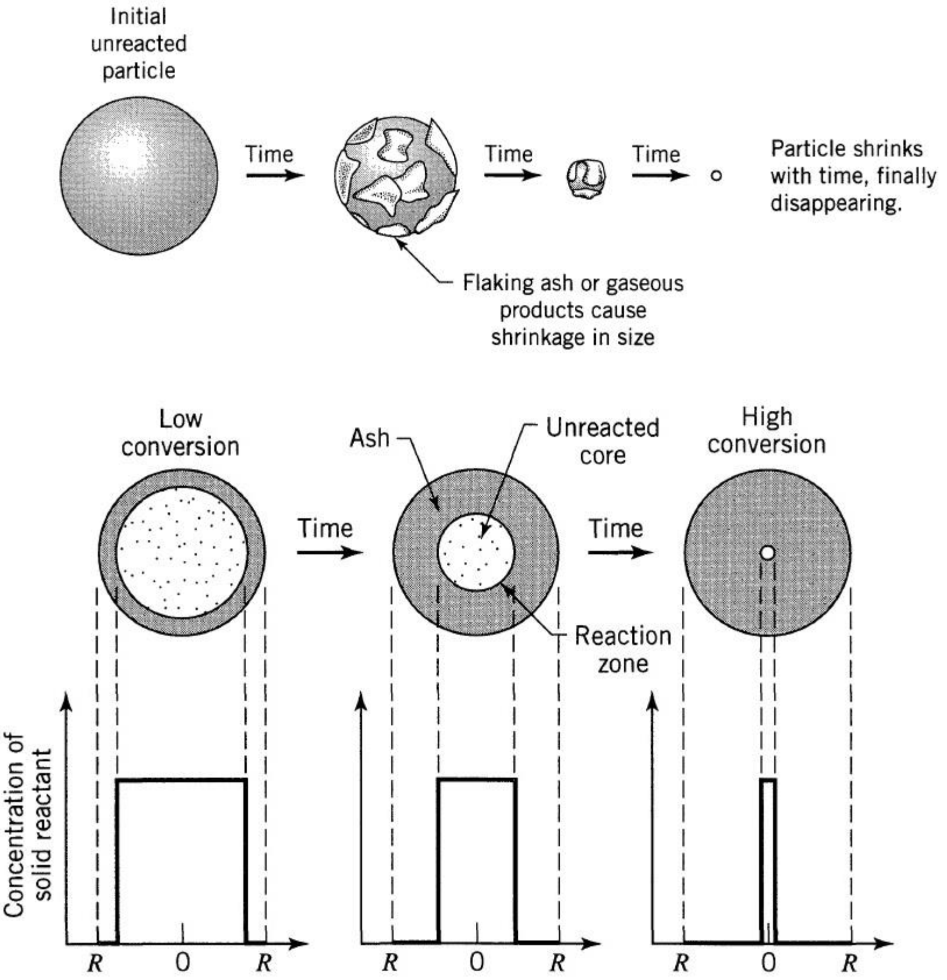
Initial unreacted particle
Time
Time
Time
Particle shrinks with time, finally disappearing.
Flaking ash or gaseous products cause shrinkage in size
Low conversion
Ash
Unreacted core
High conversion
Time
Time
Reaction zone
Concentration of solid reactant
R
0
R
R
0
R
R
0
R

Figure 3: Visual representation of the shrinking core model, adapted from [5, p. 567 and 579]

It should be noted that each model has specific rate equations. For actual development of the rate expressions as well as the use of these expression in designing a reactor, refer to chapter 25 and 26 of the book Chemical reaction engineering by Levenspiel [5].

2.4 Thermodynamics of roasting

The thermodynamics of roasting can be visualized in predominance diagrams, which are useful to understand the phase equilibria during roasting. Specifically for roasting of sulphidic tailings, it is interesting to display a diagram with the logaritmic partial pressures of SO_2 and O_2 at a given roasting temperature. Such a diagram is called a Kellogg diagram. For each point in the diagram, the stable product that can be formed in the specific Me-S-O system is presented [8]. The general Kellogg diagram for a Me-S-O system is shown in Figure 4. It is displayed in 2D because the temperature is considered as a contant, the only variables are the partial pressure of SO_2 and O_2. If the temperature is included as a variable, a 3D graph must be contructed. Mostly roasting is performed at a constant pressure, and while constructing the Kellogg diagram the temperature is contant. Therefore, the integer[1] in the Gibbs phase rule (Equation 11) becomes 0. For a three component system (Me, S and O) the phase rule can be simplified to F = 3 - P (C = 3; integer = 0) [8], [17], [18].

$$\mathrm{P = C - F + 2} \tag{11}$$

P: number of phases; C:components; F: degree of freedom

The gas phase consist mainly of SO_2 and O_2, yet also SO_3 and S_2 gasses are usually present in relevant amounts. Once the partial pressures of SO_2 and O_2 are known, the pressures of SO_3 and S_2 can be calculated from the equilibria among the gaseous components (Equation 12 and 13) [8], [17].

$$\mathrm{S_2(g) + 2O_2(g) \rightleftarrows 2SO_2(g)} \tag{12}$$
$$\mathrm{2SO_2(g) + \ O_2(g) \rightleftarrows 2SO_3(g)} \tag{13}$$

In general there are three rules to the predominance diagram.

1) If one condensed phase exists (*e.g.* MeS; P = 1), the partial pressures of SO_2 and O_2 may be changed independently as the system with constant temperature has two degrees of freedom. (F = 3 – 1 + 0 = 2; integer = 0 temperature and total pressure are constant)
2) On the lines between two condensed phases (*e.g.* MeS – MeO “line 5” Figure 4; P = 2), the system has only one degree of freedom. (F = 3 – 2 + 0 = 1; integer = 0 temperature and total pressure are constant). This means that either the partial pressure of SO_2 or O_2 can be changed, the other one is fixed.
3) The system is non variant at places where three phases are in equilibrium (P = 3), because the degree of freedom is 0 (F = 3 – 3 + 0 = 0). This means that the partial pressure of SO_2 and O_2 are fixed.

---

[1] The integer (a number which is not a fraction; a whole number – Oxford Dictionary) in the Gibbs phase rule is related to the number of intensive parameters such as temperature and pressure that are being considered.

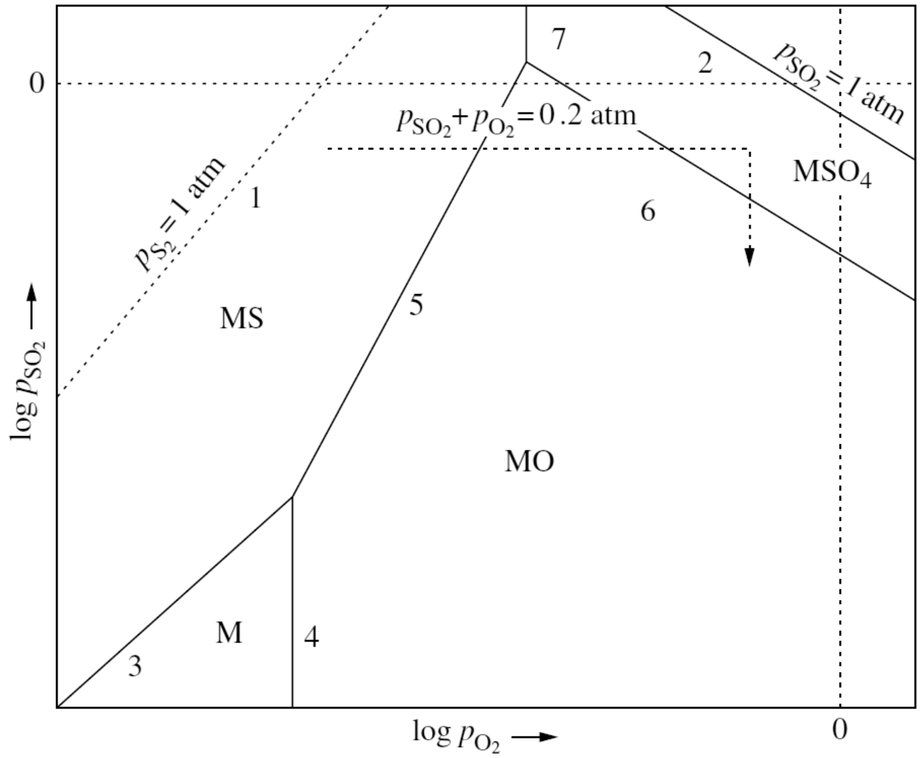

Figure 4: General Kellogg diagram of a Me-S-O system for a given temperature [8, p. 44]

Based on the equilibrium between two phases, the boundary lines can be constructed by finding the relation between the logarithmic partial pressures of SO_2 and O_2. Reactions regarding these equilibriums are presented by Equations 14 to 18 [8], [14], [17], [18]. Certain metals form several sulphides and oxides at which additional equilibria must be considered for forming Me_2S, Me_2O and $Me_2(SO_4)$ [17]. Additionally the basic sulphate $MeO.MeSO_4$ may exist. The equilibrium constants can be calculated from the free energy equations, which can be found in literature for the specific systems, by solving Equation 19. Equilibrium constant equations include the activities (*a*), which are considered to be equal to 1, for solids and partial pressures (*p*) for gases from which the relation between the partial pressures of SO_2 and O_2 can be derived (Equation 20 to 26) for the M-S-O system [14]. The relation shows the slope of the respective equilibrium line that can be drawn in the Kellogg diagram. For example consider Equation 16, the respective equilibrium Equation 24 can be transformed in function of the partial pressure of O_2 ($\log p_{SO2} = 0.5 \log K_5 + 1.5 \log O_{2)}$ which shows the slope (1.5) of that particular equilibrium line in the Kellogg diagram. This can be done for all equilibrium equations, after which the Kellogg diagram is constructed.

$$\mathrm{Me} + \mathrm{SO_2} \rightleftarrows \mathrm{MeS} + \mathrm{O_2} \qquad (14)$$
$$2\,\mathrm{Me} + \mathrm{O_2} \rightleftarrows 2\,\mathrm{MeO} \qquad (15)$$
$$2\,\mathrm{MeS} + 3\,\mathrm{O_2} \rightleftarrows 2\,\mathrm{MeO} + 2\,SO_2 \qquad (16)$$
$$2\,\mathrm{MeO} + 2\,SO_2 + \mathrm{O_2} \rightleftarrows 2\,\mathrm{MeSO_4} \qquad (17)$$
$$\mathrm{MeS} + 2\,\mathrm{O_2} \rightleftarrows \mathrm{MeSO_4} \qquad (18)$$

$$\log K = \frac{-\Delta G^0}{2.303\ RT} \quad (19)$$

$$K_{12} = \frac{p_{SO_2}^2}{p_{S_2} \cdot p_{O_2}^2} \quad (20)$$

$$K_{13} = \frac{p_{SO_3}^2}{p_{SO_2}^2 \cdot p_{O_2}} \quad (21)$$

$$K_{14} = \frac{a_{MeS} \cdot p_{O_2}}{a_{Me} \cdot p_{SO_2}} = \frac{p_{O_2}}{p_{SO_2}} \quad (22)$$

$$K_{15} = \frac{1}{p_{O_2}} \quad (23)$$

$$K_{16} = \frac{p_{SO_2}^2}{p_{O_2}^3} \quad (24)$$

$$K_{17} = \frac{1}{p_{SO_2}^2 \cdot p_{O_2}} \quad (25)$$

$$K_{18} = \frac{1}{p_{O_2}^2} \quad (26)$$

It should be noted that Kellogg diagrams are useful, however, for metallurgists ‘roaster diagrams’ are a more useful representation. In roaster diagrams, stable phases are shown as a function of temperature and oxygen percentage at a given total pressure [18]. Roaster diagrams are “projections of the intersection of the total pressure plane with the equilibrium planes on a predominance area diagram extended in the temperature dimension” [18, p. 196].

2.4.1 The Cu-S-O system

The selective sulphation of copper sulphides is controlled by the roasting conditions, as given in the Cu-S-O system. An example of such system at 727 °C is given in Figure 5. It is generally accepted that: Cu, CuS, Cu_2S, CuO, Cu_2O, $CuSO_4$, and $CuO \cdot CuSO_4$ are the condensed phases for the Cu-S-O system. The corresponding reactions, free energy relations and equilibrium line equations, needed to construct the Kellogg diagram, are presented in Table 2. For these calculations, it is assumed that a) the condensed phases are pure; and that b) all gasses behave as ideal gas at all temperatures. Figure 5 also shows total pressure loci[2] equal to 0.25 atm and 1 atm, which represent roasting under atmospheric and pure oxygen conditions respectively. It also shows the isobaric lines for the gasses SO_3 and S_2, calculated from reaction 1 and 2 of Table 2 [8], [17].

---

[2] Locus: a curve formed by all the points satisfying a particular equation of the relation between coordinates, or by a point, line, or surface moving according to mathematically defined conditions – Oxford Dictionary.

Table 2: Thermodynamic data used for calculating the Cu-S-O system [17, p. 66]

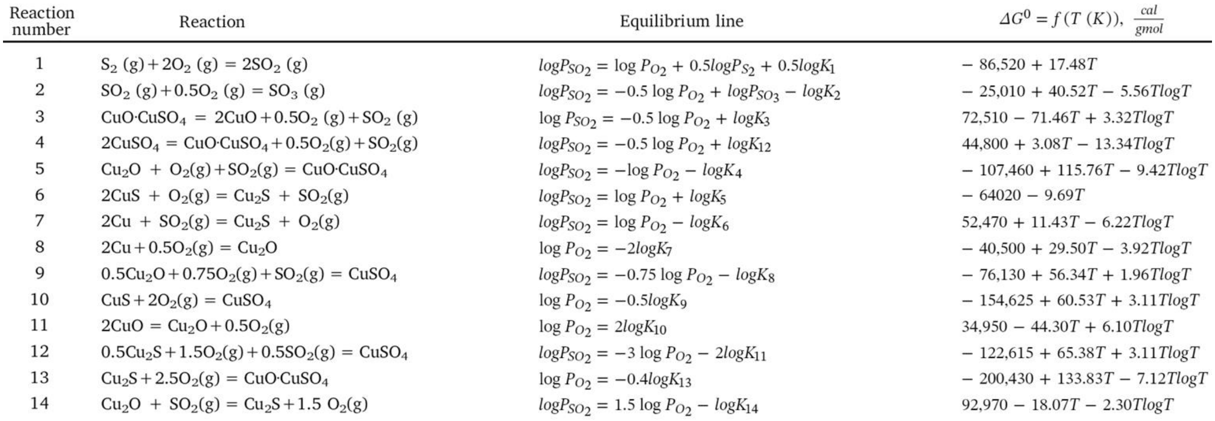

Reaction number	Reaction	Equilibrium line	$\Delta G^0 = f(T\ (K)),\ \frac{cal}{gmol}$
1	$S_2\ (g) + 2O_2\ (g) = 2SO_2\ (g)$	$logP_{SO_2} = \log P_{O_2} + 0.5logP_{S_2} + 0.5logK_1$	$-\ 86{,}520 + 17.48T$
2	$SO_2\ (g) + 0.5O_2\ (g) = SO_3\ (g)$	$logP_{SO_2} = -0.5 \log P_{O_2} + logP_{SO_3} - logK_2$	$-\ 25{,}010 + 40.52T - 5.56TlogT$
3	$CuO{\cdot}CuSO_4 = 2CuO + 0.5O_2\ (g) + SO_2\ (g)$	$\log P_{SO_2} = -0.5 \log P_{O_2} + logK_3$	$72{,}510 - 71.46T + 3.32TlogT$
4	$2CuSO_4 = CuO{\cdot}CuSO_4 + 0.5O_2(g) + SO_2(g)$	$logP_{SO_2} = -0.5 \log P_{O_2} + logK_{12}$	$44{,}800 + 3.08T - 13.34TlogT$
5	$Cu_2O + O_2(g) + SO_2(g) = CuO{\cdot}CuSO_4$	$logP_{SO_2} = -\log P_{O_2} - logK_4$	$-\ 107{,}460 + 115.76T - 9.42TlogT$
6	$2CuS + O_2(g) = Cu_2S + SO_2(g)$	$logP_{SO_2} = \log P_{O_2} + logK_5$	$-\ 64020 - 9.69T$
7	$2Cu + SO_2(g) = Cu_2S + O_2(g)$	$logP_{SO_2} = \log P_{O_2} - logK_6$	$52{,}470 + 11.43T - 6.22TlogT$
8	$2Cu + 0.5O_2(g) = Cu_2O$	$\log P_{O_2} = -2logK_7$	$-\ 40{,}500 + 29.50T - 3.92TlogT$
9	$0.5Cu_2O + 0.75O_2(g) + SO_2(g) = CuSO_4$	$logP_{SO_2} = -0.75 \log P_{O_2} - logK_8$	$-\ 76{,}130 + 56.34T + 1.96TlogT$
10	$CuS + 2O_2(g) = CuSO_4$	$\log P_{O_2} = -0.5logK_9$	$-\ 154{,}625 + 60.53T + 3.11TlogT$
11	$2CuO = Cu_2O + 0.5O_2(g)$	$\log P_{O_2} = 2logK_{10}$	$34{,}950 - 44.30T + 6.10TlogT$
12	$0.5Cu_2S + 1.5O_2(g) + 0.5SO_2(g) = CuSO_4$	$logP_{SO_2} = -3 \log P_{O_2} - 2logK_{11}$	$-\ 122{,}615 + 65.38T + 3.11TlogT$
13	$Cu_2S + 2.5O_2(g) = CuO{\cdot}CuSO_4$	$\log P_{O_2} = -0.4logK_{13}$	$-\ 200{,}430 + 133.83T - 7.12TlogT$
14	$Cu_2O + SO_2(g) = Cu_2S + 1.5\ O_2(g)$	$logP_{SO_2} = 1.5 \log P_{O_2} - logK_{14}$	$92{,}970 - 18.07T - 2.30TlogT$

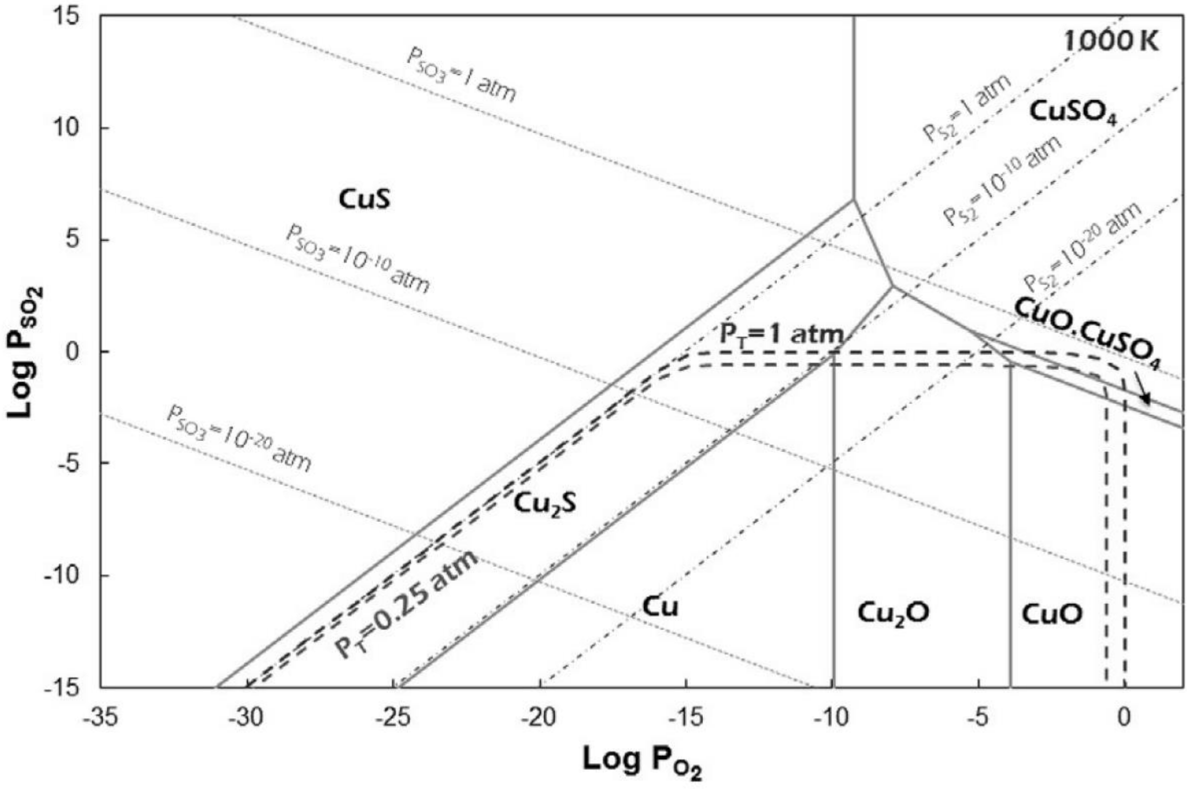

Figure 5: The Kellogg diagram of the Cu-S-O system [17, p. 67]

A roaster diagram can be constructed from a Kellogg diagram, and is more useful because during roasting oxygen and temperature are the controllable factors. Figure 6, shows such roaster diagram for the Cu-S-O system with the total pressure fixed at 0.25 atm. It shows the stability of the condensed phases ($CuSO_4$, CuO.SO_4 and CuO) relative to temperature and percent oxygen. If a second roaster diagram was constructed for a total pressure of 1 atm, the equilibrium lines would shift to higher temperatures (790 °C to 860 °C at 50% oxygen). This shift essentially means that for constant temperatures, lower total pressures benefit the CuO formation [17].

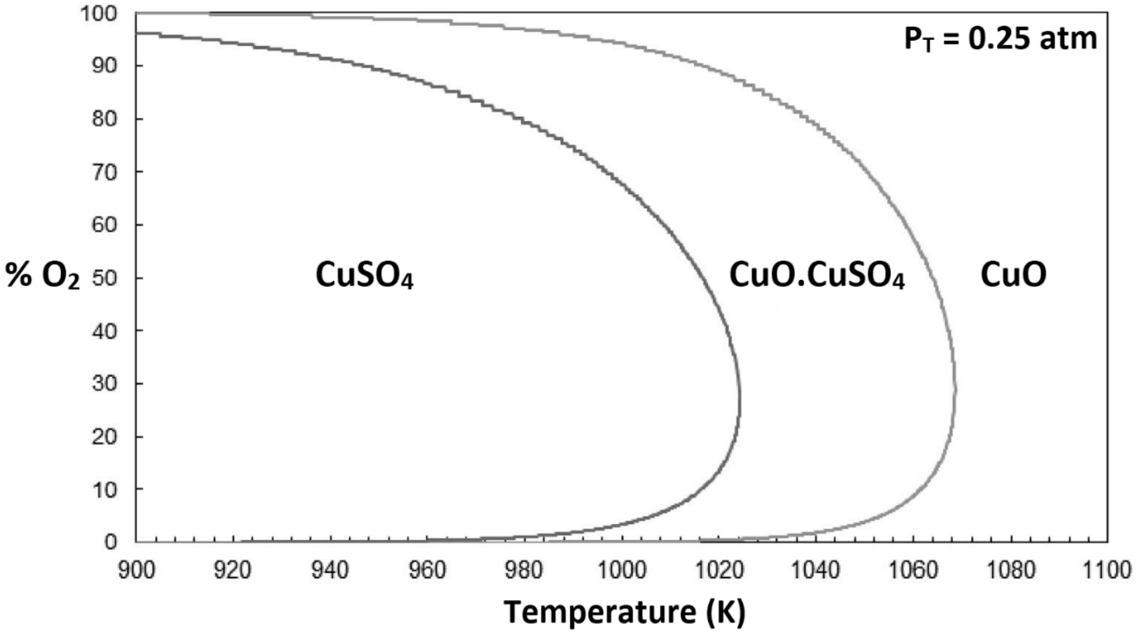

Figure 6: Roaster diagram for the Cu-S-O system at a total pressure of 0.25 atm, adapted from [17, p. 69]

2.5 Influence of temperature on conventional roasting

The temperature at which the roasting is performed, strongly affects the phases. In Table 3, an overview of phases formed with conventional roasting is given for certain products and temperatures.

A review of $CuFeS_2$ (chalcopyrite) roasting was done by Prasad *et al.* [19]. The review discussed that the oxidation of CuS and Cu_2S (cupric sulphides) results in $CuSO_4$ formation at 415 °C, which decomposes in CuO at 510 °C. With increasing temperature, the following phase changing sequence is accepted: $CuS \rightarrow Cu_2S \rightarrow Cu_2O \rightarrow CuSO_4 \rightarrow CuO.CuSO_4 \rightarrow CuO$ [19]. Roasting of FeS initially produces Fe_3O_4 (magnetite), which further oxidizes into Fe_2O_3 (hematite), if the temperature keeps rising. FeS can also convert to $Fe_2(SO_4)_3$ (Mikasaite) which transforms to Fe_2O_3 in the range of 375 °C – 650 °C [19].
Chalcopyrite ($CuFeS_2$) transforms into Cu_5FeS_4 (bornite), Fe_2O_3 and $CuSO_4$ at 500 °C but, when roasted at 800 °C, CuO, Fe_2O_3 and $CuFe_2O_4$ (cuprospinel) are formed [19].

After the review [19], a thermo-analytical study on $CuFeS_2$ was performed by Prasad *et al.* [20]. The initial phase transformation in inert atmosphere of $CuFeS_2$ (chalcopyrite) is the transformation into Cu_5FeS_4 at 160 °C. At 355 °C, sulphur removal was found due to FeS_2 (pyrite) oxidation to FeS (iron sulphide). Chalcopyrite was also transformed into Cu_2S and FeS at 524 °C [20]. Prasad *et al.* [20] also conducted $CuFeS_2$ to oxidation by heating in air. They found a mass gain of 8% between 477 °C and 667 °C that attributed to either direct transformation to Fe_2O_3, $CuSO_4$ and $FeSO_4$ or decomposition to Cu_2S and FeS which oxidize themselves. Iron sulphate, which initially formed decomposes at 460 °C to ferric oxide. The cupric sulphides (Cu_2S and CuS) generated from $CuFeS_2$ oxidize to CuO and Cu_2O which on their turn undergo an *in-situ* reaction with SO_2, O_2 and SO_3 to form $CuSO_4$. This means that rather than a direct formation of $CuSO_4$ from $CuFeS_2$, intermediate steps are taking place. Copper sulphate decomposes above 667 °C up until 745 °C to cupric ferrite ($CuO.Fe_2O_3$). During the oxidation of $CuFeS_2$, Cu_2S, CuS and FeS the released SO_2 is converted to SO_3 when in the presence of Fe_2O_3. The SO_3 further reacts with copper oxides to the formation of additional sulphates. This was tested by adding 10 wt% Fe_2O_3 (ferric oxide) to cupric sulphide and by roasting the mixture. This test confirmed that Fe_2O_3 catalyzes the reactions to form additional sulphates, because an increase in mass gain up to 14% was observed in the range temperature range of 496 °C to 650 °C [20]. The following sequence is suggested when roasting chalcopyrite with addition of ferric oxides: $CuFeS_2 \rightarrow Cu_2S \rightarrow Cu_2O \rightarrow CuO \rightarrow CuO.CuSO_4 \rightarrow CuSO_4$.

Both Zivkovic *et al.* [21] and Mitovski *et al.* [22] describe the reactions which occur during phase transformation of chalcopyrite-pyrite concentrates. A comparison was made to give a "general overview". Both articles deal with similar chalcopyrite-pyrite concentrates. Nonetheless the mineral and elemental composition of the concentrate used in Zivkovic *et al.* [21] is: 53.68 wt% $CuFeS_2$, 22.19 wt% FeS_2, 2.19 wt% CuS and 1.5 wt% Cu_2S or 21.26 wt% Cu, 26.69 wt% Fe, 37.57 wt% S. While, Mitovski *et al.* [22] only describes the elemental composition: 15.84 wt% Cu, 33.19 wt% Fe, 35.80 wt% S.

The initial heating from 40 °C to 138 °C removes moisture, while phase transformations of FeS_2 (pyrite) are reported to start between 173 °C - 261 °C [22]. In that range, FeS_2 starts oxidizing to FeS with the released sulphur being oxidized to SO_2 (Equation 27 to 29) [22]. Zivkovic *et al.* [21] and Ozer *et al.* [2] also, mention the dissociation of pyrite but between the interval 287 - 394 °C.

$$2\ \mathrm{FeS_2} \rightarrow 2\ \mathrm{FeS} + \mathrm{S_2} \qquad (27)$$
$$\mathrm{S_2} + 2\ \mathrm{O_2(g)} \rightarrow 2\ \mathrm{SO_2(g)} \qquad (28)$$
$$\mathrm{FeS_2} + \mathrm{O_2(g)} \rightarrow \mathrm{FeS} + \mathrm{SO_2(g)} \qquad (29)$$

The FeS which is formed by decomposition of FeS_2, further oxidizes forming $FeSO_4$ (350 °C [21], Fe_3O_4 and Fe_2O_3 in the interval of 275 °C to 596 °C [22]. Simultaneously, $CuFeS_2$ and Cu_5FeS_4 decompose into Cu_2S, $FeSO_4$, Fe_3O_4 and Fe_2O_3 during that interval [22]. Reactions describing these transitions are shown in Equations 30 to 35 [22]. The desulphation reaction (Equation 32) also occurs in the same interval supposedly around 480 °C [21]. Zivkovic *et al.* [21] and Ozer *et al.* [2], agree with these reactions. The decomposition of $CuFeS_2$ (Equation 34) to FeS was found to start at 287 °C [2] or 300 °C [21]. At 350°C [21] the FeS formed, due to dissociation of $CuFeS_2$, is oxidized to $FeSO_4$ (Equation 31) [21]. While, the formation of Fe_3O_4 (magnetite) and Fe_2O_3 (hematite) occur above 370°C (Equation 30 and 33) [21].

$$3\ \mathrm{FeS} + 5\ \mathrm{O_2(g)} \rightarrow \mathrm{Fe_3O_4} + 3\ \mathrm{SO_2(g)} \qquad (30)$$
$$\mathrm{FeS} + 2\ \mathrm{O_2(g)} \rightarrow \mathrm{FeSO_4} \qquad (31)$$
$$2\ \mathrm{FeSO_4} \rightarrow \mathrm{Fe_2O_3} + \mathrm{SO_2(g)} + \mathrm{SO_3(g)} \qquad (32)$$
$$2\ \mathrm{FeS} + 4\ \mathrm{O_2}\ \mathrm{(g)} \rightarrow \mathrm{Fe_2O_3} + \mathrm{SO_2(g)} + \mathrm{SO_3(g)} \qquad (33)$$
$$2\ \mathrm{CuFeS_2} + \mathrm{O_2(g)} \rightarrow \mathrm{Cu_2S} + 2\ \mathrm{FeS} + \mathrm{SO_2(g)} \qquad (34)$$
$$2\ \mathrm{Cu_5FeS_4} + \mathrm{O_2(g)} \rightleftarrows 5\ \mathrm{Cu_2S} + 2\ \mathrm{FeS} + \mathrm{SO_2(g)} \qquad (35)$$

The next transformation is Fe_3O_4 that oxidizes to Fe_2O_3 at 474 °C [22] or 480 °C [21] (Equation 36). Increasing the temperature to 525 °C, results in the sulphation of FeS and Cu_2S (Equations 31, 37 and 38) [2], [21]. These reactions stop at 620 °C [22]. Iron sulphide will decompose completely to hematite between 525 °C and 660 °C (Equation 32) [2], [21]. Thereafter, Fe_3O_4 is more stable than Fe_2O_3 at 700 °C and above, therefore transforming back [22] (Equation 39) [21], [22].

$$4\ \mathrm{Fe_3O_4} + \mathrm{O_2(g)} \rightarrow 6\ \mathrm{Fe_2O_3} \tag{36}$$
$$\mathrm{Cu_2S} + \mathrm{SO_2(g)} + 3\ \mathrm{O_2(g)} \rightarrow 2\ \mathrm{CuSO_4} \tag{37}$$
$$\mathrm{Cu_2S} + 2.5\ \mathrm{O_2(g)} \rightarrow 2\ \mathrm{CuO.CuSO_4} \tag{38}$$
$$6\ \mathrm{Fe_2O_3} \rightarrow 4\ \mathrm{Fe_3O_4} + \mathrm{O_2(g)} \tag{39}$$

Finally, between 700 °C - 847 °C, CuO.$CuSO_4$ and $CuSO_4$ start decomposing [21], [22] to CuO and at 900 °C $CuFe_2O_4$ (copper ferrite) formation occurs [22]. These reactions are shown in Equations 40 to 42 [21], [22]. According to Ozer *et al.* [2], the temperature range is lower namely 600°C - 700°C with formation of $CuFe_2O_4$ above 700°C. In their experiment decomposition of copper sulphates even started at 550 °C.

$$\mathrm{CuO.CuSO_4} \rightarrow 2\ \mathrm{CuO} + \mathrm{SO_3(g)} \tag{40}$$
$$2\ \mathrm{CuSO_4} \rightarrow \mathrm{CuO} + \mathrm{SO_3(g)} \tag{41}$$
$$\mathrm{CuO} + \mathrm{Fe_2O_3} \rightarrow \mathrm{CuFe_2O_4} \tag{42}$$

The reactions above describe the roasting mechanism for chalcopyrite-pyrite, with stepwise transitions. XRD analysis of samples roasted at 450 °C, 600 °C and 1000 °C [21] confirmed the mineral compositions (Table 3). The phases: FeS, $FeSO_4$, and $CuSO_4$ were not detected as there was not enough time for them to crystallize [21]. Ozer *et al.* [2], roasted copper-bearing materials and found similar results to [21] and [22] for their chalcopyrite concentrate (16.52 wt% Cu, 29.88 wt% Fe, 38.85wt% S) roasting. They confirmed mineral composition with XRD for samples roasted at 500 °C, 550 °C, 600 °C and 680 °C. Generally it can be concluded that during roasting of chalcopyrite-pyrite concentrates, the sequence of reaction between 0 °C - 800 °C can be given as: $CuFeS_2$ – Cu_2S – $CuSO_4$ – CuO.$CuSO_4$ – CuO – $CuFe_2O_4$ and FeS_2 – FeS – $FeSO_4$ – $Fe_2(SO_4)_3$ – Fe_3O_4 – Fe_2O_3 for chalcopyrite and pyrite respectively [2].

Table 3: Overview of phases during roasting at different temperatures of different starting products

Samples	Unroasted/ un-treated	400 °C	450 °C	500 °C	550 °C	600 °C	650 °C	680°C	800 °C	1000 °C	Source
Chalcocite	Cu_2S	$CuSO_4$	$CuSO_4$	CuO, $CuO.CuSO_4$							[19]
			$CuSO_4$, $CuO.CuSO_4$			$CuSO_4$				CuO	[21]
Pyrite	FeS_2		Fe_2O_3, $Fe_2(SO_4)_3$			Fe_2O_3, $Fe_2(SO_4)_3$			Fe_2O_3		[21]
Iron sulphide	FeS	Fe_3O_4, Fe_2O_3, $Fe_2(SO_4)_3$		Fe_3O_4, Fe_2O_3, $Fe_2(SO_4)_3$,		Fe_3O_4, Fe_2O_3 $Fe_2(SO_4)_3$,	Fe_3O_4, Fe_2O_3 $Fe_2(SO_4)_3$,				[19]
				Fe_2O_3, Fe_3O_4							[20]
Chalcopyrite	$CuFeS_2$			Cu_5FeS_4, Fe_2O_3, $CuSO_4$					CuO, Fe_2O_3, $CuFe_2O_4$		[19]
	$CuFeS_2$ (25.2 wt% Cu, 28.28 wt% Fe, 31.6 wt% S)			Fe_2O_3, $CuSO_4$, $FeSO_4$, Cu_2S, CuS					$CuO.Fe_2O_3$		[20]
Cupric sulphide + 10 wt% ferric oxide	CuS / Cu_2S + 10 wt% Fe_2O_3			CuO, $CuSO_4$, Cu_2O							[20]

Chalcopyrite-pyrite concentrates	FeS_2, $CuFeS_2$, CuS, Cu_2S, CaO		FeS_2, $CuFeS_2$, Fe_3O_4, Fe_2O_3			$CuFeS_2$, Fe_2O_3				Fe_2O_3, CuO, Cu_2O (727 °C)	[21]
	FeS_2,$CuFeS_2$,$CaCO_3$, Fe_2O_3, Cu_5FeS_4, ZnS		$CuSO_4$, Fe_2O_3, Fe_3O_4, Cu_2S				$CuSO_4$, Fe_2O_3, $Cu_2O(SO_4)$			CuO, $CuFe_2O_4$, Fe_2O_3, Fe_3O_4	[22]
	FeS_2, $CuFeS_2$, SiO_2			$FeSO_4$, $CuSO_4$, SiO_2	Fe_2O_3, $FeSO_4$, $CuSO_4$, SiO_2	Fe_2O_3, $CuSO_4$, SiO_2		Fe_2O_3, Fe_3O_4, $CuSO_4$, $CuO.CuSO_4$, SiO_2			[2]
Run of mine	FeS_2, SiO_2, Fe_2O_3, $KFe_3(SO_4)_2(OH)_6$, $CuFeS_2$, Mg-Al Silicate			SiO_2, Fe_2O_3, $FeSO_4$, $CuSO_4$	SiO_2, Fe_2O_3, $FeSO_4$, $CuSO_4$	SiO_2, Fe_2O_3, $Cu.CuSO_4$		SiO_2, Fe_2O_3, CuO			[2]
Flotation tailing	FeS_2, SiO_2, Fe_2O_3, $KFe_3(SO_4)_2(OH)_6$, $CuFeS_2$, Mg-Al Silicate			SiO_2, Fe_2O_3, $FeSO_4$	SiO_2, Fe_2O_3, $FeSO_4$	SiO_2, Fe_2O_3		SiO_2, Fe_2O_3, Fe_3O_4			[2]

2.6 Introducing carbonates to the roasting process

The presence of carbonates in the roasting process of sulphidic ores (mostly iron) can result in a decrease of desulphurization of the ore due to retention of sulphur in the form of sulphate in the roasted material. During the roasting process, the sulphur from the metal sulphides transform to $CaSO_4$ (anhydrite) if $CaCO_3$ (calcium carbonate) is present. However, roasting at elevated temperatures also causes sulphates to decompose ($FeSO_4$ at 480 °C [21], $CuSO_4$ 550 °C - 847 °C [2], [21], [22]). The formed $CaSO_4$, however, remains stable up to 1000 °C when Fe_2O_3 is present. Above 1000 °C Fe_2O_3 loses its catalytical effect and even starts to promote $CaSO_4$ decomposition [23]. The SO_2 fixation in the presence of $CaCO_3$ is represented by Equation 43 and 44, which occur above 460 °C [7], [15], [24], [25].

$$\mathrm{CaCO_3} \rightleftarrows \mathrm{CaO} + \mathrm{CO_2(g)} \qquad (43)$$

$$\mathrm{CaO} + \mathrm{SO_2} + 0.5\mathrm{O_2} \rightarrow \mathrm{CaSO_4} \qquad (44)$$

Abzalov *et al.* [24] found that the desulphurization process of iron pellets, which contain carbonates could be divided into three temperature regions: 1) a lower region up to 600 °C; 2) an intermediate region between 600 °C - 1000 °C and; 3) a high temperature region of above 1000 °C (Figure 7). In the lower temperature region desulphurization corresponds with the removal of SO_2. In the intermediate region desulphurization slows down and hardly any sulphur is removed. At 600 °C - 1000 °C, the limestone decomposes, causing the formed lime to react with SO_2 to form calcium sulphate (Equation 43 and 44). In the higher temperature region (> 1000 °C), desulphurization increases, due to the increasing decomposition of calcium sulphates (Equations 45 and 46) [23], [24]. This suggests that if CaO is added at the beginning of a roasting experiment, less desulphurization might occur due to S being fixated in the material during roasting.

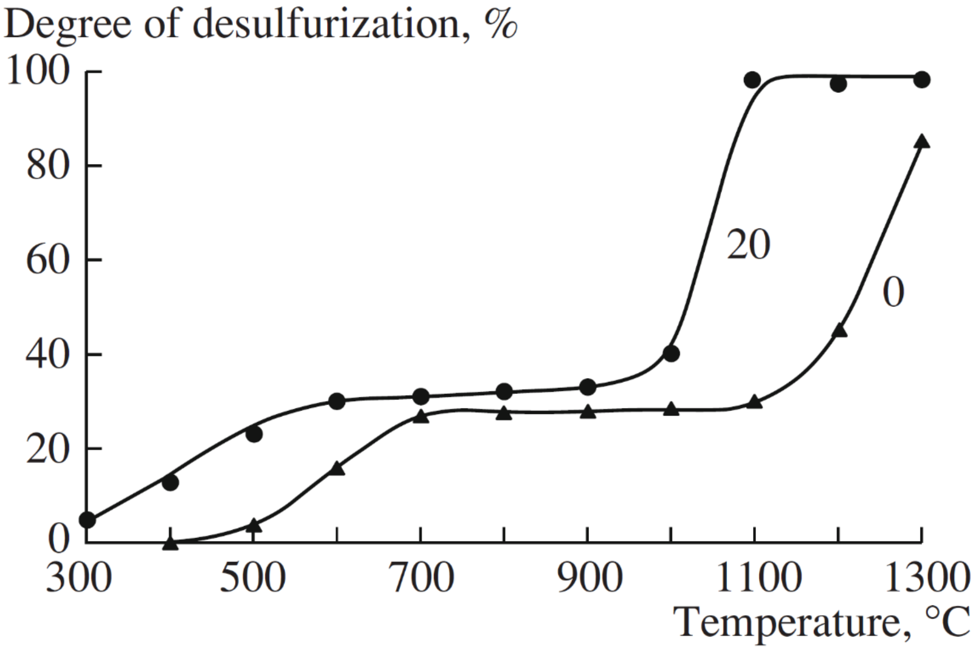

Figure 7: Kinetic curve of the desulphurization of fluxed Sokolovsk-sarbaisk pellets during a holding time of 20 min and 0 min as shown on the graph [24, p. 1004]

$$CaSO_4 + Fe_2O_3 \rightleftarrows CaO.Fe_2O_3 + SO_2 + 0.5\ O_2 \qquad (45)$$
$$CaSO_4 + SiO_2 \rightleftarrows CaO.SiO_2 + SO_2 + 0.5\ O_2 \qquad (46)$$

It is shown that if the roasted sample contains more $CaO/CaCO_3$ initially, sulphur is maintained at a higher rate during the roasting process (Figure 8) [24]. The addition of a certain stoichiometric amount of carbonates to a sulphide containing material, *i.e.* the ratio between these two materials, can be used to optimize SO_2 retention.

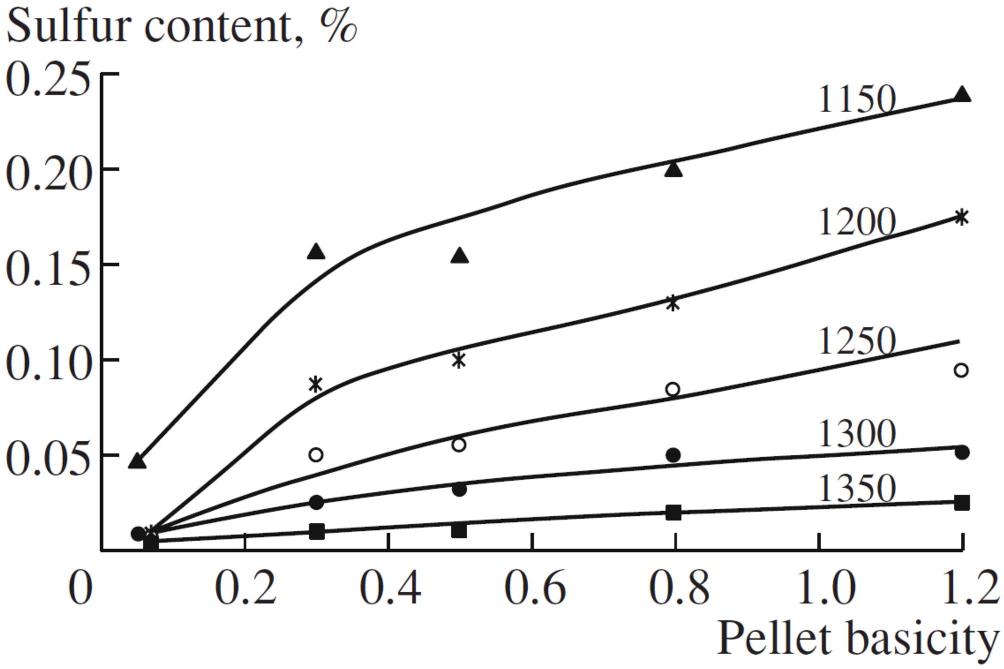

Figure 8: Sulfur content in Kostomuksha pellets relative to the roasting temperature and basicity, *i.e.* initial limestone quantity in sample pellet; the roasting temperature (° C) is given on the curves [24, p. 1004]

Riveros *et al.* [25] studied the roasting of mineral copper concentrates with addition of lime at 500 °C. As mentioned before, limestone reacts with SO_2 above 460 °C [24]. The sulphating reaction, which is assumed to occur in these conditions, is given in Equation 4746. Sulphur retention was found to be 90.5 wt% with addition of 100 wt% excess dry limestone.

$$CuFeS_2 + CaCO_3 + 4.25\ O_2(g) \rightleftarrows CuSO_4 + 0.5\ Fe_2O_3 + CaSO_4 + CO_2(g) \qquad (47)$$

XRD analysis of the roasted product showed Fe_2O_3, $CaSO_4$, $CuSO_4$, $CaCO_3$, $CuO.CuSO_4$ and CuO phases to be present. Therefore, it can be concluded that copper concentrate pellets combined with limestone can be roasted together to reduce SO_2 emission to a minimum, which is convenient for further copper leaching [25].

2.7 Microwave-assisted roasting

Microwave heating, is based on electromagnetic energy at high frequency waves of which 915 MHz and 2.45 GHz are often used for heating. They are associated with electric and magnetic fields that are responsible for interactions with matter and heating, respectively. Materials that absorb microwave radiation are called dielectrics and contain dipoles. Upon absorbing microwaves, the electric field polarizes the material. However, the polarization can’t follow the rapid change of the electric field. This introduces orientation (dipole) polarization (Figure 9), which is one of the most important mechanism of several dielectric polarization types. When applying microwave irradiation to the material, the electric and magnetic components are alternating and the molecules cannot respond quickly to the change in direction, therefore align and flip around. Subsequently, stored energy is lost giving rise to friction causing them to heat up [26], [27], [28].

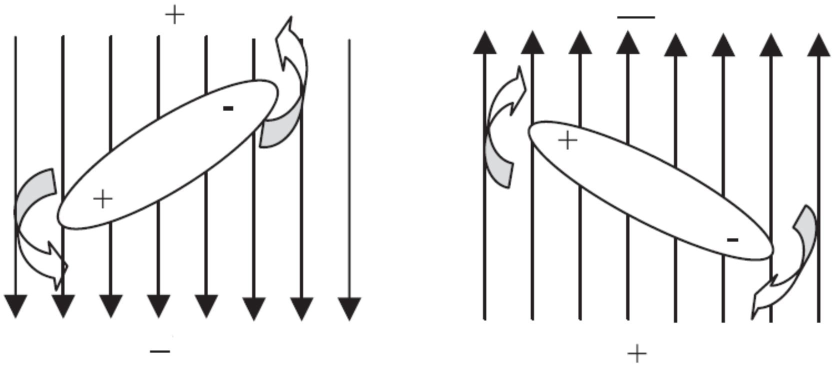

Figure 9: Dipole realignment in an electromagnetic field [26, p. 191]

A second mechanism of heating under microwave radiation is ionic conduction, where ions in a solution move due to their charge. As a result of these movements, they collide and transform kinetic energy to thermal energy. The higher the ion concentration, the more thermal energy is produced. This is explained by the fact that with higher ion concentrations the chance of collision becomes higher, thus faster heating of the solution occurs [26].

Three main material classes can be differentiated (Figure 10), with respect to how materials interact with a microwave field:

1) absorbers dissipate the electromagnetic energy as heat, depending on the dielectric loss factor;
2) conductors/reflectors have high dielectric loss factors and little to no penetration depth *e.g.* metals;
3) transparent materials have low dielectric loss factors which result in large penetration depth as microwaves pass through without any losses thus little energy is absorbed.

Materials that consist of a combination of different phases can react differently to microwaves resulting in selective heating of the high dielectric loss phase and passing the low loss phase [26], [29].

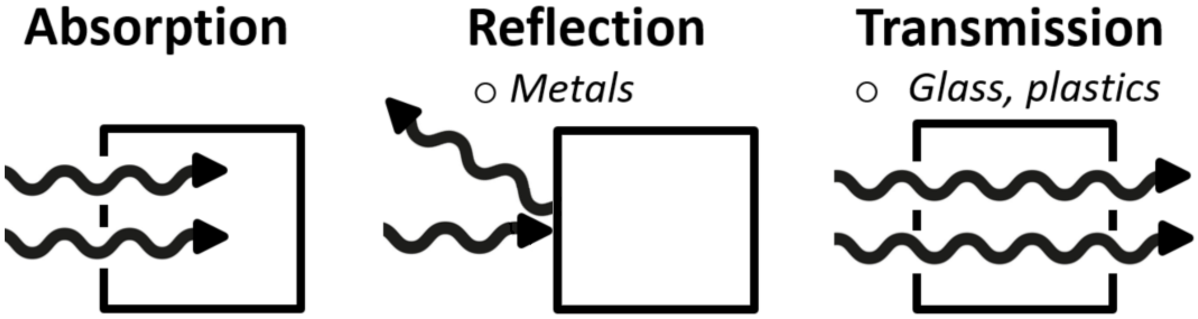

Figure 10: Interactions to a microwave field

The dielectric response of materials to microwaves can be described using the dielectric constant (ε') and dielectric loss constant (ε"). The dielectric constant (ε') relates to the ability of a material to absorb microwave energy. Thus, molecules with high dipolar moment have a high dielectric constant. The dielectric loss factor (ε") relates to the ability of a material to convert the absorbed energy into heat. The two quantities are commonly expressed as the complex dielectric constant (ε^*) shown in Equation 4847 [26].

$$\varepsilon^* = \varepsilon' - i\varepsilon'' \qquad (48)$$

The fraction of the dielectric loss factor and dielectric constant (Equation 49) indicates how a material can absorb microwave energy and convert it into heat. This relation is also known as the loss tangent (tan δ) at a given frequency and temperature [26].

$$\tan\delta = \frac{\varepsilon''}{\varepsilon'} \qquad (49)$$

The power density P (*i.e.* the volumetric absorption of microwave energy W/m^3) in a material due to exposure to microwave energy is shown in Equation 5049, where ε_0 is the permittivity of free space, ε''_{eff} the effective loss factor, E the electric field strength inside the material (V/m), μ_0 the permeability of free space, μ''_{eff} the effective magnetic loss factor and H the magnetic field strength (A/m). The second term is only added if the material shows magnetic losses, thus if the effect of the magnetic field must be considered [26].

$$P = 2\pi f \varepsilon_0 \varepsilon''_{eff} E^2 + 2\pi f \mu_0 \mu''_{eff} H^2 \qquad (50)$$

The microwave heating expression is given in Equation 5150, where ΔT is the average temperature related to the heated ore bulk (sample), P is the microwave power, t is the time of microwave heating, V is the volume, C_p the heat capacity and ρ the density [29].

$$\Delta T = \frac{P.t}{V.C_p.\rho} \qquad (51)$$

The penetration depth (D_p) is presented in Equation 5251, where f is frequency (Hz) and c the speed of light (m/s). It shows that the depth is inversely proportional to the frequency. However, the greatest heating is achieved with higher frequencies thus only heating the exterior of the material [26], [29].

$$D_p = \frac{c}{2\pi f \sqrt{2\varepsilon'}\left[\sqrt{1+\tan^2\delta}-1\right]^{0.5}} \tag{52}$$

Important parameters for heating materials (*i.e.* roasting) are mineralogy, microwave time, microwave power and particle size. Examples of these parameters are described in the following sections.

2.7.1 Mineralogy and temperature

Microwave irradiation penetrates the object and, if the material can absorb the microwaves, this essentially heats it from the inside out through conduction. This in contrast with conventional heating, which results in a thin layer of the material being heated from the outside. Heating of the rest of the material depends on the heat transfer properties of the material itself [26], [28]. This introduces the common problem with measuring the exact temperature of the samples in a microwave experiment. Thermocouples are used but only give the temperature of the chamber and not the exact temperature within the sample. Kingman *et al.* [27], used a sheathed metal thermocouple directly in contact with the sample and found maximum temperatures achieved during irradiation at 1000 W, 2.45 GHz as listed in Table 4.

Table 4: Heating results of different products at 1000 W, 2.45 GHz microwave irradiation [27, p. 1082]

Mineral	Chemical composition	Max temperature achieved (°C)	Time (min)
Chalcopyrite	$CuFeS_2$	920	1
Galena	PbS	956	7
Magnetite	Fe_3O_4	1258	2.75
Orthoclase	$KAlSiO_3O_8$	67	6
Pyrite	FeS_2	1019	6.75
Quartz	SiO_2	79	7
Sphalerite	ZnS	88	7

Materials can be classified as hyperactive, active or inactive materials based on their heating rate in the microwave. Minerals might have a high heating rate, which puts them in the hyperactive class, but the maximum temperature they reach is independent and could be relatively low. Internally gathered results (at VITO) of some minerals are presented in Table 5. This shows that some materials can't heat up in a microwave. On the other hand, this inactivity of materials could be interesting for selective heating. However, it could be seen as a disadvantage if reactions between an active an inactive material are desired. A partial solution could be to place a SiC-plate above the samples. This plate itself does heat up with microwave irradiation, after which it can release heat to the sample chamber by convection and thermal radiation.

Table 5: Mineralogy effect on microwave heating

Material classification	**Heating rate (°C/min)**	**Maximum Temperature (°C)**
Hyperactive materials		
Fe_3O_4	1200	500-1000
FeS_2	1200	500
Active materials		
CuO	200	800
Fe_2O_3	170	1000
FeS	135	800
Inactive materials		
CaO	5	200
$CaCO_3$	5	130
SiO_2	2-5	70

2.7.2 Influence of power, sample mass, time and ratio

The absorbed microwave power (*i.e.* power density) depends largely on microwave input power, sample mass and time as seen in Figure 11 for a typical nickeliferous silicate laterite oxide ore [28]. The effect of input power is explained by the fact that, as the electric field increases when the input power is higher, the power density increases (Equation 50). The influence of sample mass is explained by both microwave absorption and heat loss. Due to volumetric heating of microwaves an increase in sample mass causes an increase in absorbed microwave power. The heat loss is reduced because: a) the surface area to volume ratio is lower for higher sample masses; and b) the distance for heat conduction increases. The microwave absorbed power increases rapidly at a certain process time due to the internal temperature of the sample being equal to the critical temperature. Because the sample reaches its critical temperature, the permittivity also rises rapidly [28].

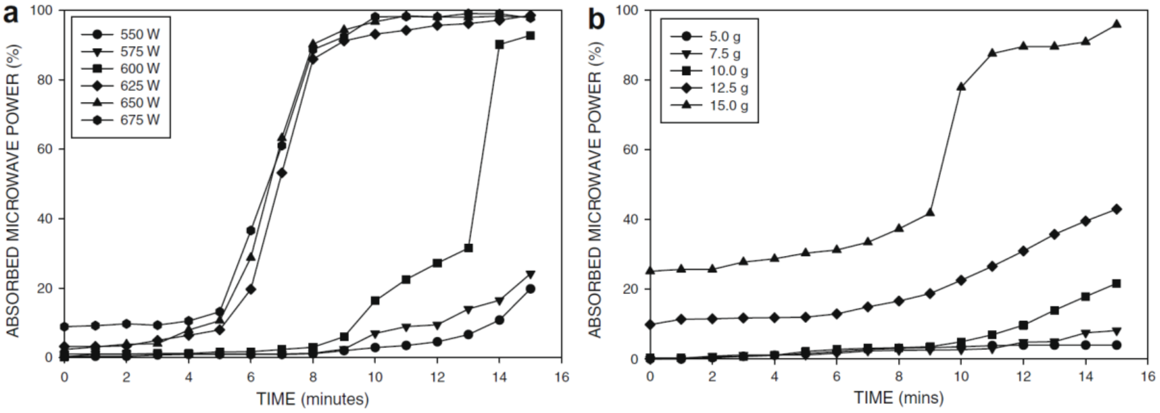

Figure 11: The influence of microwave power (a) and sample mass (b) on the absorbed microwave power [28, p. 1107]

An increase in heating rate of chalcopyrite-calcite particles with increasing microwave power for a constant ratio of chalcopyrite-calcite was found by Hua *et al.* [10]. However, if the content of $CaCO_3$ in the pellets increased, the heating rate dropped. This is in agreement with the chalcopyrite being an active material and $CaCO_3$ an inactive material. The effect of microwave power was again tested but on the leachability of copper which showed that from a certain point increase in power lead to a decrease in copper leachability. In this particular case it was 575W that showed a maximum of copper leaching, with the other variables being: i) a particle size of 3 mm diameter; ii) a sample mass of 30 g; iii) a chalcopyrite-calcite ratio of 1:2 and; iv) an exposure time of 10 min. It is to no surprise that all of the previous parameters affect the roasting and leachability. For sample mass with the other variables kept as mentioned above, an optimal mass of 33 g was found when varying between 20 to 40 g. Finally the exposure time was evaluated for different microwave powers on the leachability of copper for a sample mass of 33 g and the other parameter kept the same as mentioned before. Copper leachability showed a decrease at 7 min for 750 W, 10 min for 575 W and 20 min for 452 W, all corresponding to an obtained ore temperature of 400 °C at that time. This could be attributed to the sample being sintered, because the microwave exposure time was too long. Due to the long exposure time, the sample temperature was too high resulting in sintering of the sample. Thus, copper extraction initially increases due to rise of the temperature but decreases after 400 °C due to the sample being sintered. This introduces a reduction in the porosity of reaction products meaning the leaching reaction slows down. It should be noted that temperature measurements are an indication and real temperature of the samples may well exceed 400 °C.

2.7.3 Influence of particle size

A simulation of pyrite-calcite ore was performed to predict several influences such as power density on the temperature as well as the influence of particle size [30]. The maximum temperature reached in pyrite-calcite ore, for microwave exposure of 1 and 10 ms, with increasing power density for different particle sizes is recorded by Jones *et al.* [30] (Figure 12). Firstly, it should be noted that there is an increase in temperature with increasing particle size. Secondly, when the particle size decreases there is a proportionally lower increase of temperature with increasing power density (slope is lower). The conclusion was that if the particle size was low, more energy was needed to sufficiently raise the temperature because heat losses also increased. A final conclusion would be the selective heating of pyrite phase in the pyrite-calcite ore, as seen from Table 5 which shows pyrite to be a hyperactive material and calcite to be an inactive material. Therefore, longer exposure would lead to higher temperatures due to the pyrite heating up.

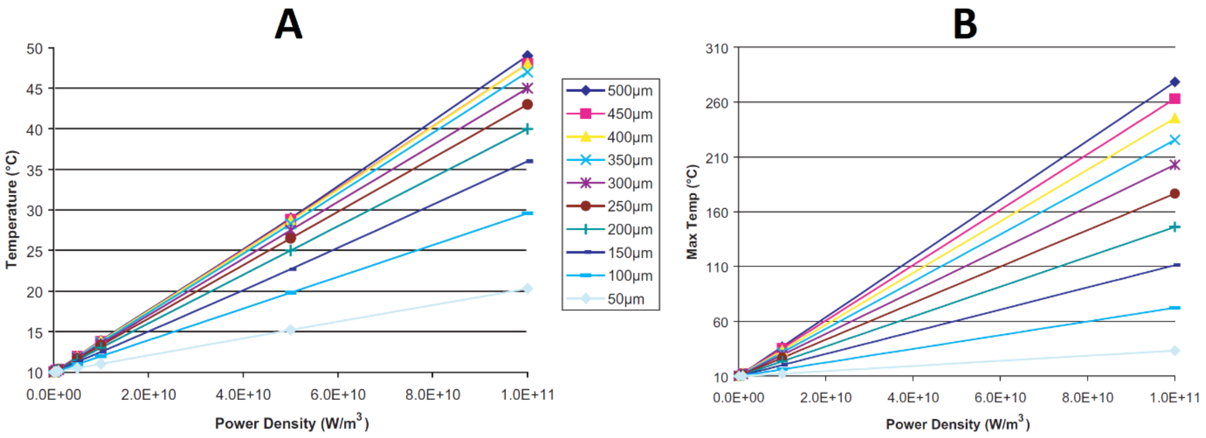

Figure 12: The influence of particle size for various power densities on the temperature for an exposure of 1 ms (A) or an exposure of 10 ms (B) [30, p. 666]

2.7.4 Phase changes of $CuFeS_2$-$CaCO_3$ roasting

A chalcopyrite-calcite pellet was roasted in a microwave (750W, 2.45GHz) and in a conventional furnace at 600 °C and 800 °C by Hua *et al.* [10]. The phases present in the obtained materials are shown in Table 6. It is found that iron was transformed to Fe_2O_3 during all treatments, while copper is transformed to $CuSO_4$ and CuO at respectively low and higher temperatures during conventional roasting. Both copper phases exist in the microwave treated samples because of the selective heating that occurs. This means that, although the bulk temperature was about 400 °C, the temperature within the sample is not homogeneous. Therefore, local increase in temperature cause the decomposition of $CuSO_4$ to CuO during microwave roasting. However, sulphur retention showed to be more than 96% by absorption in standard iodine solution for both microwave and conventional roasting [10].

Table 6: Phases present in chalcopyrite-calcite microwave and conventional (600 °C and 800 °C) roasted product [10]

$CuFeS_2$-$CaCO_3$ pellet				
Oxidized products for $CuFeS_2$	Oxidized products for $CaCO_3$	Microwave	Conventional 600 °C	Conventional 800 °C
$CuSO_4$		$CuSO_4$	$CuSO_4$	
CuO		CuO		CuO
Fe_2O_3		Fe_2O_3	Fe_2O_3	Fe_2O_3
	$CaSO_4$	$CaSO_4$	$CaSO_4$	$CaSO_4$
	$CaCO_3$ (excess)	$CaCO_3$	$CaCO_3$	$CaCO_3$
$CuO.CuSO_4$				
Cu_2O				
$Fe_2(SO_4)_3$				
Fe_3O_4				

2.8 Chemical Leaching

2.8.1 Acid leaching

Sulphide copper concentrates that consisted of 7.70% Cu, 28.80% Pb, 20.52% Fe and 23.72% S, were roasted together with CaO in a 2:1 ratio, at 820 °C by Liao *et al.* [31]. The raw material contains FeS_2, $CuFeS_2$ and PbS. After roasting, most of the sulphur was fixated by CaO as $CaSO_4$ and $PbSO_4$. The roasted product also consisted of CuO and Fe_3O_4 due to decomposition of $CuFeS_2$. The residu from H_2SO_4 leaching contained $CaSO_4$, $PbSO_4$ and Fe_2O_3. Measurement with ICP-OES concluded that sulphur retention was 99.77%, which is possible because the reaction between CaO and SO_2 to $CaSO_4$ can easily take place above 460 °C. Leaching with H_2SO_4 showed that, in order to reach maximum Cu extraction, the temperature should be 90 °C, stirring speed 500 r/min, S:L ratio 1:6 and the concentration 1.20 mol/L. Reaction 53 to 55 describe the leaching process [31].

$$\mathrm{CuO} + \mathrm{H_2SO_4} \rightarrow \mathrm{CuSO_4} + \mathrm{H_2O} \tag{53}$$

$$\mathrm{Fe_3O_4} + \mathrm{H_2SO_4} \rightarrow \mathrm{FeSO_4} + \mathrm{Fe_2O_3} + \mathrm{H_2O} \tag{54}$$

$$\mathrm{PbO} + \mathrm{H_2SO_4} \rightarrow \mathrm{PbSO_4} + \mathrm{H_2O} \tag{55}$$

Roasted copper converter slag that consisted of 52% Fe, 2.60% Cu and 4.90% S with $Fe_2(SO_4)_3.H_2O$ as sulphating agent was studied by Altundogan *et al.* [32]. X-ray analysis detected the following phases to be present: Fe_2SiO_4, Fe_2O_3 and CuS. The highest copper recovery was found when roasting at around 500 °C - 550 °C. Above these temperatures sulphates would decompose. The copper extraction was 95% when the ratio of $Fe_2(SO_4)_3.H_2O$:slag was 2.5. Leaching with H_2SO_4 showed a recovery up to 98.21% at 75 °C for 4h in a 1:2 acid, slag ratio [32].

In general it can be concluded that leaching with H_2SO_4 works fine for copper recovery, but is not very selective. This results in high acid consumption as the dissolution of gangue materials with copper extraction can't be avoided. Especially, when copper oxides are leached and contain alkaline gangues. Carbonates present in these gangues are the major problem, as they are acid soluble and result in high acid consumption [33], [34]. Therefore, a selective leaching reagent is often preferred for copper extraction from a more complex material [35].

2.8.2 Alkaline leaching

Ammonia is a selective reagent for copper extraction. The ammonia-water system is, however, not buffered and ammonia vaporizes easily. This results in pH fluctuations, which is suboptimal for ore leaching. To resolve these problems, a salt such as $(NH_4)_2CO_3$ must be added [35]. Carbonate phases in a solid material do not react with ammonia in solution, while copper mineral phases do interact. Therefore, selective leaching of copper is possible with ammonia leaching and little gangue materials is leached with it [33]. The main advantages of alkaline leaching over acid leaching are the fact that alkaline leaching is less corrosive, more selective and that carbonate gangues consume less of the leaching agent [34]. Equations 56 and 57 show an example of chrysocolla ($CuSiO_3{\cdot}2H_2O$) and malachite ($CuCO_3{\cdot}Cu(OH)_2$) leaching with $NH_3.H_2O/(NH_4)_2CO_3$ [33]. Equation 58 shows the leaching of malachite with $NH_3OH/(NH_4)_2CO_3$ with formation of a stable copper(II) tetraammine complex [34].

$$\mathrm{CuSiO_3.2H_2O + 2\,NH_3.H_2O + (NH_4)_2CO_3 \rightarrow Cu(NH_3)_4CO_3 + H_2SiO_3 + 4\,H_2O} \tag{56}$$
$$\mathrm{CuCO_3.Cu(OH_2) + 6\,NH_3.H_2O + (NH_4)_2CO_3 \rightarrow 2\,Cu(NH_3)_4CO_3 + 8\,H_2O} \tag{57}$$
$$\mathrm{Cu_2(OH)_2CO_3 + 6\,NH_4OH + (NH_4)_2CO_3 \rightarrow 2\,Cu(NH_3)_4CO_3 + 8\,H_2O} \tag{58}$$

The leaching of copper from the Baifang copper mine tailing was studied by Zhoa *et al.* [36]. They used ammonia/ammonium chloride as leaching solution. Their findings were that the optimal S:L ratio of 1:4, a leaching time of 4 h at 40 °C and the use of 3 mol/L NH_4^+ resulted in a Cu extraction yield of 75%. The study was also mentioned in Radmehr *et al.* [37], who listed studies on ammonium leaching in the copper industry, which can be seen in Table 7. Ammonia leaching on copper is a neutralization method, meaning that the metals are dissolved without any oxidizing or reducing agents. In Table 7 can be seen that ammonia/ammonium carbonate leaching yields the highest copper recovery. Therefore, this leaching agent was used in this study as well. On top of that, Hue *et al.* [10] studied the microwave-enhanced roasting of copper sulphide in the presence of $CaCO_3$ and used $NH_3/(NH_4)_2CO_3$ for leaching.

Table 7: Copper leaching studies performed in the past decade with ammonium/ammonium carbonates lixivent [37, p. 2515]

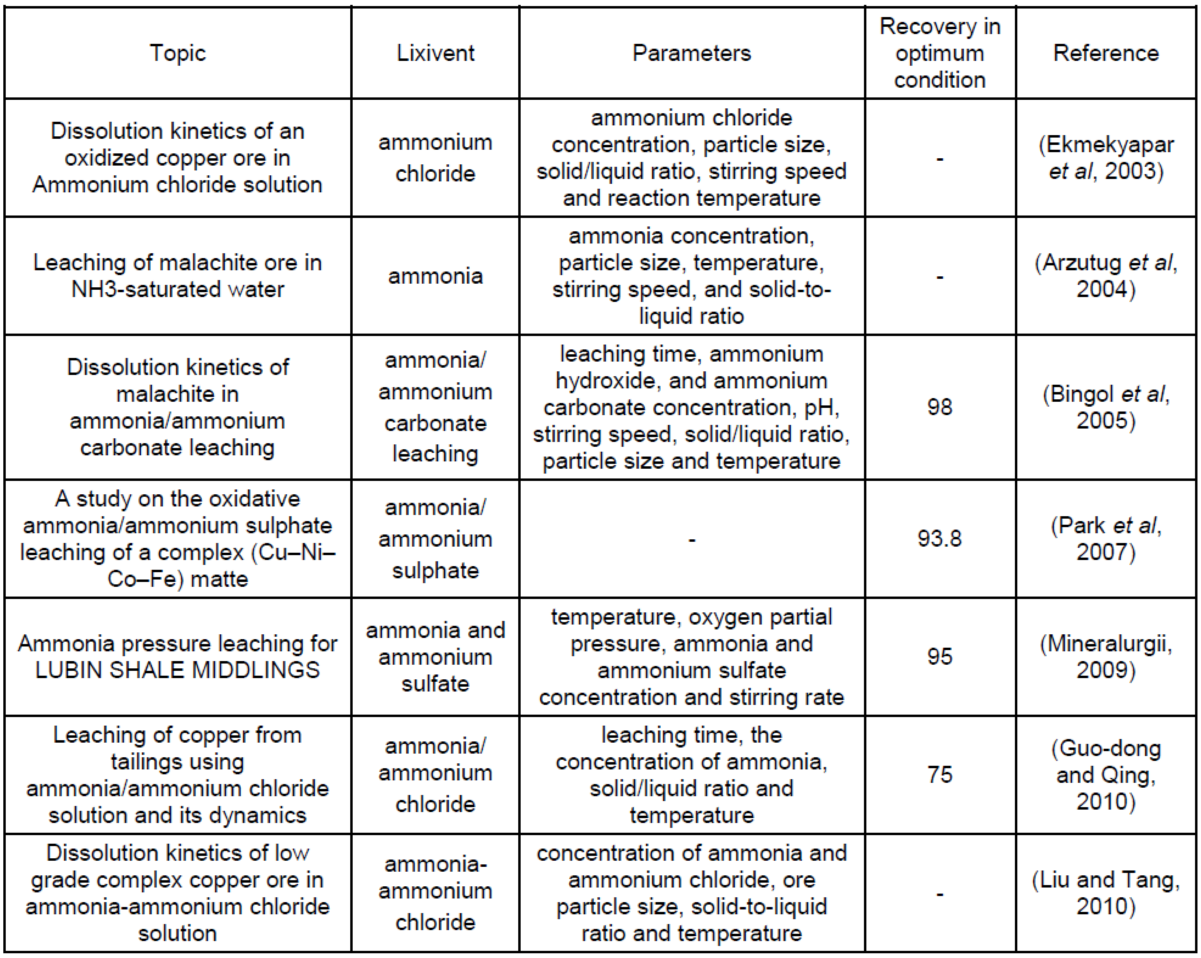

Topic	Lixivent	Parameters	Recovery in optimum condition	Reference
Dissolution kinetics of an oxidized copper ore in Ammonium chloride solution	ammonium chloride	ammonium chloride concentration, particle size, solid/liquid ratio, stirring speed and reaction temperature	-	(Ekmekyapar *et al*, 2003)
Leaching of malachite ore in NH3-saturated water	ammonia	ammonia concentration, particle size, temperature, stirring speed, and solid-to-liquid ratio	-	(Arzutug *et al*, 2004)
Dissolution kinetics of malachite in ammonia/ammonium carbonate leaching	ammonia/ ammonium carbonate leaching	leaching time, ammonium hydroxide, and ammonium carbonate concentration, pH, stirring speed, solid/liquid ratio, particle size and temperature	98	(Bingol *et al*, 2005)
A study on the oxidative ammonia/ammonium sulphate leaching of a complex (Cu–Ni–Co–Fe) matte	ammonia/ ammonium sulphate	-	93.8	(Park *et al*, 2007)
Ammonia pressure leaching for LUBIN SHALE MIDDLINGS	ammonia and ammonium sulfate	temperature, oxygen partial pressure, ammonia and ammonium sulfate concentration and stirring rate	95	(Mineralurgii, 2009)
Leaching of copper from tailings using ammonia/ammonium chloride solution and its dynamics	ammonia/ ammonium chloride	leaching time, the concentration of ammonia, solid/liquid ratio and temperature	75	(Guo-dong and Qing, 2010)
Dissolution kinetics of low grade complex copper ore in ammonia-ammonium chloride solution	ammonia-ammonium chloride	concentration of ammonia and ammonium chloride, ore particle size, solid-to-liquid ratio and temperature	-	(Liu and Tang, 2010)

3 Materials and methods

3.1 Materials

The selected sulphidic tailing and marl (waste rock) originate from the Cobre Las Cruces mine, located in Spain. The sulphidic tailing was dried at 40 °C, while the marl was dried at 105 °C. After drying, both materials were stored in closed containers. Initially, the marl had a coarse particle size in comparison with the sulphidic tailing. Therefore, the marl was ground in a Disc Mill (*Retsch® Disc Mill DM 200* - Figure 13), and sieved over a 1 mm sieve. Further crushing for solid sample preparation of the tailing and the marl, or a mixture of both was done using pestle and mortal. The use of chemical agents was limited and only required during leaching experiments and ICP-OES sample preparation (Table 8).

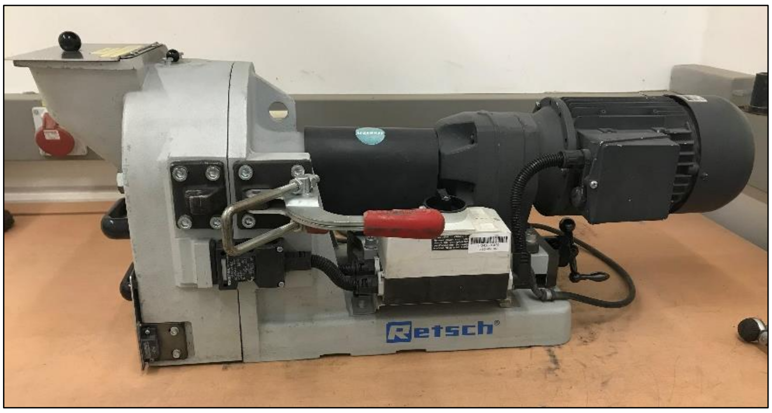

Figure 13: *Retsch® Disc Mill DM 200*, used for grinding the marl

Table 8: List of used chemical agents

Chemical name	**Chemical Formula**	**Purity**	**Brand**
Ammonium carbonate	$(NH_4)_2CO_3$	ACS, ≥30% NH_3	Sigma-Aldrich
Nitric Acid 65%	HNO_3	Suprapur	Merck
Ammonia solution 25%	NH_3	Analysis	Emsure

3.2 Experiments

3.2.1 Roasting

3.2.1.1 Experimental design conventional roasting

The roasting experiments with a conventional furnace (*Nabertherm LH 60/14*) were performed in five batches. The batches differed in the roasting temperature to which they were exposed, which was either: 400 °C, 500 °C, 600 °C, 700 °C or 800 °C. Each batch contained 14 samples of which 2 replicates from 7 different weight ratios of the sulphidic tailing and the marl (Table 9). Samples were prepared by separately weighing the tailing and the marl, after which they were added together and mixed to a fine powder with pestle and mortar. The actual sample mass in the crucibles was 10 g for mixed samples and 5 g for reference samples, *i.e.* pure tailing and marl (tolerance of ±5 mg). The total sample weight prepared was 11 g and 5.5 g for mixed and reference samples, respectively, due to possible losses during mixing and transport to the crucibles. In total 70 samples were obtained. Figure 14 shows the sample setup for roasting in a conventional furnace.

Table 9: Theoretical sample ratios, prepared for one batch of conventional roasting

Sample	wt% Tailing	wt% Marl	Tailing (g)	Marl (g)
1	100%	0%	5.5	0
2				
3	80%	20%	8.8	2.2
4				
5	60%	40%	6.6	4.4
6				
7	50%	50%	5.5	5.5
8				
9	35%	65%	3.85	7.15
10				
11	20%	80%	2.2	8.8
12				
13	0%	100%	0	5.5
14				

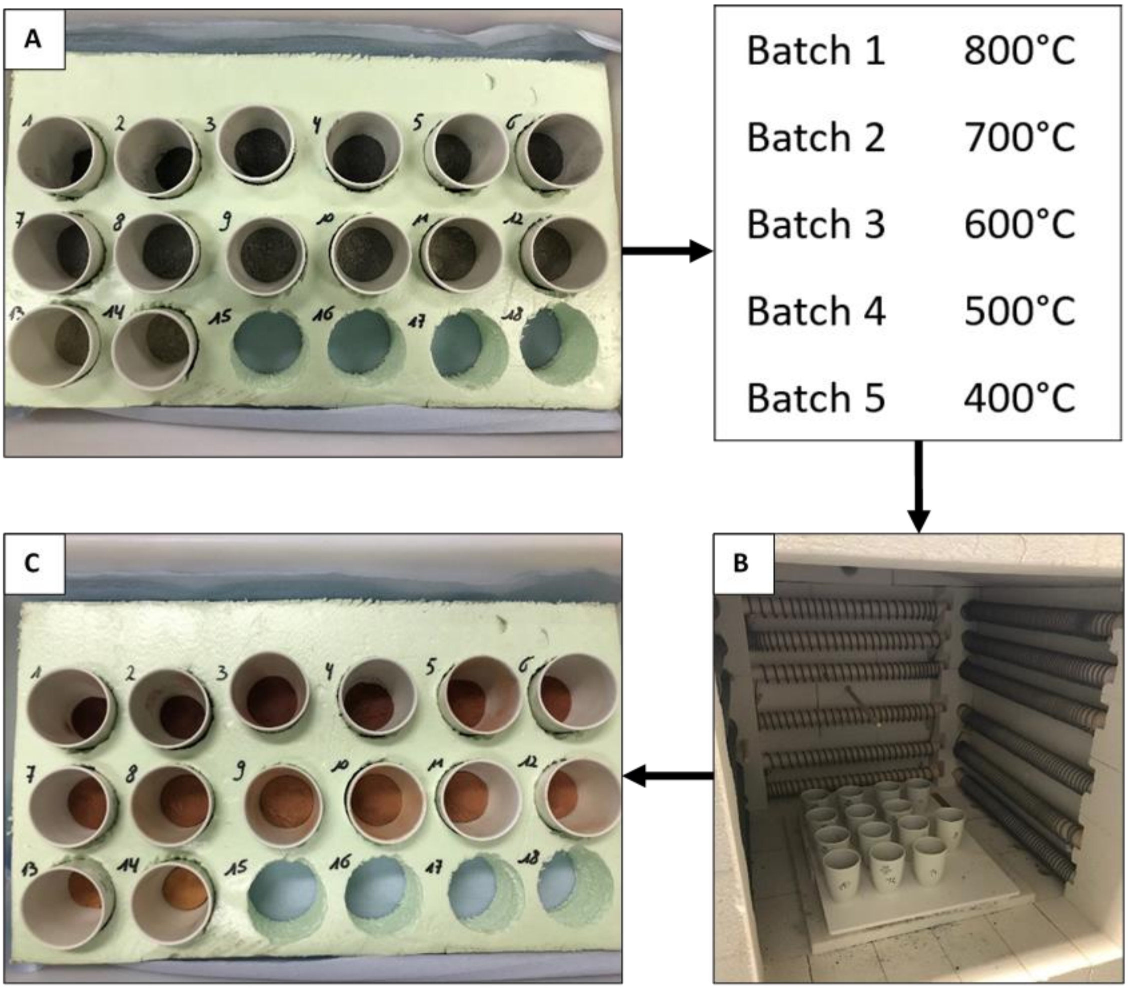

Figure 14: Conventional roasting setup with corresponding temperatures for each batch, A) unroasted samples; B) oven setup; C) roasted samples (*e.g.* Batch 1 - 800 °C)

3.2.1.2 Temperature profile during conventional roasting

The theoretical temperature profile for the conventional furnace is given in Figure 15. Heating was started immediately, therefore the wait time was set to 0 min. The ramp up (Time 1) to the desired temperature (T1) was set at 100 °C/h, after which a dwell time (Time 2) of 1 hour was maintained. Cool down to room temperature was also set at a rate of 100 °C/h (Time 3). However, the actual cooling rate was significantly slower than this set cooling rate, especially at lower temperatures. Due to the extensive cool down time, the furnace was slightly opened when the temperature reached 150 °C and completely opened below 100 °C to speed up the cooling step. Samples were removed when the temperature reached about 40 °C, after which they were kept at room temperature to further cool down. After the samples reached room temperature, they were weighed and transferred to closed containers.

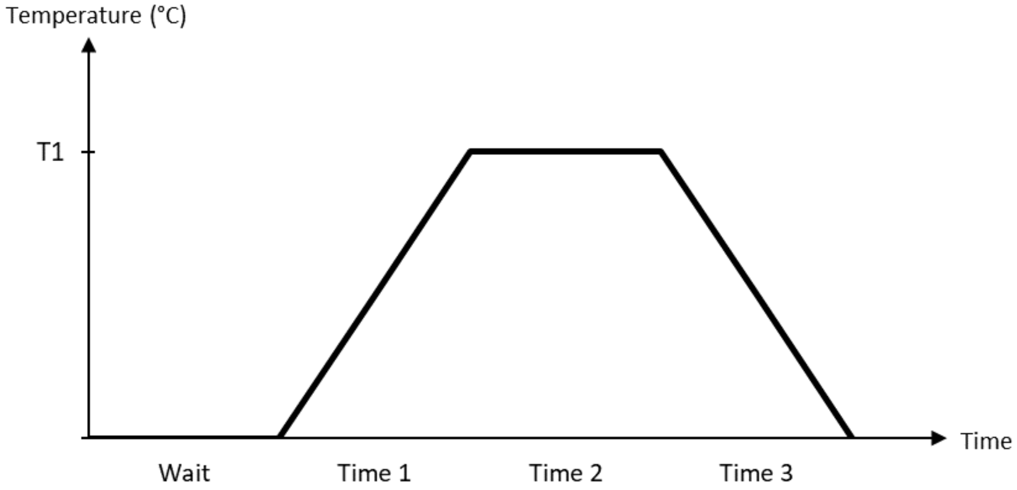

Figure 15: Theoretical temperature profile of the conventional roasting

3.2.1.3 Experimental design microwave-assisted roasting

The roasting experiments with the microwave furnace (*Milestone PYRO advanced microwave furnace*) were performed in five batches. The microwave was equipped with a 1.8 kW magnetron and operating at a frequency of 2450 MHz. The first three batches differed in roasting temperature to which they were exposed, which was either 300 °C, 400 °C or 500 °C. The two other batches were conducted at 500 °C but with dwell times of 15 min or 30 min in contrary to the 1 hour dwell time which was used previously. Each batch contained 6 samples of which 2 replicates from 3 different ratios of the sulphidic tailing and the marl (Table 10). Samples were prepared by separately weighing the tailing and the marl, after which they were added together and mixed to a fine powder with pestle and mortar. The actual sample mass in crucibles was 5 g for both mixed and reference samples (tolerance of ±5 mg). The total sample weight prepared was 5.5 g due to possible losses during mixing and transport to the crucibles. In total 30 samples were obtained. Table 11 shows the settings for roasting in the microwave furnace.

Table 10: Theoretical sample ratios, prepared for one batch of microwave roasting

Sample	wt% Tailing	wt% Marl	Tailing (g)	Marl (g)
1	100%	0%	5.5	0
2				
3	0%	100%	0	5.5
4				
5	50%	50%	2.75	2.75
6				

Table 11: Microwave settings, values marked with “*” may change depending on the experiment that was conducted

Step	Time (h:min:s)	Power (W)	Temperature (°C)	Fan speed
1	00:30:00	1800	500 *	✤✤✤
2	01:00:00 *	1800	500 *	✤✤✤

Cooldown	60 min

The features of the microwave setup are shown in Figure 16. With microwave heating, phases in the samples can interact more strongly with the microwave irradiation and, therefore, the exact temperature of the samples are unknown. Hence, the microwave was equipped with a silicon carbite plate (SiC) (Figure 16). The SiC plate introduces the effect of a normal furnace by heating up itself under microwave irradiation and giving heat by convection and thermal radiation to the sample chamber. Thus, the plate was used to ensure that the temperature inside the chamber reached the set temperature. The off-gas was removed and runs through a scrubber setup (Figure 17). Ice was placed around the first unit to prevent the water to evaporate completely, as the gas leaving the microwave reaches high temperatures, during the experiment. A second scrubber unit was also in place after which the final external scrubber unit was placed which was cooled down with an external cooling unit. Finally, an external logger was coupled to the thermocouple inside the oven to measure the temperature in function of the time.

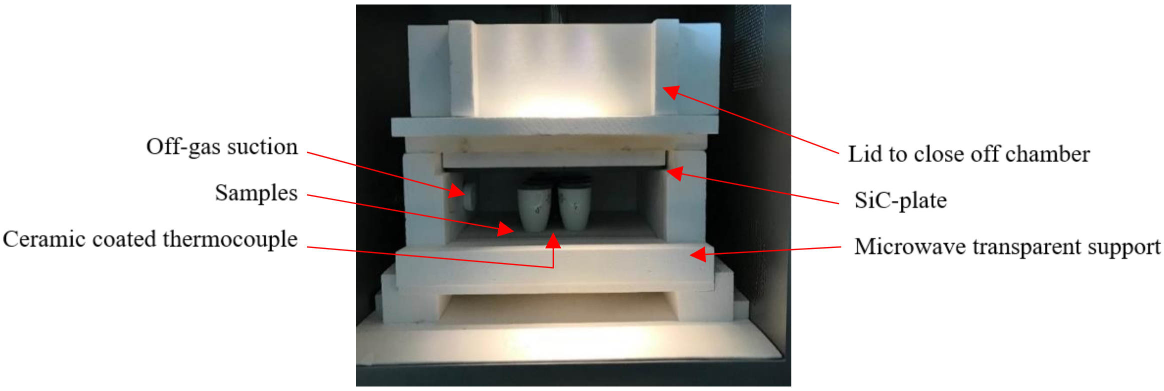

Figure 16: Internal microwave furnace setup

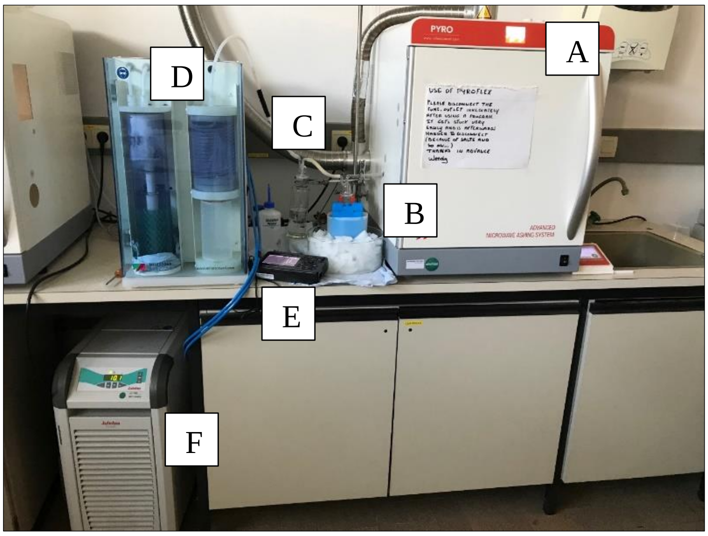

A	Milestone PYRO advanced microwave furnace
B	Off-gas suction outlet, first scrubber unit and ice bath
C	Second scrubber unit
D	Third external scrubber unit (20% NaOH)
E	Temperature logger
F	External cooling unit

Figure 17: External microwave furnace setup

3.2.1.4 Temperature profile during microwave-assisted roasting

The temperature profile was different to the one used for conventional roasting, due to faster heating and cooling. Since these roasting experiments were steered on temperature, the microwave must deliver a variable power. As shown in Figure 18, the power was maximum at the start (1800 W) and varied depending on the temperature, which was measured with the thermocouple inside. The exact settings for an experiment are shown in Table 11. Once the temperature dropped below 80 °C, at the end of the temperature profile, the door unlocked (safety) and was opened to promote faster cooling. Samples were removed when the temperature reached about 40 °C, after which they were kept at room temperature to further cool down. After the samples reached room temperature, they were weighed and transferred to closed containers.

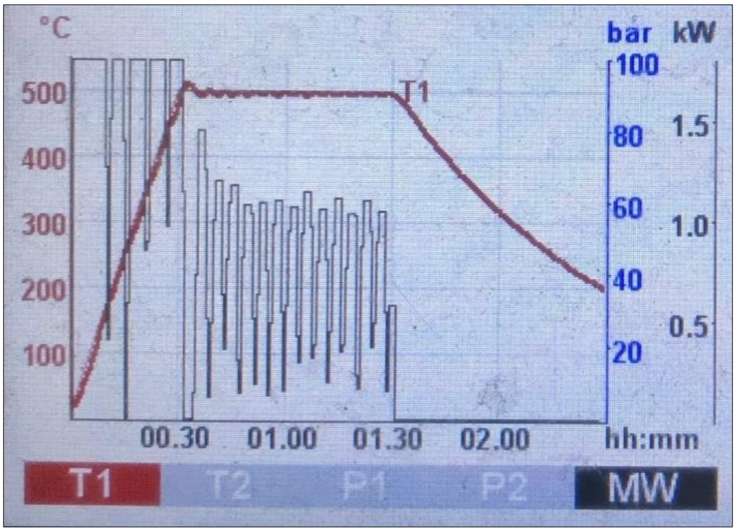

Figure 18: Temperature profile of microwave furnace (*e.g.* 500 °C - 1 hour dwell time)

3.2.2 Ammoniacal leaching

The original sulphidic tailing, the marl and all roasted samples were subjected to a leaching step, using a 1:10 solid to liquid ratio. This ratio was obtained by weighing 2 g of sample (tolerance of ±5 mg) and adding 20 mL of leaching solution (Figure 19). The leaching solution consisted of 3.5 M NH_3 and 3 M $(NH_4)_2CO_3$ and was prepared with the chemicals listed in Table 8**Error! Reference source not found.**. The original sulphidic tailing and the marl were first ground with mortar and pestle. The roasted materials could be used directly.

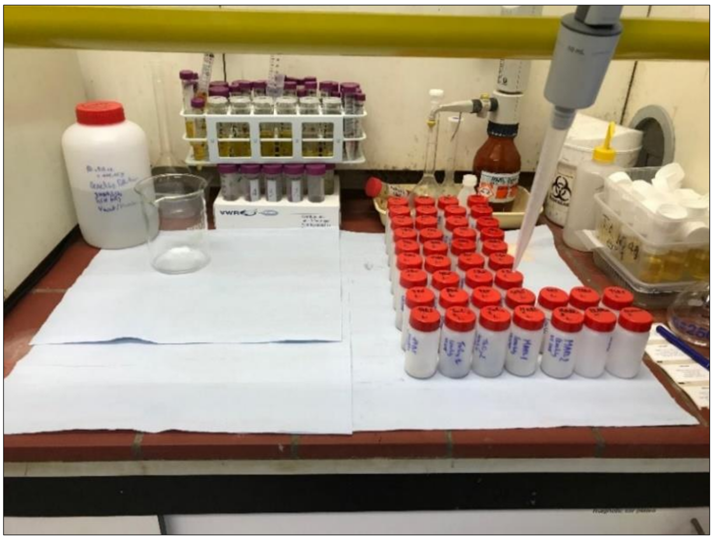

Figure 19: Setup for adding leaching solution

Subsequently, the samples were placed in a linear shaking water bath (*Grant GLS 400*) at 60 °C for 4 hours at shaking speed of 300 (Figure 20). After this treatment, they were put aside and left for a couple of minutes so the residue could settle down.

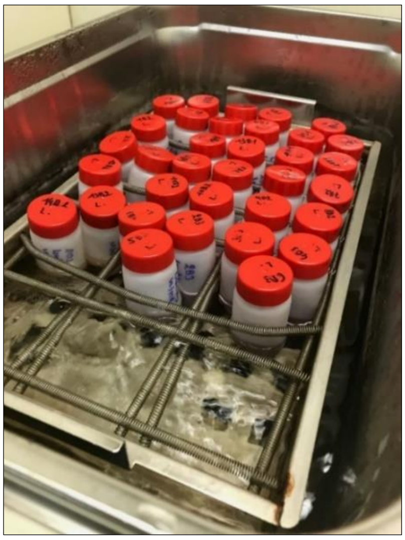

Figure 20: *Grant GLS 400*, linear shaking water bath setup

The leachate was carefully taken out using a syringe and was filtered over a disposable syringe filter (*chromafil*® *RC-45/25 – 0.45 µm*). The setup is shown in Figure 21. At least 10 up to 15 mL leachate was recovered for each sample and stored in a fridge at ±10 °C. However, due to precipitate formation after a couple of days, the subsequent obtained leachates (microwave and leaching kinetic samples) were stored in a dark place at room temperature.

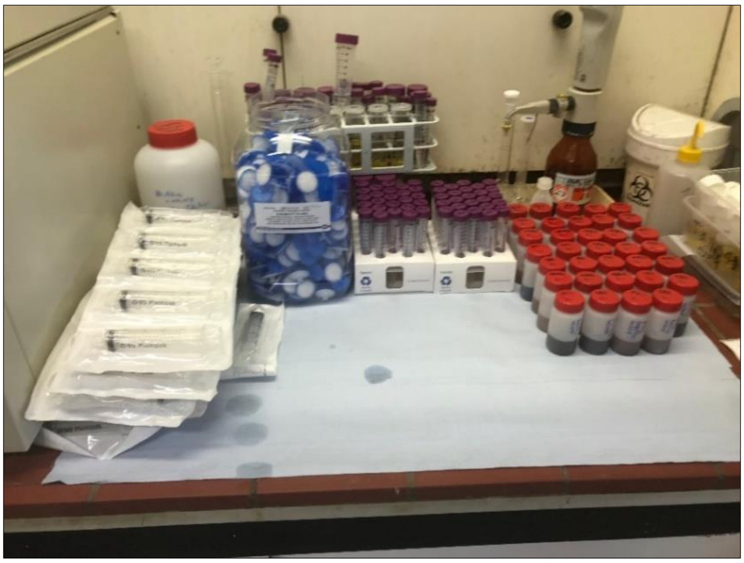

Figure 21: Setup for leachate recovery

3.2.3 Leaching kinetics

The kinetics of the leaching reaction were investigated. Similar to the conventional furnace experiment, 10 samples were prepared at a 50 wt% tailing/50 wt% marl ratio. They were roasted at 500 °C at a dwell time of 1 hour. All other parameters were identical to these described in previous sections. The leaching steps involved the same treatments as explained in previous sections, except for the residence time in the linear shaking bath. The time when two replicates were retrieved was varied between either 30 min, 1 hour, 2 hours, 3 hours or 4 hours.

3.3 Analyses

3.3.1 X-ray fluorescence (XRF)

The original sulphidic tailing, the marl and all roasted samples were measured with a handheld (*Niton XL3T GOLDD+*) XRF analyzer to determine the elemental composition (Figure 22). The samples must be a fine powder and homogeneous. Therefore, the original sulphidic tailing and the marl were ground using mortar and pestle. The roasted samples did not need this pretreatment as they received this treatment before roasting during sample preparation. Each sample was measured thrice for 2 min, and results were combined later on, *i.e.* the average and the standard deviation were determined.

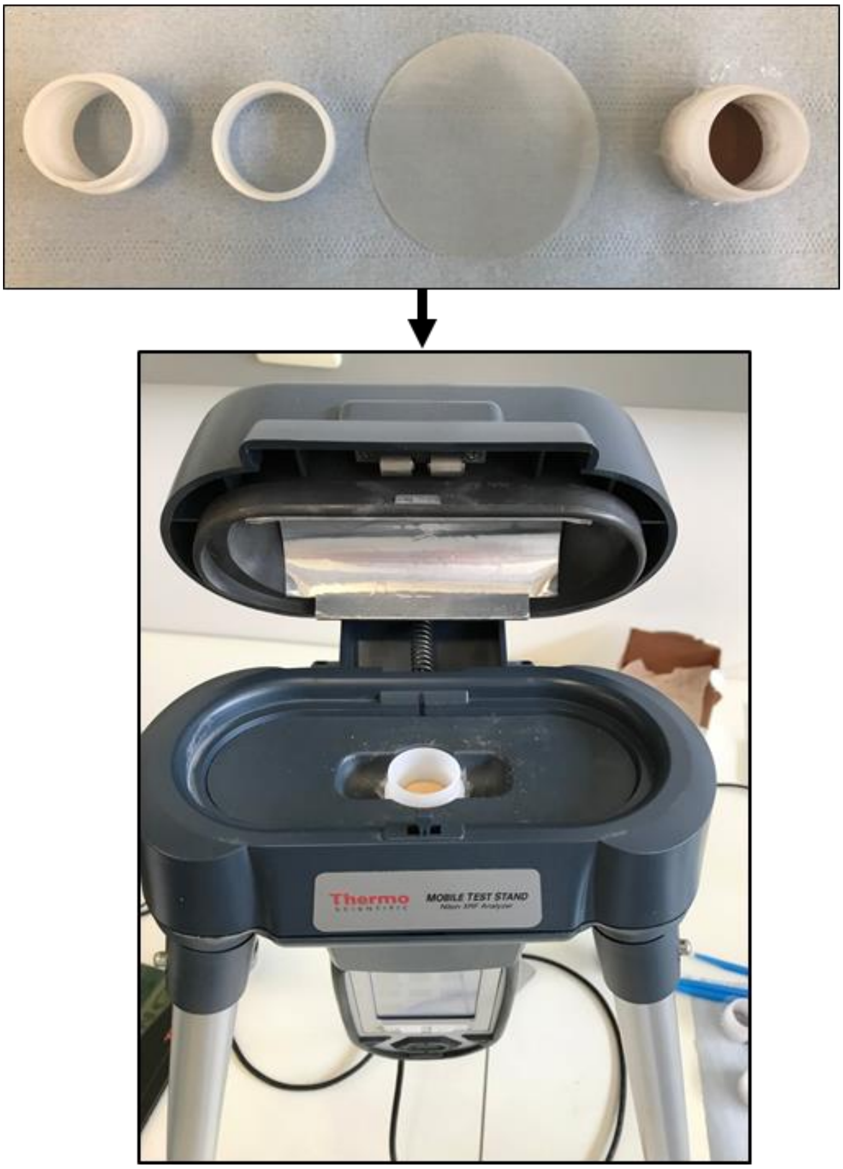

Figure 22: XRF sample preparation and handheld stand setup

3.3.2 X-ray diffraction (XRD)

3.3.2.1 Sample preparation

The original sulphidic tailing, the marl and each first replicate of the roasted samples were measured with XRD (*PANalytical Empyrean XRD Diffractometer*) to determine the crystalline phases present in the samples (Figure 23). The samples must be fine powders. Therefore, the original sulphidic tailing and marl were ground using mortar and pestle. The roasted samples were fine enough for direct measurement. The samples were prepared upside down (normal procedure) to prevent introducing stress, which is a measure of strain in the samples. After use, the sample holders were cleaned with ethanol to prevent contamination.

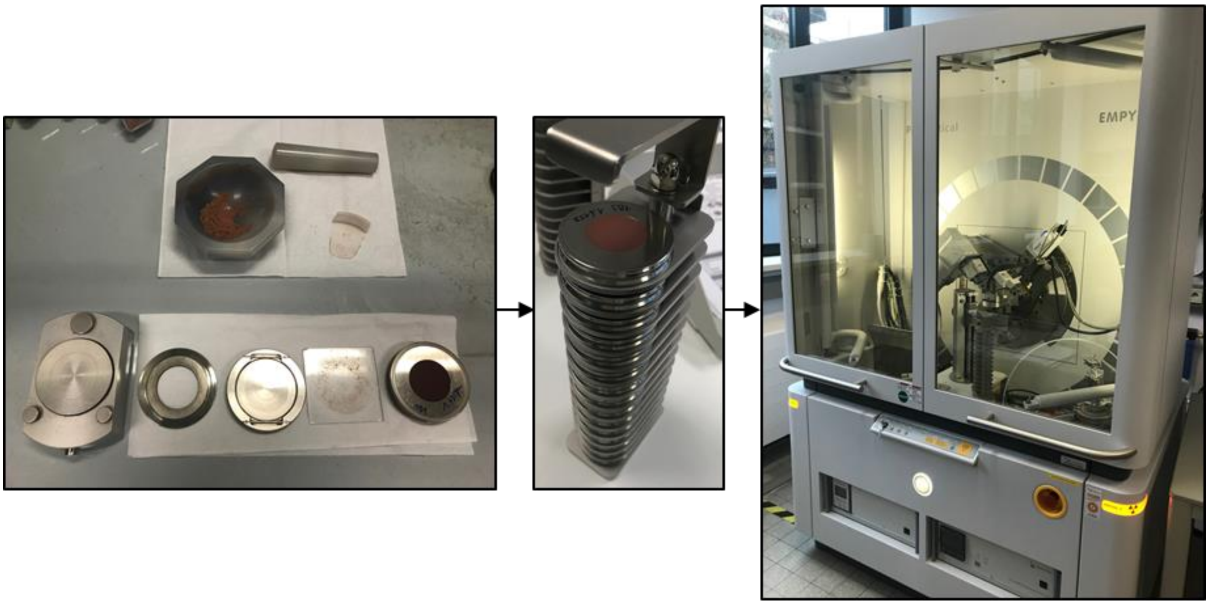

Figure 23: XRD sample preparation, sample rack and diffractometer

3.3.2.2 Rietveld analysis

Once the samples were measured, the diffraction data were analyzed to identify the crystalline phases. After that, Rietveld refinement was performed using the *PANalytical HighScore Plus* software. The Rietveld refinement is a fitting procedure, by the least square method, that calculates the diffraction pattern from the reflections of the identified phases. The concentration level as well as the amorphous content of the samples can be determined by this refinement.

3.3.3 Thermogravimetric analysis (TGA)

The Thermogravimetric Analysis (*Netzsch – STA 449 F3 Jupiter*®) was performed on five samples (Table 12). A mass loss (%) as a function of temperature (°C) graph is plotted during measurement. The samples were prepared by separately weighing (tolerance of ±5 mg) the sulphidic tailing and the marl, after which they were added together and mixed to a fine powder with pestle and mortar. The total sample mass prepared was about 2 g. Because the samples were powdered solid samples, no further preparation was needed. The crucible was cleaned with acetone, after which ±50 mg of the sample could directly be weighed (accuracy ±0.01 mg) and evenly distributed into the crucible. The heating range was 30 °C up to 1050 °C and the gas used was air.

Table 12: Theoretical sample ratios, prepared for TGA analysis

Sample	wt% Tailing	wt% Marl	Tailing (g)	Marl (g)
1	100%	0%	2	-
2	80%	20%	1.6	0.4
3	50%	50%	1.0	1.0
4	35%	65%	0.7	1.3
5	0%	100%	-	2

3.3.4 Inductively coupled plasma optical emission spectroscopy (ICP-OES)

Primary dilutions of the filtered leachates, with a dilution factor of 10, were prepared immediately after collection (Figure 24). The dilution was prepared by adding 2 mL of filtered leachate, 17 mL of MiliQ water (2x 8.5 mL) and 1 mL of HNO_3 65% in a 50 mL container. Samples were stored in a fridge at ±10 °C. However, due to precipitate formation, the subsequent obtained leachates (microwave and leaching kinetic samples) were stored in a dark place at room temperature. The samples showing precipitation were filtered before ICP-OES measurement.

However, the microwave and leaching kinetic samples still showed precipitate formation after resting for a day despite the different storage method. Therefore, the pH was checked and corrected from pH 7 to pH 1 by adding another 0.5 mL of HNO_3 65% to the 10x diluted samples. All the precipitates dissolved quickly when shaken, and the problem was solved this way.

Subsequently, secondary dilutions (dilution factor 100) were prepared for the microwave and leaching kinetic samples. These dilutions were prepared from the 10 times diluted samples by taking 1.2 mL sample and combining it with 10.2 mL of MilliQ water and 0.6 mL HNO_3.

The samples were measured with an ICP-OES (*Perkin Elmer - Avio 500* with an *Elemental Scientific - prepFAST* autosampler). Due to the prep*FAST* autosampler, the 100 and 1000 time dilutions were made automatically from the 10x diluted samples, when required.

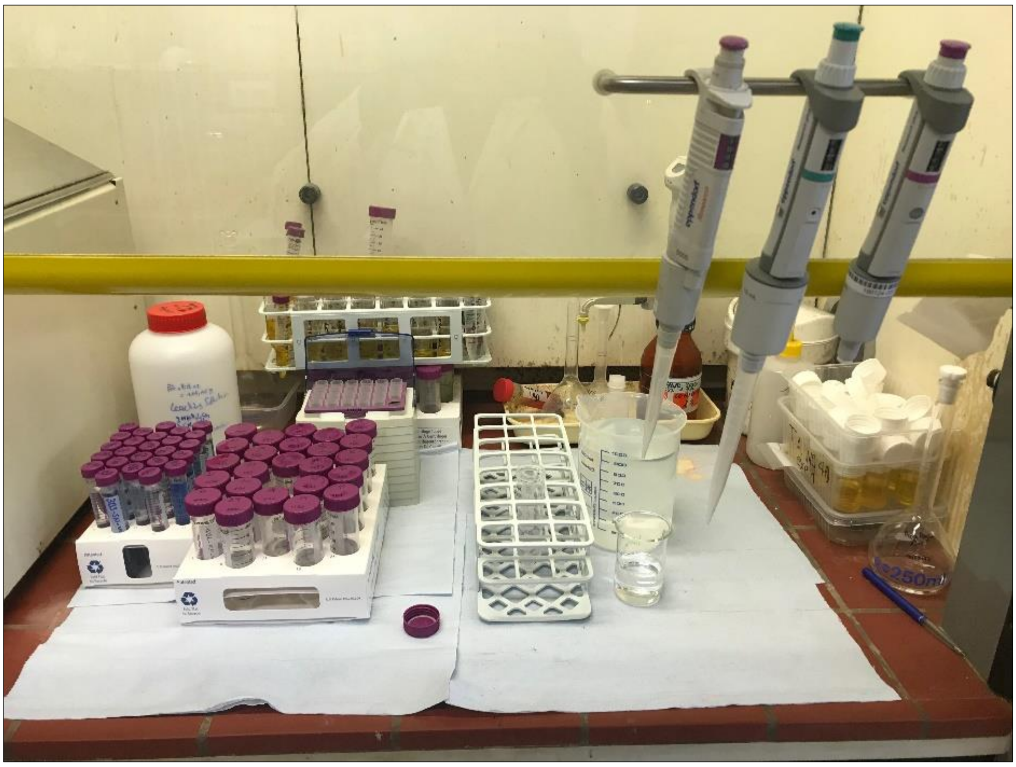

Figure 24: Primary dilution of filtered leachates setup

4 Results and discussion

4.1 Composition of the sulphidic tailing and the marl

The elemental composition of the sulphidic tailing and the marl were determined utilizing two measuring techniques: a) Handheld XRF and; b) ICP-OES after destruction of the material ($HCl/HNO_3/HBF_4$ (3/1/2), 2 h, 105°C). The most relevant elements are given in Table 13, while all measured elements are shown in Annex A. A comparison between both techniques showed similar values for Cu, Fe and S, the main elements of interest in this study.

Table 13: Composition of sulphidic tailing and marl, determined with XRF and ICP-OES

	Handheld XRF		**ICP-OES***	
Element	**Sulphidic Tailing (%)**	**Marl (%)**	**Tailing (mg/kg dm)**	**Marl (mg/kg dm)**
Al	1.14	4.53	3640	44800
As	0.29	<dl	2270	4.4
Bi	0.03	<dl	238	0.42
Ca	2.10	13.60	8380	99400
Co	0.07	<dl	323	13
Cu	**0.50**	<dl	**4370**	**25**
Fe	**27.72**	**3.65**	**305000**	**33900**
K	0.20	1.67	763	18300
Mg	<dl	<dl	290	15100
Mn	0.02	0.02	102	418
Na	<dl	<dl	318	6740
Pb	0.71	0.002	6700	16
S	**35.48**	**0.44**	**348000**	**4370**
Sb	0.03	<dl	316	<4
Si	11.54	17.26	n.d.	n.d.
Ti	0.26	0.34	1380	2190
Zn	0.11	0.01	1120	89

<dl: below detection limit; n.d. not determined

* Conversion from mg/kg dm to percentage is done by dividing the number by 10 000 (*e.g.* XRF - Cu = 0.50 %; ICP-OES - Cu = 0.43 %)

Diffraction patterns were gathered from the untreated original tailing and the marl and are presented in Figure 25. Major mineral phases in the tailing include Pyrite (FeS_2) and Quartz (SiO_2). The marl consists mainly of Muscovite-2M1-ferroan ($K(Al, Fe)_2(AlSi_3O_{10})(OH)_2$), Calcite ($CaCO_3$), Quartz ($SiO_2$) and Dickite ($Al_2Si_2O_5(OH)_4$). The Rietveld refinement of the untreated original tailing and marl is shown in Table 15

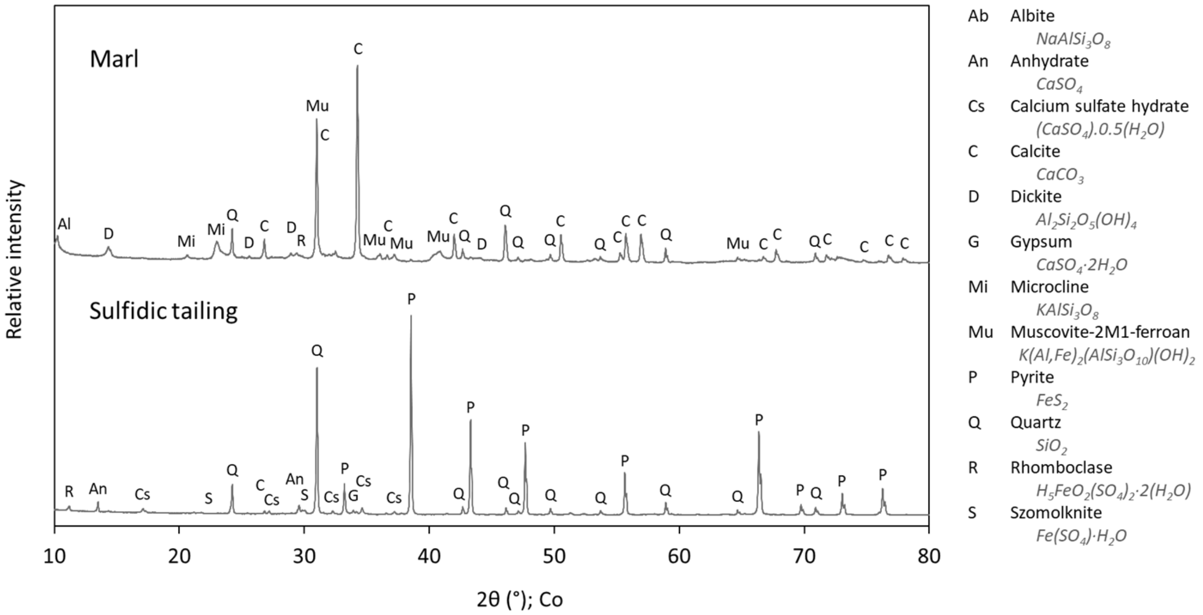

Figure 25: Diffractograms of the original sulphidic tailing and the marl

4.2 Conventional roasting

4.2.1 Mass loss

The mass loss during roasting was determined by weighing the crucibles containing the sample before and after roasting (Equation 59). In general, the mass loss increased with roasting temperature (Figure 26). The graph can be divided into two zones (A and B). Zone A shows a decrease in mass loss with increasing marl content, a trend consistent for all roasting temperatures. This trend likely was a result of a more pronounced sulphur fixation as sulphate with increasing marl content. The sulphur was thus being captured and not able to escape the material as SO_2. However, some sulphur or even sulphate might still be converted to SO_2 explaining the occurring mass loss with increasing marl content. The reactions regarding the pure tailing correspond to FeS_2 oxidation during which sulphide is set free and interacts with oxygen to the formation of SO_2 (Equation 27 to 33). Zone B shows an increase in mass loss with increasing marl content. In this region it was suggested that most sulphur was captured as sulphate and that the remaining (excess) carbonates decomposed whereby the carbonates were converted to CO_2. This is confirmed in the following section where the retained sulphur is plotted. For the mixtures it gets more complex. Therefore, XRD and Rietveld refinements were conducted on the roasted mixed samples.

$$\text{Mass loss (\%)} = \frac{\text{Spl. mass pre roast. (g)} - \text{Spl. mass post roast. (g)}}{\text{Spl. mass pre roast. (g)}} \qquad (59)$$

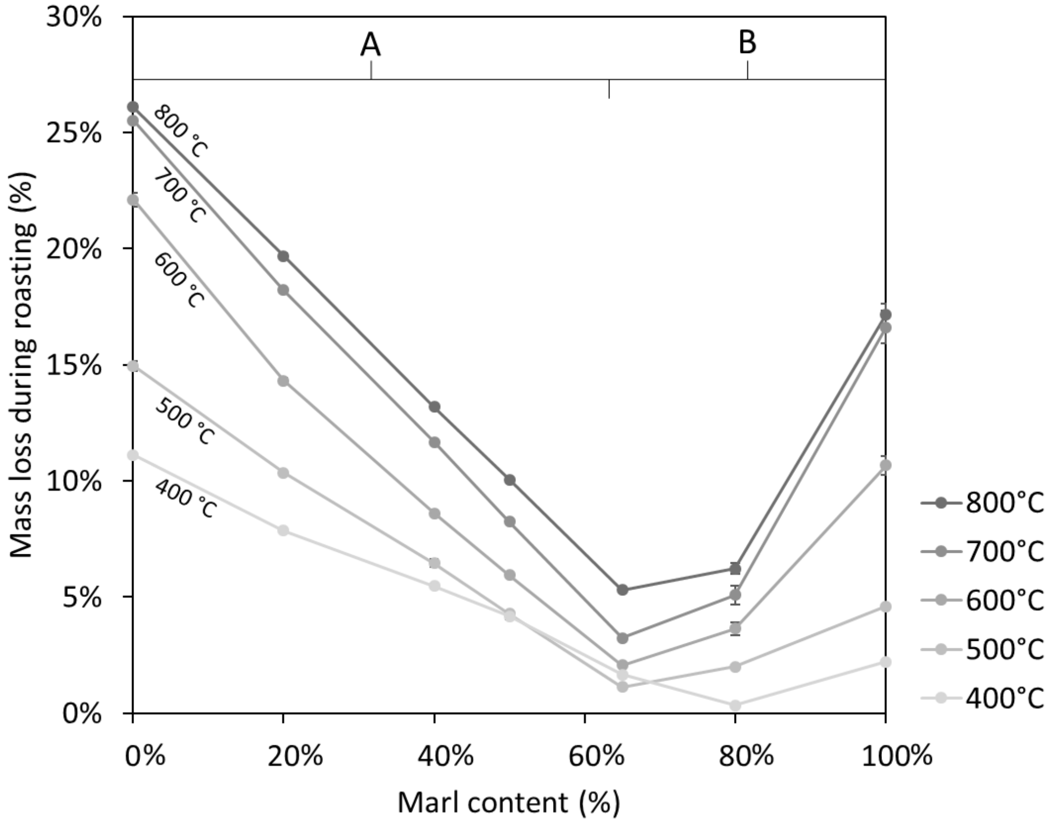

Figure 26: Mass loss during conventional roasting

TGA analysis was performed to accurately determine the mass loss as a function of temperature (Figure 27). This could help in describing the possible reactions that take place in the different samples. Firstly, a slight decrease in mass (±3 %) occurred in the range of 34 °C to 247 °C. This was related to the removal of moisture in the samples, *i.e.* water and water of crystallization.

The tailing showed two major mass losses. The first mass loss (±14%; 388 °C to 504 °C) was linked to FeS_2 oxidation. During this oxidation, SO_2 was set free which caused the majority of the mass loss (mainly Equation 27 to 33). Between 504 °C and 554 °C a slight mass gain was observed (±0.5%). The second mass loss (±9%) occurred between 554 °C and 693 °C, after which the sample weight more or less stabilized. This second mass loss related to the transformation of iron phases to Fe_2O_3 during which SO_2 gas was released. (Equation 30, 32 and 33)

The mass of the marl material kept decreasing from 310 °C until 774 °C, after which it stabilized. This mass loss (±17%) was mainly attributed to the decomposition of $CaCO_3$ in the material (Equation 43 and 44). At ≥600 °C $CaCO_3$ decomposition increased [25], which is shown as a more pronounced mass loss from that point on.

The mixture containing 65% marl showed mass loss (±6%) between 372 °C and 482 °C. For the mixture with 50% marl content the first mass loss (±3.5%) occured between 372 °C and 440 °C. The weight of the sample kept dropping but a more pronounced mass loss (±3%) occurred at the interval of 482 °C to 505 °C. With further increase in temperature, the mixtures containing 50% and 65% marl only slightly decreased in weight (±3%)

For the mixture containing 20% marl a mass loss (±8%) was shown between 372 °C and 450 °C. The mass loss levelled off, but the sample weight kept dropping slightly. A second more pronounced mass loss (±2.5%) occurred in the interval 500 °C to 530 °C. Finally a mass loss of (±6 %) was found between 530 °C and 700 °C. Further increase in temperature lead to slight mass loss.

The mass loss between roughly 372 °C and 500 °C was always related to the FeS_2 oxidation during which SO_2 is released. From the comparison of the mass loss, from the different mixtures, it was clear that the mass loss decreased with increasing marl content. This was related to the fact that samples with a higher marl content form more sulphates which caused mass gain. The sulphate formation can also be noticed clearly within the samples containing 20% and 50% marl, because the curve levelled off at roughly 425°C to 500 °C, and 535 °C to 600 °C (sample containing 20 % marl) which are the temperature ranges at which sulphates are formed. Secondly, mass loss showed from roughly 600 °C and up was related to formation of Fe_2O_3 from other iron minerals during which SO_2 is set free. Subsequent mass losses at elevated temperatures were related to $CaCO_3$ remainders that decomposed to CO_2 or due to sulphate phases that started to decompose.

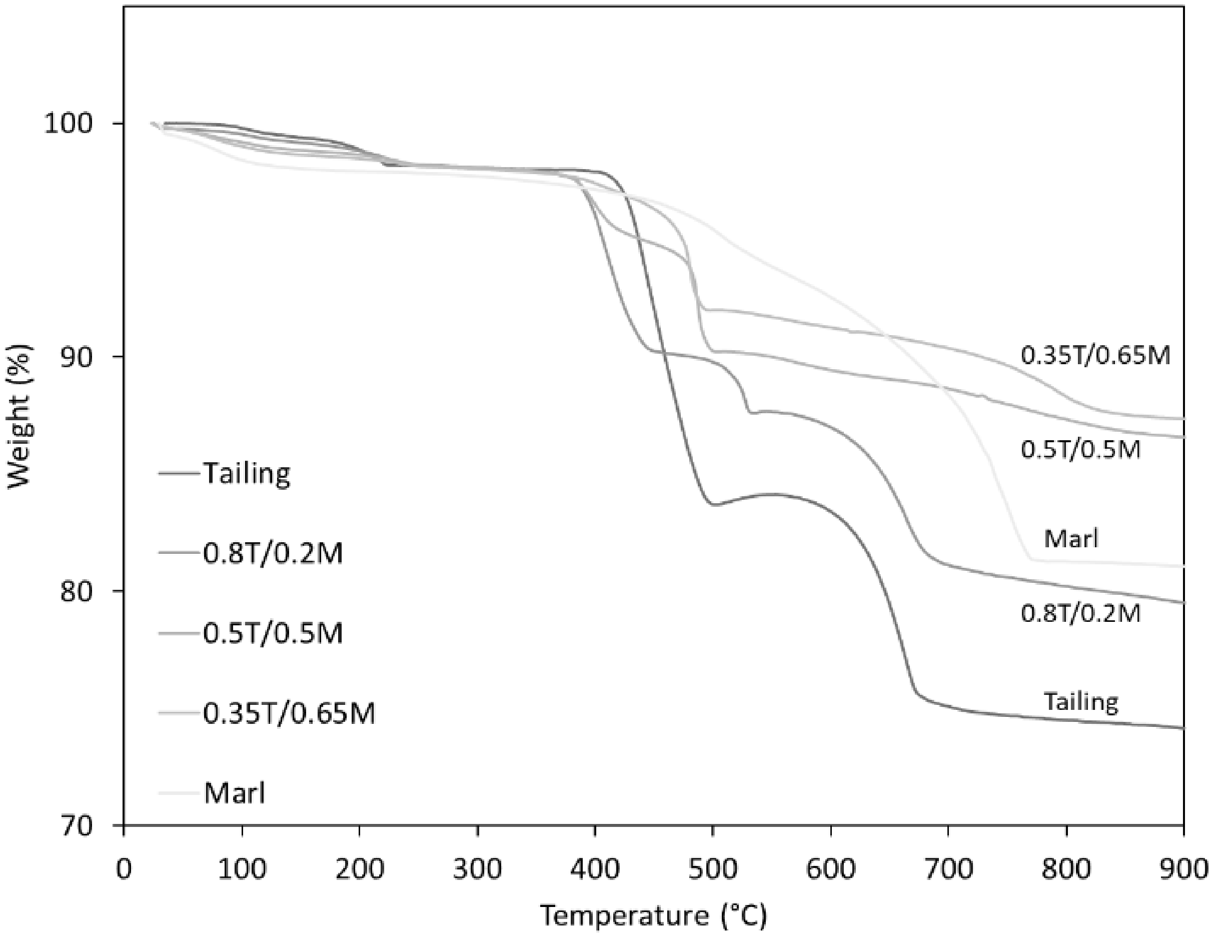

Figure 27: TGA analysis of the starting materials and three tailing/marl mixtures

A comparison between the mass losses at 800 °C in a conventional furnace and TGA was done and shown in Table 14. In general the mass losses were similar to each other, except for the samples containing 50% and 65% marl. This can be explained due to the fact that the amount of sample in the crucibles was of major difference. Hence, the SO_2 released at the bottom of the sample first had to reach the surface before it was removed from the sample. During its travel through the sample, which was longer in the conventional furnace, the SO_2 had more potential and time to be reacting into sulphates. This means that in the conventional furnace more sulphates were formed, which caused mass gain. Therefore, less mass loss was found during heating in a conventional furnace relative to the TGA for the samples containing 50% and 65% marl.

Table 14: Comparison of weight loss after heating to 800 °C with TGA and in a conventional furnace

Sample (heating to 800 °C)	Weight loss (%)	
	TGA	Roasting CF
Tailing	25.5	26.1
80% T/20% M	19.8	19.7
50% T/50% M	12.6	10.1
35% T/65% M	11.7	5.3
Marl	18.7	17.2

4.2.2 Sulphur fixation

The sulphur retained in each sample was calculated according to Equation 60, and presented in Figure 28 as a function of the marl content. Generally, more sulphur was retained in the solid samples as the marl content increased. At 65% marl addition, almost all sulphur in the initial sample was captured. The excess carbonates from the added marl (ratios containing either 65% or 80% and the pure marl) would now purely start to convert to CO_2 as no sulphur was left to be fixated. Upon increasing the roasting temperature, the amount of sulphur retained in the sample decreased. This was related to decomposition reactions, which were more prominent at elevated temperatures, in which sulphur and sulphates decomposed to SO_2. When comparing the pure tailings, less SO_2 formation was prominent at lower temperatures, likely due to incomplete oxidation of the sample, *i.e.* mainly FeS_2. At temperatures ≥600 °C the pure tailing sample was fully oxidized. However, the addition of the marl lead to more sulphur fixation at 600 °C than 700 °C and 800 °C. This was due to decomposition of sulphates. However, the decomposition of $CaSO_4$ seemed unlikely because Yan *et al.* [23] reported that $CaSO_4$ remains stable up to 1000 °C in the presence of Fe_2O_3 and only starts to rapidly decompose above 1000 °C.

$$\text{Relative retained sulphur in solid spl.}\,(\%) = \frac{\text{S\%} * \text{spl. mass post roast. (g)}}{\text{S\%} * \text{spl. mass pre roast. (g)}} \tag{60}$$

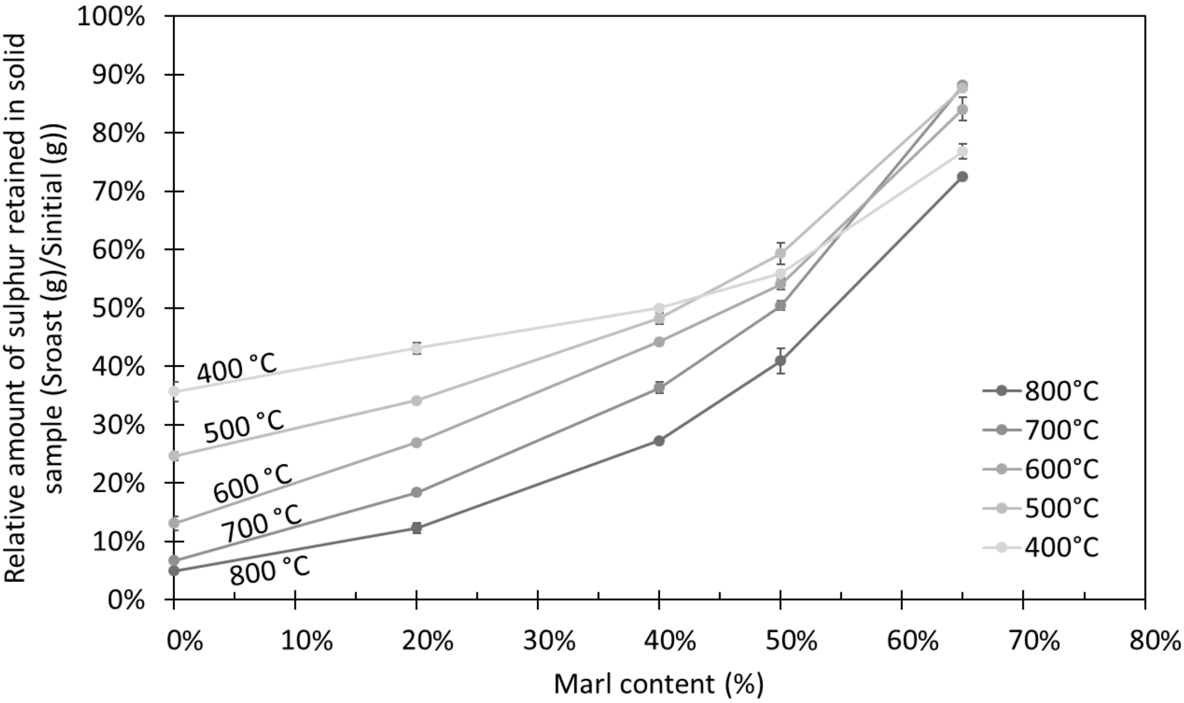

Figure 28: The relative amount of sulphur retained during roasting (%) in relation to the marl content (%) (conventional roasting)

4.2.3 Mineral phase analysis

Diffraction patterns were gathered from each first replicate of the conventional roasted samples. However, quantitative analysis, *i.e.* Rietveld refinement, was performed on the initial materials and on the roasted samples containing either 20%, 40%, 50% or 65% marl. Therefore, displaying the diffractograms of the mixed samples was less relevant. The mixed samples undergo complex interactions and, therefore, the mineral composition and quantity of each phase can help clarifying these interaction. The Rietveld refinement of the untreated original tailing, marl and mixed samples are shown in Table 15, while the phase composition of a specific tailing/marl mixture after roasting is also presented as a function of the roasting temperature in Figure 29.

Table 15: Overview of Rietveld refinement on conventional roasted samples

Roasting Condition		Pre-roast	Pre-roast	Post roasting: 400 °C				Post roasting: 500 °C				Post roasting: 600 °C				Post roasting: 700 °C				Post roasting: 800 °C				
wt % Tailing		100	0	80	60	50	35	80	60	50	35	80	60	50	35	80	60	50	35	100	80	60	50	35
wt % Marl		0	100	20	40	50	65	20	40	50	65	20	40	50	65	20	40	50	65	0	20	40	50	65
Mineral phase	Composition	wt % (Rietveld refinement)																						
Albite	$NaAlSi_3O_8$		1.6	0.2	0.8	1	1					1.1		0.6	1.1									
Anglesite	$PbSO_4$			0.2	0.3	0.2	0.1	0.5	0.3	0.3	0.1	0.1	0.1	0.2										
Anhydrite	$CaSO_4$	1.2		8.7	12.7	14.5	17.2	12.1	18.0	21.4	26.4	12.6	19.3	21.1	26.1	14.5	19.4	21.7	25.1	5.8	11.5	19.1	22.0	30.8
Anorthite	$CaAl_2Si_2O_8$				0.3	0.1	0.2					1.1	1	1.4	2.2									
Calcite	$CaCO_3$	0.2	34	2.7	4.5	5.3	5.9	0.9	1.7	1.6	1.6			0.1	0.2									
Calciumsulfate hydrate	$Ca(SO_4)0.5H_2O$	5.6																						
Dickite	$Al_2Si_2O_5(OH)_4$		11.3	1.1	0.9	1.1	1.2																	
Gypsum	$CaSO_4.2H_2O$	3.3																						
Hematite	Fe_2O_3			11.8	14.2	13.6	11.0	22.5	21.7	21.5	18.6	38.1	30.3	29.5	22.5	56.5	37.6	31.7	19.8	65.7	57.9	46.1	38.4	28.6
Iron sulfate	$FeSO_4$			4	6.3	4.9	3.4																	
Maghemite	Fe_2O_3			8.3	3.9	3.0	1.2	5.8	3.4	1.4	0.3													
Microcline	$KAlSi_3O_8$		1.4	2.9	0.3	0.5	1.0	0.5	0.7	0.7	1.0	0.7	0.3	2.4	3.1	0.8	1.5	1.5	2.1	2.0	3.0			
Mikasaite	$Fe_2(SO_4)_3$			4.7	5.0	4.6	3.3	11.8	10.9	9.5	5.4	5.6	3.5	1.1										
Muscovite-2M1 ferroan	$K(Al,Fe)_2AlSi_3O_{10}(OH)_2$		37.5	18.8	23.8	27.7	35.0	17.2	21.7	23.7	28.3	15.3	22.8	20.9	23.0		16.9	23.2	33.8			8.8	13.9	16.8
Perkovaite	$CaMg_2(SO_4)_3$											3.3	3.9	3.4	3.3	2.4	3.6	2.9	3.5		0.2	2.4	3.1	4.2
Pyrite	FeS_2	56.3		12.5	5.9	3.8	1.2	4.8	1.0	0.3		0.2	0.4	0.3										
Quartz	SiO_2	27.9	14.1	24.1	21.0	19.6	18.3	23.9	20.7	19.7	18.2	21.9	18.6	19.1	18.6	25.8	21.0	19.1	15.8	26.4	27.4	23.6	22.5	19.7
Rhomboclase	$H_5FeO_2(SO_4)_2.2(H_2O)$	1.5																						
Sulfur	S	2.2																						
Szomolknite	$Fe(SO_4).(H_2O)$	1.9																						
Total composition		100.1	99.9	100.1	99.9	99.9	100	100	100.1	100.1	99.9	100	100.2	100.1	100.1	100	100	100.1	100.1	99.9	100	100	99.9	100.1

The tailing mainly consisted of FeS_2 and Rietveld refinement showed that FeS_2 was already partly transformed at the lowest temperature, which was 400 °C. FeS_2 oxidation was reported to start between 173 °C and 394 °C (Mitovski *et al.* [22], Zivkovic *et al.* [21] and Ozer *et al.* [2]), which initially resulted in the formation of FeS (iron sulphide). At 400 °C some $FeSO_4$ (iron sulphate) was present in the samples, which indicated the FeS_2 oxidative reaction mechanism (Equation 31). In addition, $Fe_2(SO_4)_3$ (mikasaite) was formed, supposedly from FeS_2 and FeS, but this phase disappeared at 700 °C. The formation of $Fe_2(SO_4)_3$ corresponded to the finding of Zivkovic *et al.* (Table 3). Furthermore, γ-Fe_2O_3 (maghematite) and Fe_2O_3 (hematite) were also formed, as a step during FeS_2 oxidation (Equation 30, 32 and 33). At 600 °C, γ-Fe_2O_3 completely transformed to α-Fe_2O_3 (hematite). FeS_2 itself disappeared fully around 500 °C to 600 °C and was less pronounced at higher marl content due to lower initial tailing content. The contribution of the Fe_2O_3 phase strongly increased with temperature as the oxidative reaction mechanism of FeS_2 lead to the formation of it.

With higher marl content, $CaSO_4$ (anhydrite) became more prominent. This was due to the reaction of $CaCO_3$ with released SO_2 (Equations 43 and 44), which increased as more $CaCO_3$ was available. $CaSO_4$ was also the most important phase in which sulphur was fixated.

As mentioned $FeSO_4$ and $Fe_2(SO_4)_3$ were present at low temperatures, while at higher temperatures $CaMg_2(SO_4)_3$ (perkovaite) was present. This suggested that, at high temperatures, Fe was incorporated in phases such as Fe_2O_3 and that Ca coming from excess $CaCO_3$ reacted to $CaMg_2(SO_4)_3$.

Muscovite-2M1-ferroan, was mainly present in the marl material. Therefore, the increasing contribution of this phase with increasing marl content could be expected.

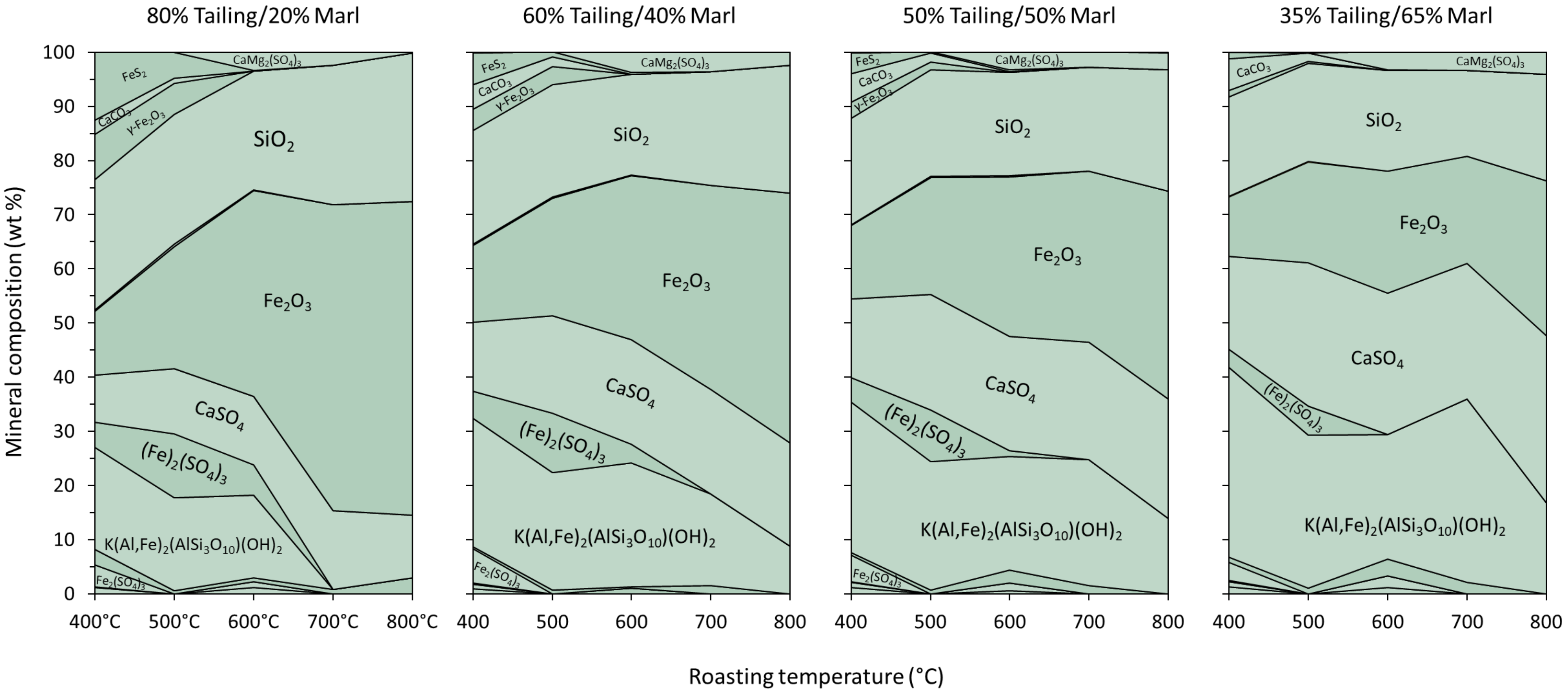

Figure 29: Representation of the Rietveld data from mixed conventional roasted samples

4.2.4 Molar amount of sulphide, sulphate and carbonate

The Rietveld refinement is restricted to the weight percentage of each mineral phase. Therefore, it does not give a direct value for the amount of sulphide, sulphate and carbonate present in the sample material. Hence, the molar amount of sulphide, sulphate and carbonate was calculated from the Rietveld refinement. This calculation took the amount of sulphide, sulphate and carbonate present in the identified phases into account (Figure 30). For example, the calculation of the molar concentration of carbonate is briefly explained. Firstly, the phases containing carbonates were listed. For carbonates, only calcite ($CaCO_3$) was present in the material. Secondly, the molar amount was calculated by dividing the $CaCO_3$ content by the molar mass of $CaCO_3$. Thirdly, the previous value was corrected to mmol. This value now gives the amount of $CaCO_3$ in mmol/g sample. A second series of graphs can be constructed by multiplying the previous value with the actual sample mass. Now, the mmol of $CaCO_3$ in that particular sample is given. The calculations for the sulphide and sulphate content are analogous.

The sulphide was considered to be coming from FeS_2 present in the tailing, while the carbonate was coming from the marl ($CaCO_3$). Therefore, the pre-roast mixture consisted of both sulphide and carbonate, of which their amount in each mixture depended on the mixing ratio of tailing and marl. The sulphate content in the tailing was very low (0.088 mmol/g), and even zero in the marl. Obviously, the previous reflected to the sample mixture as well.

Firstly it should be noted that FeS_2 oxidation was incomplete until after 500 °C to 600 °C. FeS_2 almost completely disappeared at 500 °C for the 40%, 50% and 65% marl ratios.

Secondly, the carbonate content in the samples was 0 or 0.01 mmol/g material and 0.02 mmol/g material for 50% and 65% marl, respectively after treatment at 600 °C. This suggested that all carbonates were consumed through sulphur fixation and decomposition of carbonate minerals at high roasting temperature occurred.

Thirdly, with elevated roasting temperatures (≥600 °C), the sulphate formation gradually decreased. This was due to decomposition reactions of the formed sulphates.

Roasting at 500 °C seemed to be optimal for sulphate formation because: a) nearly all FeS_2 was oxidized (40% marl ratio and higher); b) carbonates were used for sulphate formation with low decomposition of both; and c) the sulphate formation peaked at this roasting temperature. The sulphate peak occured because, most of the sulphide was released as almost all FeS_2 was oxidized. Therefore, SO_2 could react with the carbonates for sulphate formation. The higher the marl content, the more carbonates were present, and therefore the reaction with SO_2 was more likely. At roasting temperatures above 500 °C decomposition of sulphates occurred, which was not yet the case at 500 °C for $CaSO_4$ and $CuSO_4$ [2], [21].

Note that increasing the marl content suggested to improve FeS_2 oxidation. However, it should be considered that less FeS_2 was present in these materials, pre-roasting (“dilution” effect).

Based on the handheld XRF results of the roasted samples, the amount of sulphur retained in these samples was calculated. The amount of sulphur in the mixed sample was considered as 100%. The sulphur concentrations in the roasted samples were compared to the initial concentration in the mixed sample and thus show the retained sulphur content. These values are presented by the small crosses in Figure 30 and show the same trend as the Rietveld-derived value for the sulphur in each sample, which equals the sum of the sulpide and sulphate content.

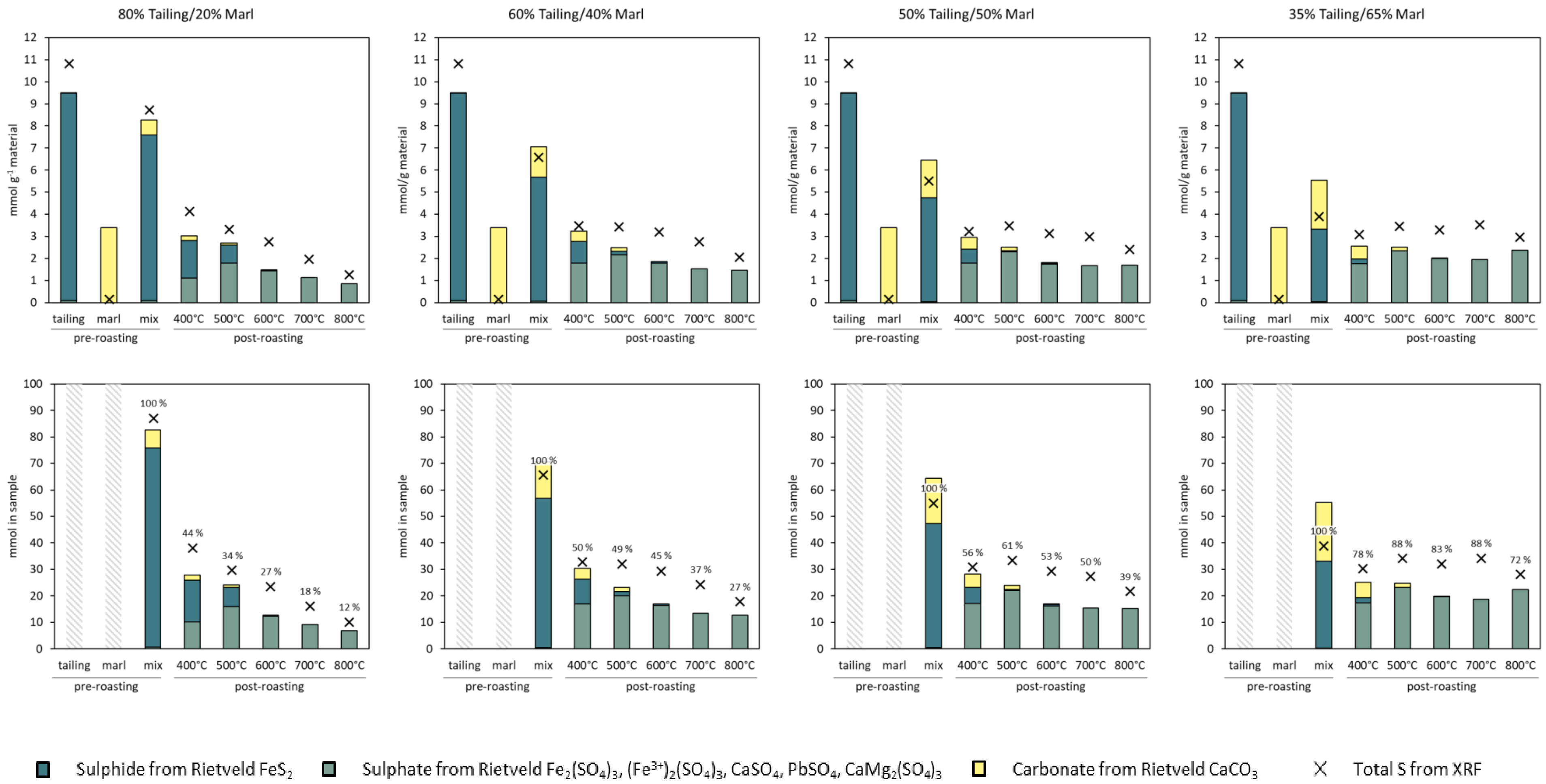

Figure 30: The molar amount of sulphide, sulphate and carbonate in the conventional roasted samples, represented as the amount per gram material (mmol/g material) or as the total amount in each sample (mmol)

4.2.5 Sulphate formation relative to sulphide and carbonate consumption

To give a more clear view on the roasting temperature and marl content at which the sulphate formation was the highest, a comparison between the sulphate formation and sulphide or carbonate consumption was made Figure 31.

Figure 31 a and b are closely related, because sulphate formation could only happen if sulphide was consumed, *i.e.* FeS_2 oxidation. At 400 °C, the sulphide oxidation was limited, which resulted in low sulphate formation. Sulphide oxidation was good at 500 °C, which was also shown by the fact that the amount of sulphate formed increased with more than 50% over the sulphate formed at 400 °C (Figure 31 a). At higher temperatures, sulphide oxidation was complete, but sulphate decomposition could take place. Therefore, the sulphate content in the products diminished with increasing temperature.

Figure 31 c shows the molar ratio of sulphate formation to carbonate consumption relative to the marl content at different roasting temperatures. The carbonate consumption was related to the sulphur oxidation and thus increased from 400 °C to 500 °C, as more sulphides were set free. Hence, the molar ratio of sulphate formed over carbonate consumed rose, as sulphate formation was at its highest and carbonate was mainly consumed due to reaction with sulphide. The carbonate consumption increased at higher temperatures ($\geq$600 °C) as it decomposed to CO_2, which did not contribute to the sulphate formation thus the trend lowered.

The general trend with increasing marl content was that the amount of sulphate formed increased as more sulphide was fixated. However, less sulphide was fixed per mmol of $CaCO_3$.

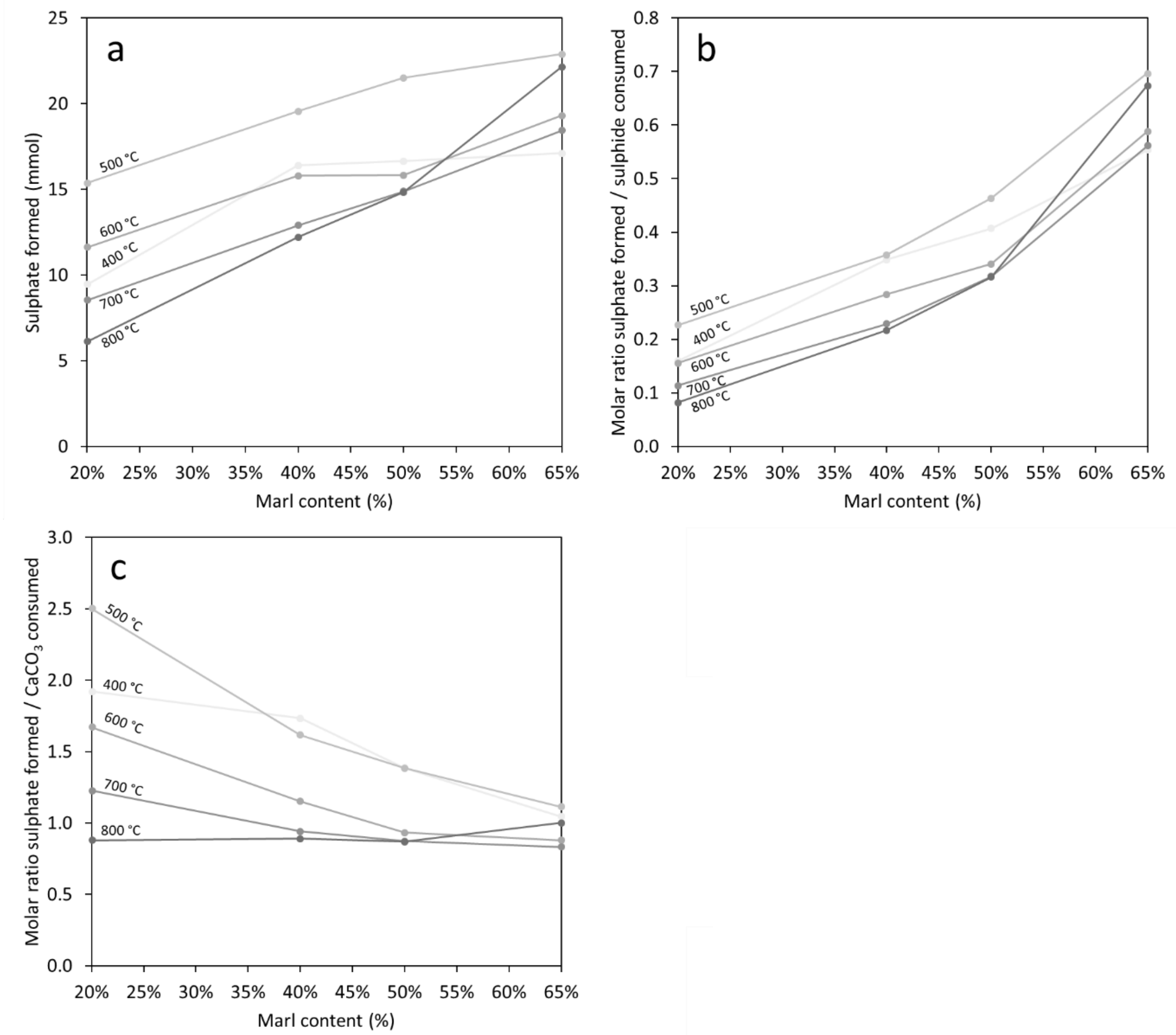

Figure 31: The sulphate formation (a), the sulphate formation to sulphide consumed (b) and the sulphate formation to carbonate consumed (c), all presented as a function of the marl content

4.2.6 Mass loss based on Rietveld refinement

The sulphate formation (mass gain), sulphide and carbonate consumption (mass loss) derived from Rietveld refinement were used to calculate an overall mass loss (Figure 32a). The obtained data showed a decrease in mass loss with increasing marl content. It also showed an increase in mass loss with increase of roasting temperature, as expected. The comparison between this graph and the mass loss graph based on pure weight (Figure 32b) showed very comparable values for each roasting temperature and each mixture. Therefore, it could be concluded that the method of Rietveld-derived quantification of sulphate formation, sulphide and carbonate consumption was able to quantify the contribution of each of these to affect the mass loss of a specific sample.

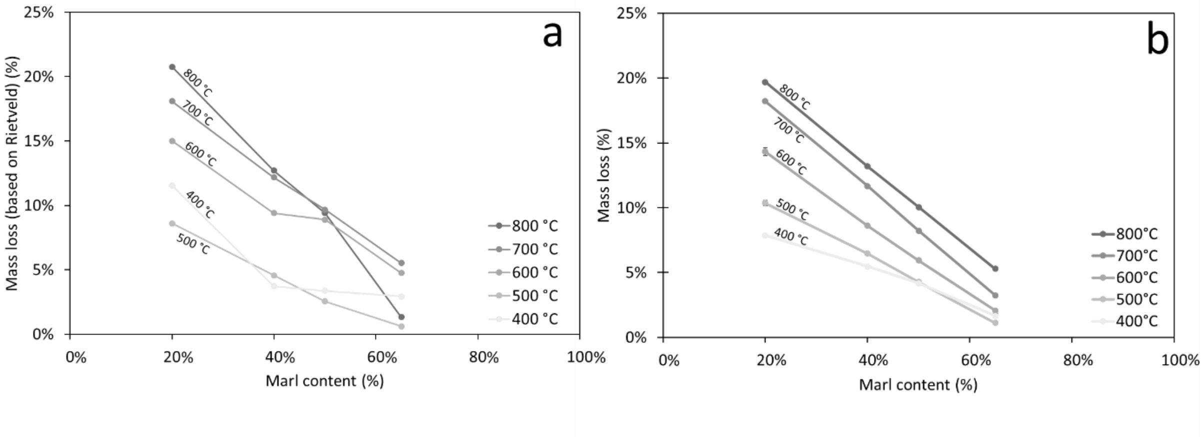

Figure 32: Mass loss based on Rietveld refinement (a) and (b = Figure 26) crucible weight for conventional roasted samples

4.3 Microwave roasting

4.3.1 Mass loss

The mass loss during microwave roasting was determined, *i.e.* by weighing the crucibles containing the sample before and after roasting (Equation 59). In general, the mass loss was positively correlated with temperature and time, *i.e.* more mass loss with higher roasting temperature or time (Figure 33). A decrease in mass loss with increasing marl content was shown, which was true for all roasting temperatures. This trend was a result of pronounced sulphur fixation as sulphate, thus sulphur being captured and not able to escape the material as SO_2. A decrease in dwell time at 500 °C from 60 min to 30 min and 15 min had little effect on the mass loss of the mixed and pure marl samples. This did not mean that there was similar sulphate formation or better FeS_2 oxidation. The results showed a difference between 30 min and 60 min for the pure tailing sample. This difference could be due to the FeS_2 oxidation reaction which was still ongoing after 30 min. Hence, more SO_2 was set free resulting in more mass loss as no marl was present. The pure marl samples showed a low mass loss, as carbonates do not readily decompose at 500°C [24].

A comparison in mass loss between conventional roasting (Figure 26) and microwave-assisted roasting at 400 °C and 500 °C (Figure 33) is presented in Table 17. The mass loss of the pure tailing samples were always lower in the microwave furnace. This suggested that in the microwave furnace less FeS_2 oxidation occurred, *i.e.* less SO_2 released thus lower mass loss. Comparing the 50% taling/50% marl samples, the mass loss was higher during microwave-assisted roasting. This was because during conventional roasting more sulphate phases were formed, contributing to a lower mass loss. They presumably were more easily formed during conventional roasting because of the heating rate (100 °C/h). Hence, samples stayed longer in a certain temperature range during which sulphates would be formed. While during microwave roasting the set temperature was reached within 30 min. The marl samples showed similar mass losses between both roasting techniques. Because of the low activity of the marl ($CaCO_3$), which heats up to only 130 °C by solely microwave irradiation (Table 5), a SiC plate was used to ensure that at least the temperature inside the microwave chamber reached the set temperature. Therefore, similar mass losses were expected. However, the actual sample temperature still partially depends on its reaction to the microwave irradiation. Therefore the exact sample temperature is unknown.

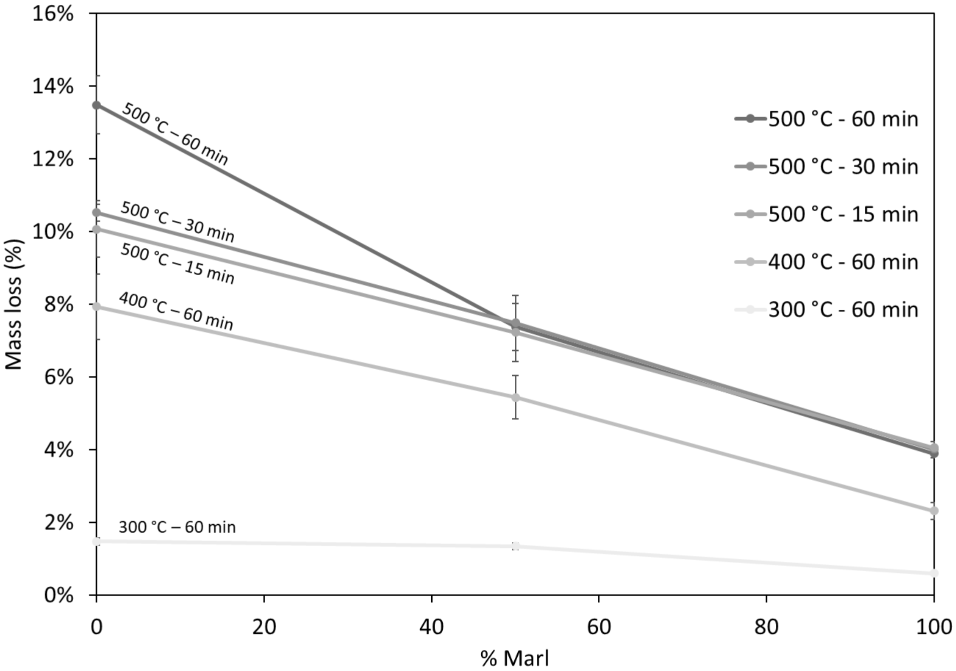

Figure 33: Mass loss during microwave roasting

Table 16: Mass loss comparison between conventional roasting and microwave-assisted roasting

Mass loss (%)	Tailing		50% T – 50% M		Marl	
	CF	MW	CF	MW	CF	MW
400 °C	11.13	7.93	4.17	5.43	2.22	2.31
500 °C	14.96	13.48	4.27	7.37	4.60	3.89

4.3.2 Sulphur fixation

The sulphur retained in each sample during microwave-assisted roasting was calculated according to Equation 60 and presented in Figure 34 as a function of the marl content. Generally, retained sulphur in the pure tailing decreased with increasing roasting temperatures, as expected due to more FeS_2 oxidation. For the mixed samples, the retained sulphur stayed the same (with respect to the error bars). Except for the samples roasted at 300 °C. In this case the maintained Sulphur was 94.40% for the pure tailing, which could be explained by a minimal FeS_2 oxidation that occured at this temperature, *i.e.* sulphide was not set free. However, the trend shows a decrease in sulfur fixation when adding marl.

The longer the dwell time, the less sulphur was retained. At least, when comparing the samples conducted to microwaves for 15 min or 30 min to these conducted at 60 min. At the dwell time of 15 min less sulphur was retained in comparison with a 30 min dwell time. However, both values are in the same error range.

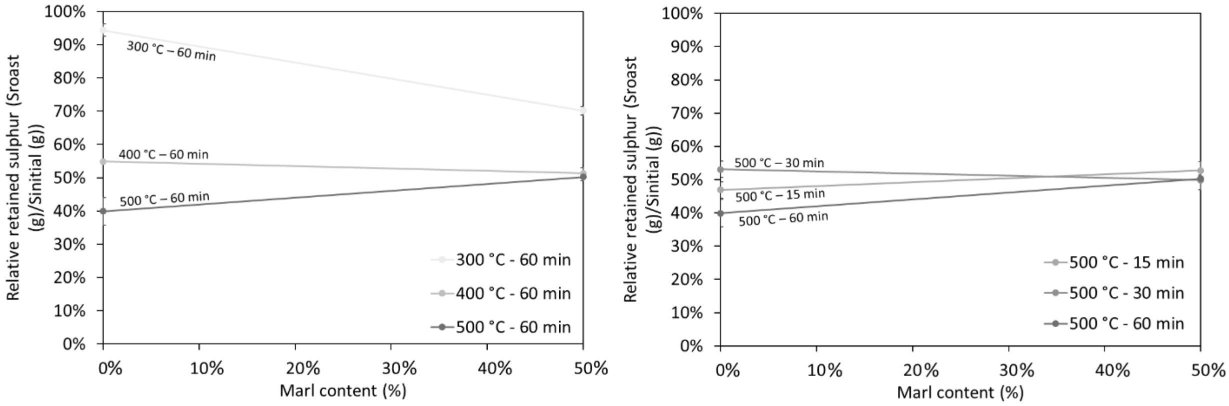

Figure 34: Relative retained sulphur in relation to the marl content (microwave roasting)

4.3.3 Mineral phase analysis

The comparison of the x-ray diffractograms of the 50% tailing/50% marl microwave roasted samples at different temperatures for 60 min are given in Figure 35. They show increased FeS_2 oxidation with increased roasting temperature, as expected. However, compared to the conventional roasting at 500 °C, the FeS_2 phase was still present. Subsequently, the amount of the $CaCO_3$ phase decreased with increased roasting temperature as more $CaCO_3$ was getting consumed in favor of sulphate formation.

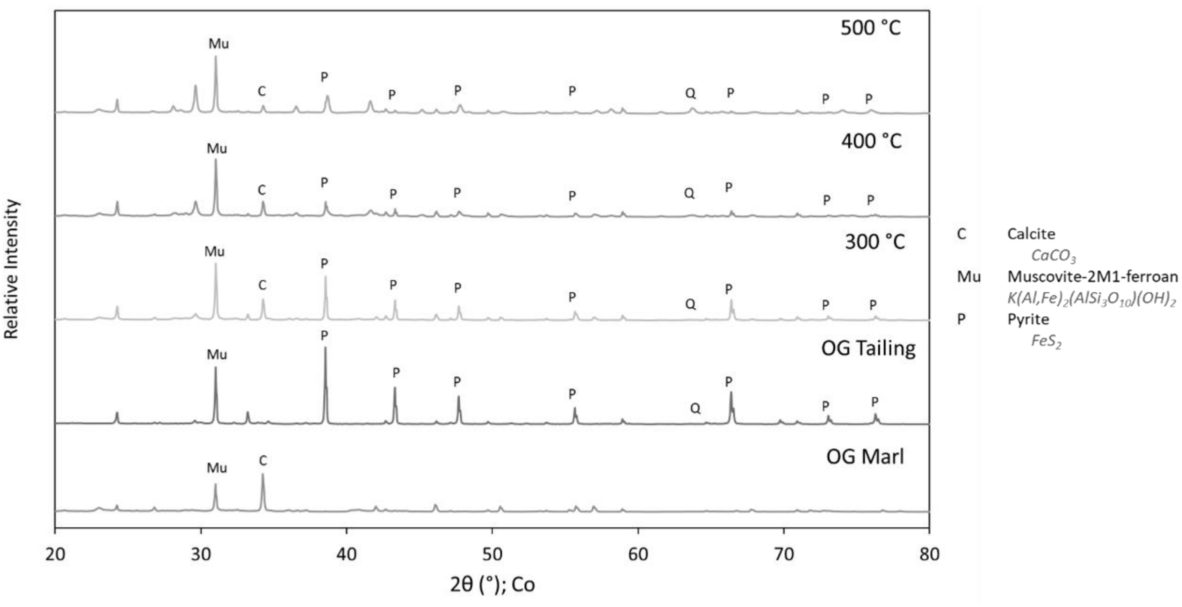

Figure 35: X-ray diffractogram of microwave roasted samples at different temperatures for 60 min

Diffractograms regarding the different dwell times (15 min, 30 min or 60 min at 500 °C) are given in Figure 36. With a longer dwell time more FeS_2 oxidation was observed, *i.e.* quantity of FeS_2 phase decreased. Again, as expected, the $CaCO_3$ phase decreased with increasing dwell time as it was relative to the FeS_2 oxidation, which increased. Rietveld analysis should be performed to see if there is a major difference between the samples conducted at 30 min or 60 min dwell time. Based on the diffractograms this was unlikely, at least no major differences could be observed, yet quantitative results may suggest otherwise.

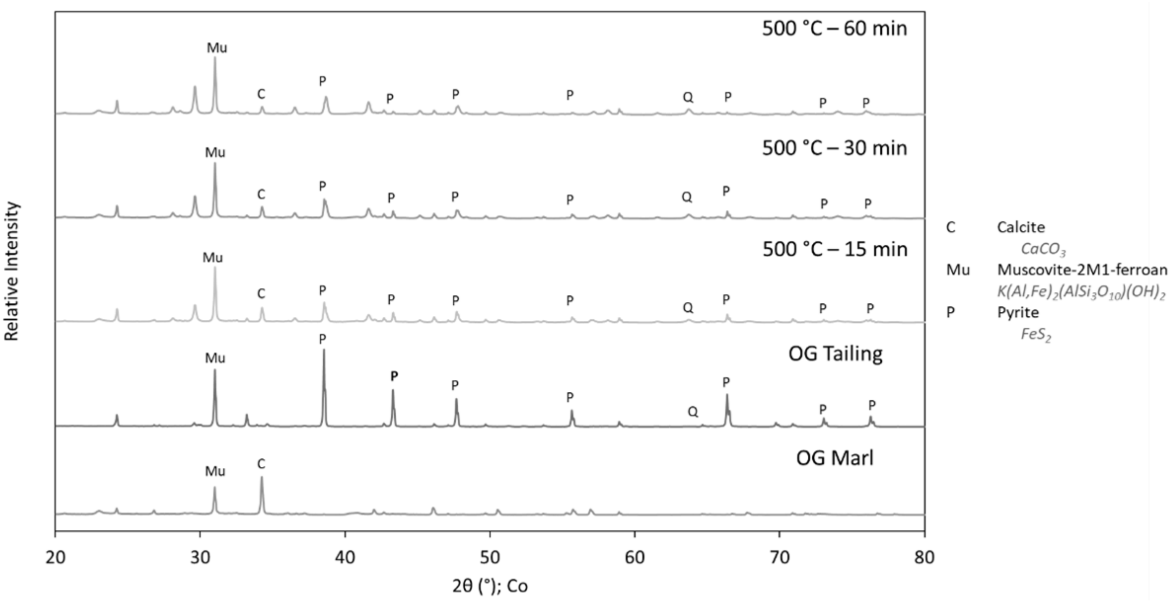

Figure 36: X-ray diffractogram of microwave roasted samples at 500 °C with different dwell times

The Rietveld refinement was only performed on the pure tailing and 50% tailing/50% marl microwave roasted sample at 500 °C for 60 min (Table 17). The Rietveld refinement on the pure tailing showed that not all FeS_2 was oxidized during the roasting at 500 °C. The fraction of the FeS_2 phase that was oxidized, was transformed into γ-Fe_2O_3, α-Fe_2O_3, $FeSO_4$ and $Fe_2(SO_4)_3$. The sulphide was removed as SO_2 during this transformation. The sample with 50% marl showed a strong presence of $CaSO_4$, this means that the released SO_2 from the FeS_2 oxidation was fixated as sulphate. The leftover FeS_2 was 2.8 wt% which was much lower than the 19.4 wt% weight contribution of FeS_2 in the roasted pure tailing. Muscovite strongly increased (up to 26.6%), but this was due to the mixture that contained 50% marl, in which muscovite was present (37.5%). Finally, it should be noted that the leftover of $CaCO_3$ was 4 wt%, the other $CaCO_3$ (roughly 13 wt%) was transformed together with SO_2 into $CaSO_4$ or decomposed to CO_2.

Table 17: Overview of Rietveld refinement on microwave roasted samples

Roasting Condition		Pre-roast	Pre-roast	Post roasting: 500 °C - conventional furnace	Post roasting: 500 °C - Microwave furnace	
wt % Tailing		100	0	50	100	50
wt % Marl		0	100	50	0	50
Mineral phase	**Composition**	**wt % (Rietveld refinement)**				
Albite	$NaAlSi_3O_8$		1.6			
Anglesite	$PbSO_4$			0.3	0.7	
Anhydrite	$CaSO_4$	1.2		21.4	5.5	19.2
Anorthite	$CaAl_2Si_2O_8$					
Calcite	$CaCO_3$	0.2	34	1.6	0.0	4
Calciumsulfate hydrate	$Ca(SO_4)0.5H_2O$	5.6				
Dickite	$Al_2Si_2O_5(OH)_4$		11.3			
Gypsum	$CaSO_4.2H_2O$	3.3				
Hematite	Fe_2O_3			21.5	18.8	20.8
Iron sulfate	$FeSO_4$				2	
Maghemite	Fe_2O_3			1.4	12.7	1.9
Microcline	$KAlSi_3O_8$		1.4	0.7	0.1	0.8
Mikasaite	$Fe_2(SO_4)_3$			9.5	5.8	2.5
Muscovite-2M1 ferroan	$K(Al,Fe)_2AlSi_3O_{10}(OH)_2$		37.5	23.7	6.7	26.6
Perkovaite	$CaMg_2(SO_4)_3$					
Pyrite	FeS_2	56.3		0.3	19.4	2.8
Quartz	SiO_2	27.9	14.1	19.7	28.3	21.4
Rhomboclase	$H_5FeO_2(SO_4)_2.2(H_2O)$	1.5				
Sulfur	S	2.2				
Szomolknite	$Fe(SO_4).(H_2O)$	1.9				
Total composition		100.1	99.9	100.1	100	100

The Rietveld refinement is restricted to the weight percentage of each mineral phase. Hence, the molar amount of sulphide, sulphate and carbonate was calculated from the Rietveld results (Figure 37). The calculations were analogous to the those for conventional roasted samples of which an example was given in section 4.2.4. Only the 50% tailing/50% marl samples, roasted at 500 °C for 60 min, could be compared between conventional and microwave roasting. Because not enough Rietveld refinements were conducted and thus available at this time.

Firstly, it was observed that the microwave treated sample contained more FeS_2 (2.8 wt%) than the conventional roasted sample (0.3 wt%). After conventional roasting at 400 °C, the contribution of the FeS_2 phase was 3.8 wt%. This suggested that the actual sample temperature during microwave roasting was situated between 400 °C and 500 °C at a set temperature of 500 °C. Subsequently, the sulphate formation as well as the carbonate consumed was less than with conventional roasting. Obviously, because less FeS_2 was oxidized thus less SO_2 was released. This suggested that the sample did not reach the set temperature inside the microwave, despite adding the SiC plate.

Note that when comparing the leftover FeS_2 between conventional and microwave roasting other influences than just temperature were possible. Because, this could also be attributed to the slower ramp up that happened during conventional roasting, *i.e.* the sample spend more time at elevated temperatures. Therefore, more FeS_2 oxidation occurred. Secondly, during microwave roasting, supposedly less oxygen could be provided into the furnace. Therefore, less oxidation may have taken place.

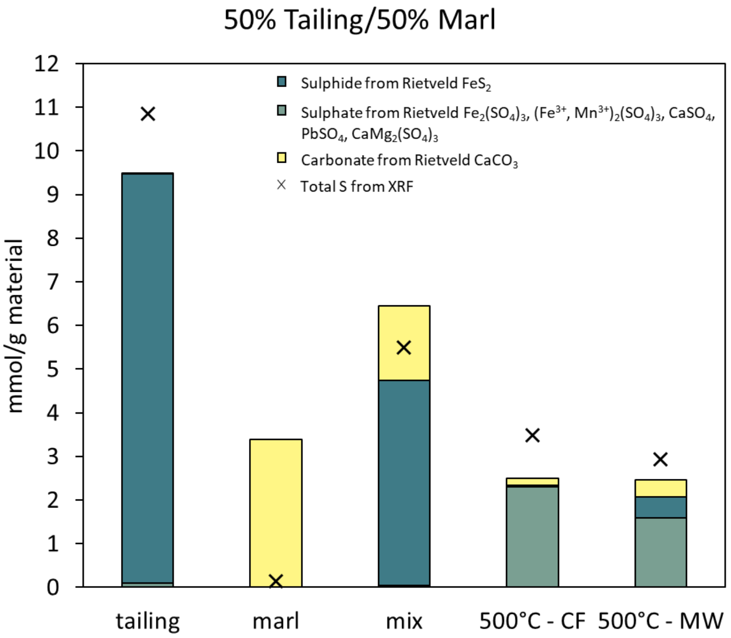

Figure 37: The molar content of sulphide, sulphate and carbonate in the microwave-assisted roasted samples, represented as the amount per gram material (mmol/g)

4.4 Leaching

4.4.1 Conventional roasted samples

A noticeable color difference was observed between the filtered leachates obtained from the materials treated at different roasting temperatures, especially when comparing the filtered leachates from the roasted pure tailing (Figure 38). The filtered leachate of the untreated tailing had a light yellow color, supposedly due to dissolution of matrix elements (iron). The filtered leachates show a blue color, which was more pronounced depending on the roasting temperature they were conducted to. The filtered leachate obtained from the pure tailing sample roasted at 500 °C, showed the most intense blue color, suggesting it contained the most copper (*i.e.* copper ammonia complexes). With roasting temperatures above 600 °C the blue color faded, thus copper dissolution diminished.

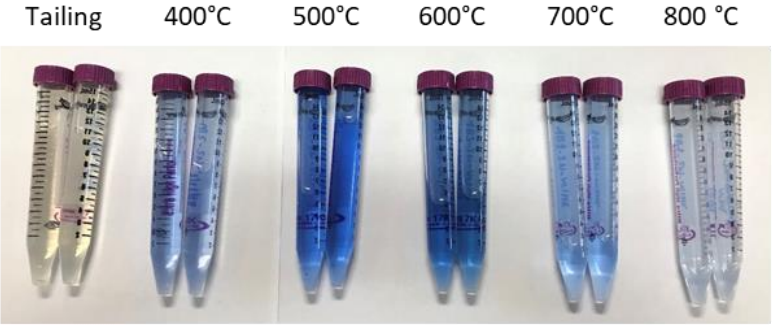

Figure 38: Filtered leachates of conventional roasted pure tailing (100%)

The leachates were analyzed with ICP-OES in which Cu, S, Zn, Pb and Fe concentrations were determined. Based on the destructive ICP-OES results of the original materials (Table 13), the initial concentration of the elements were calculated. The element recoveries (%) in function of the marl content (%) were plotted (Figure 39).

The copper recovery was at its highest (92.5%) when leaching the pure tailing, roasted at 500 °C. The samples roasted at other temperatures all showed a lower copper recovery, which followed the observations made based on the color of the filtered leachates (Figure 38).
By increasing the marl content in the samples, the copper recovery decreased significantly. For example, the sample roasted at 500 °C with the addition of only 20% marl showed a Cu recovery of only 67.3%. However, roasting at 500 °C was still the best option, compared to the other temperatures, regardless of the mixing ratio. The only exception were the samples roasted at 400 °C, which showed an increase in Cu recovery with the addition of marl. Clearly, roasting in the presence of marl caused Cu to be less accessible for leaching. At this moment, based on the available analyses data, it is unclear if the decrease in recovery was due to the physical inhibition of Cu leaching (*e.g.* Cu phases are less accessible due to deposition of inhibition layers) or due to the presence of more chemically stable Cu phases.
Low Cu recovery after roasting at 400 °C could be due to CuS and Cu_2S to be present as the main Cu mineral phases [2], [19], [20], [21].
At 500 °C to 600 °C the copper phases should be easy to dissolve in ammonia because, $CuSO_4$ should be the most common mineral phase around this temperature [2], [19], [20], [21]. In

ammonia, formation of tetraamine copper complexes ($[Cu(NH_3)_4]^{2+}$, providing the deep blue color) would then occur [38].
The extremely low copper recovery rates after roasting at elevated temperatures was also a case of evaluating in which phase copper was present. At ≥700 °C $CuFe_2O_4$ (cuprospinel) could be formed according to Ozer *et al.* [2], Prasad *et al.* [19] and Mitovski *et al.* [22]. These spinel minerals are known to be very stable thus difficult to leach, resulting in such low Cu recovery.

The leaching of sulphur increased with increased marl content. This could be expected as more sulphate was formed with increased marl content. However, sulphur recovery showed only a maximum of 76% at a roasting temperature of 500 °C of the sample containing 50% marl. Increasing the marl content any further did not increase the sulphur recovery significantly (merely 2%). Depending on the marl content, the optimal roasting temperature for sulphur leaching was 500 °C, 600 °C or 800 °C. However, in most mixtures they were comparable. Therefore, roasting at 500 °C was preferred as it is less energy consuming.

The recovery of Zn showed a maximum of 81.1% when pure tailing was roasted at 600 °C. Generally Zn should be similar in reacting with ammonia as Cu. Because Zn also forms tetraamine complexes ($[Zn(NH_3)_4]^{2+}$) [38]. By increasing the marl content the Zn recovery generally decreased. If the marl content was ≥40%, then a roasting temperature of 500 °C was desired. Roasted at 500 °C showed the highest recovery compared to other temperatures, although it was only 61.7% at a marl content of 40%. The highest roasting temperatures (700 °C and 800 °C) showed very low Zn recovery, maybe because $ZnFe_2O_4$ (Franklinite) was present, which belongs to the mineral spinel group that is very hard to dissolve and thus leach.

Lead recovery was low for all samples and roasting temperatures, with solely a maximum of 6.8% when the pure tailing was considered at 600 °C. With increased marl content the Pb recovery decreased. Considering that other elements leached better at 500 °C, Pb recovery could be averaged at 3% when roasted at 500 °C.

The Fe recovery, *i.e.* matrix dissolution, should preferably be low so only metals of interest are leached. Additionally, if Fe was leached these formed precipitates with ammonia due to the pH being around 10, thus remain in the residue. Low recoveries (maximum of ±1.5%) were found for all samples and all roasting temperatures. Thus, Fe was to some extend present in the filtered leachates of samples roasted at 400 °C, 500 °C and 600 °C. Note that at 600 °C the Fe recovery of the pure tailing was 0. This could be due to the fact that the filtered leachate was filtrated again before being measured with the ICP-OES, due to Fe-precipitates, therefore losing the iron. Finally, the Fe recovery was close to 0 in samples roasted at 700 °C and 800 °C. This was because, Fe_2O_3 (only Fe containing mineral in this range) was not being able to dissolve in ammonia.

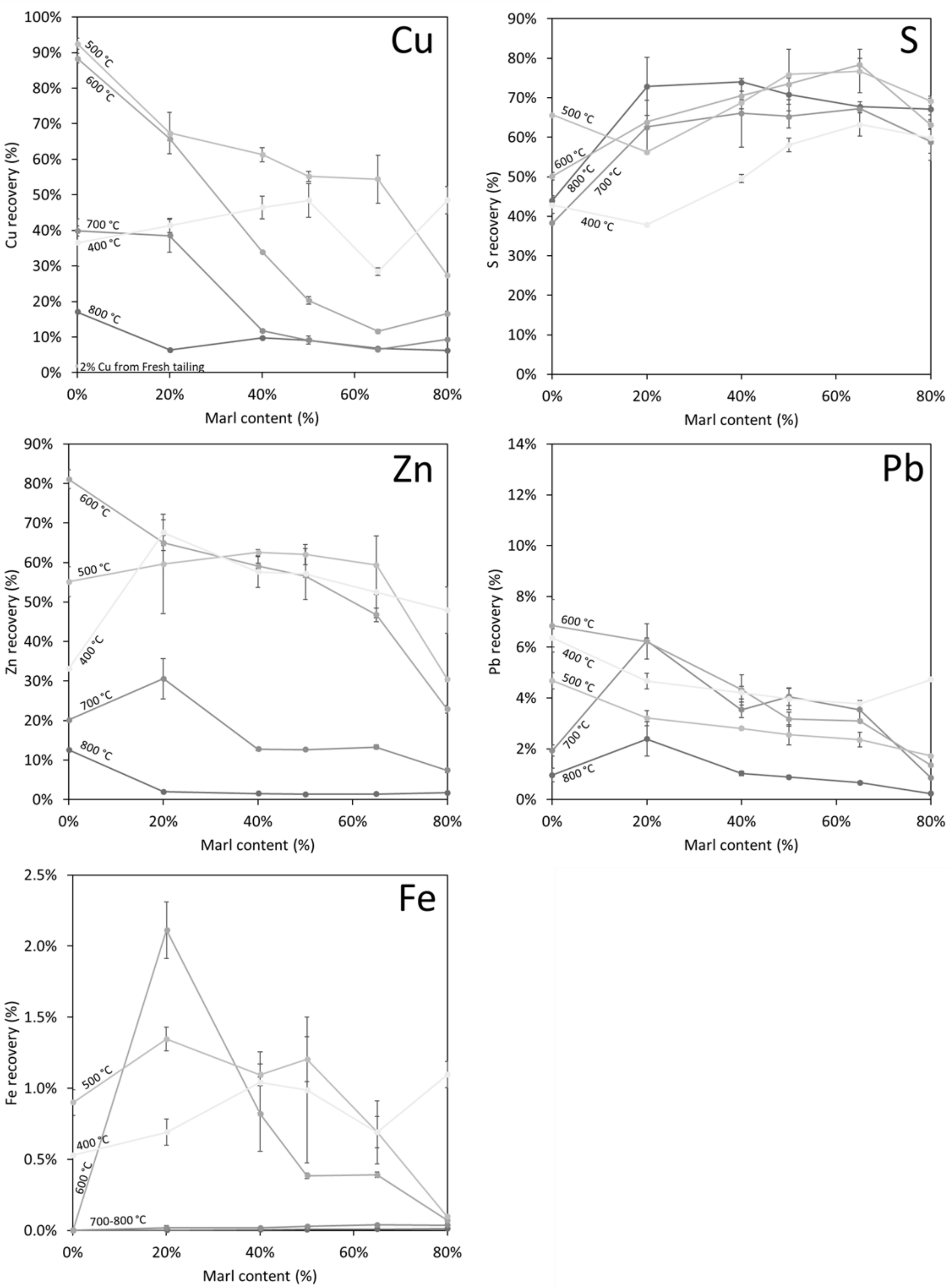

Figure 39: Elemental recovery (%) from conventionally roasted samples using ammoniacal leaching

4.4.2 Microwave roasted samples

After obtaining the filtered leachates, a noticeable color difference was observed between the leachates obtained from the materials conducted at different roasting temperatures or times, especially when comparing the filtered leachates from the roasted pure tailing (Figure 40). The filtered leachate of the tailing roasted at 300 °C had a light yellow color, supposedly due to dissolution of matrix elements (iron). The other filtered leachates showed a blue color, which was similar for the leachates roasted at 400 °C and 500 °C with a dwell time of 15 min or 30 min. The most intense blue color was observed in the leachate of the sample roasted at 500 °C with a dwell time of 60 min. These preliminary observations were similar to those observed with conventional roasting.

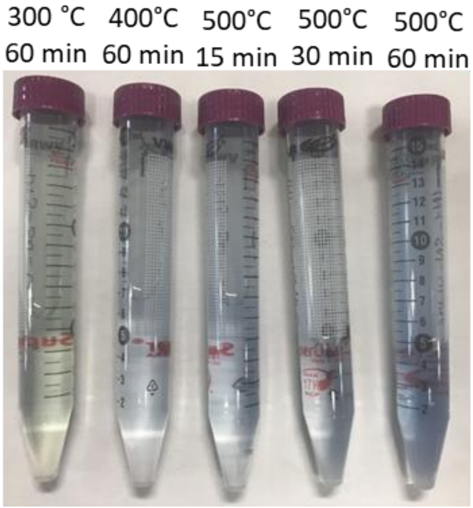

Figure 40: Filtered leachates of microwave roasted pure tailing (100%)

The elemental recoveries (%) in function of the marl content (%) are presented in Figure 41. The copper recovery of the pure tailing at 500 °C was significantly lower (31.03%) than was found with conventional roasting (92.5%). This was also true for the samples roasted at 400 °C. The highest copper recovery (49.26%) was shown for the sample containing 50% marl, roasted at 500 °C. In comparison with conventional roasting at 500 °C (54.8%) this was less, which again was true for the samples roasted at 400 °C. These results suggested that conventional roasting was preferred for copper recovery. However, when comparing the Cu recoveries after roasting at 400 °C and 500 °C in the microwave furnace, with the recoveries of samples roasted at 400 °C in the conventional furnace. The same, increasing trend in function of the marl content was shown. These results implied that the sample temperature of the microwave roasted samples was between 400 °C and 500 °C. Hence, with further optimization roasting in the microwave furnace is definitely conceivable. Comparison between the dwell times (15 min, 30 min and 60 min) when roasting at 500 °C, higher Cu recovery was obtained with a longer dwell time. This difference (14%) was very pronounced for leaching of the roasted pure tailing but diminished (4.2%) for leaching of the roasted sample containing 50% marl.

The sulphur recovery stayed relatively low, obtaining a maximum (16.23%) with the leaching of the pure tailing roasted at 400 °C. Generally though, sulphur recovery increased with increasing roasting temperature. Adding marl to the sample mixture increased the sulphur recovery as well, which was likely because more sulphates were formed during roasting. Thus, sulphur being fixated whereby otherwise they were lost as SO_2 when roasting the pure tailing. Note that the samples containing 50% marl showed a large variance on their sulphur recoveries. The maximum recovery was 57.42% when roasted at 500 °C during a 60 min dwell time. These relatively low recoveries confirmed that FeS_2 oxidation was not fully completed, thus less sulphate was formed and could be dissolved during leaching.

Zinc leaching showed a decrease with increased roasting temperature with samples containing 50% marl. The influence of dwell time was also relatively limited. However, adding marl did improve the Zn recovery by 36% for roasting at 300 °C with a maximum recovery of 52%. The average recovery with microwave roasting of the sample containing 50% marl was 40% compared to 55% when roasted in a conventional furnace. Zinc likely formed tetraamine complexes ($[Zn(NH_3)_4]^{2+}$) [38].

The lead recovery showed a decrease with increased marl content as well as increased roasting temperature. The maximum obtained Pb recovery was 15.17% in the pure tailing roasted at 300 °C. This was obvious, because with increased marl content more sulphate was formed including $PbSO_4$. Lead, generally is poorly dissolved in ammonia. Samples containing 50% marl average a lead recovery of about 5%, which was similar to the conventional roasting. However, a strong difference was observed with the pure tailing sample compared to the conventional roasting.

Iron recovery was generally low (±1%). The highest Fe recovery (1.9%) was found during the roasting of pure tailing at 300 °C. With increased marl content the Fe recovery decreased. If the roasting temperature increased, the Fe recovery also decreased with a minimum for samples roasted at 400°C. Comparison between the dwell times did not show a significant difference. It can be concluded that the Fe recovery was low, which was desired.

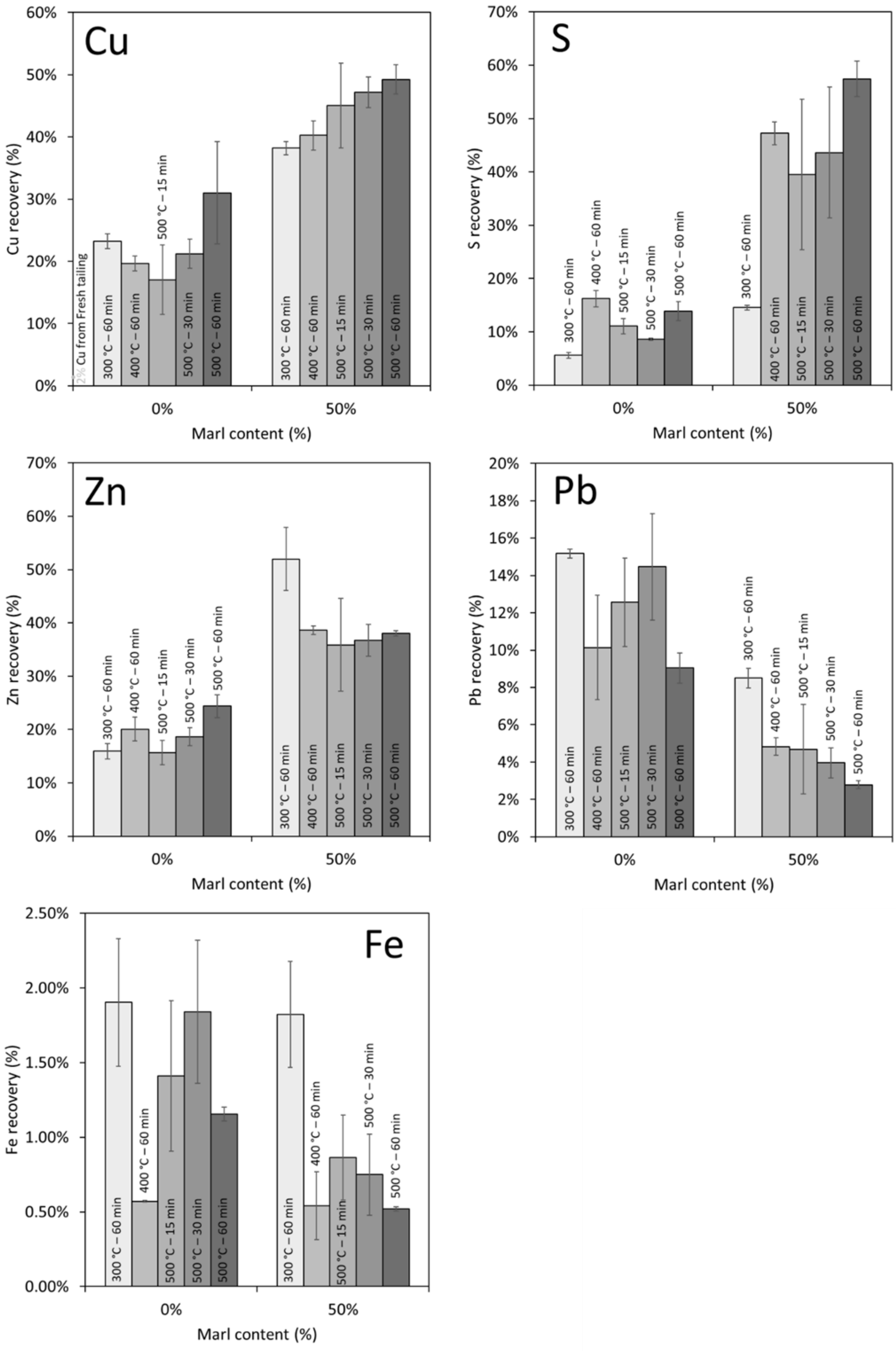

Figure 41: Elemental recovery (%) during leaching of microwave roasted samples using ammoniacal leaching

4.4.3 Leaching kinetics

Leaching experiments were performed for different leaching times (30 min, 1 h, 2 h, 3 h and 4 h) to investigate the leaching kinetics. After obtaining the filtered leachates (50% tailing/50% marl roasted at 500 °C for 60 min), a noticeable color difference was observed between these leachates conducted at different leaching times (Figure 42). The first three samples showed minor amounts of precipitation with an orange to yellow color during the time frame of 30 min to 2 h. This was probably due to iron dissolution and precipitate formation. The samples conducted at 3 h and 4 h did not show precipitates and were light blue of color, indicating copper dissolution.

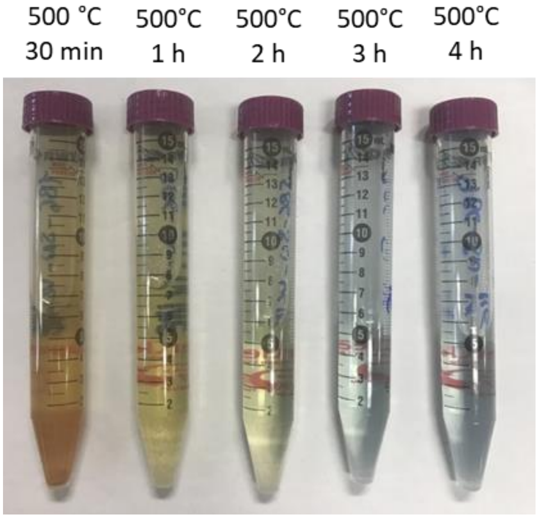

Figure 42: Filtered leachates of conventional roasted samples (50% Tailing/50% Marl) conducted at different leaching times

Visual observations were confirmed by ICP-OES measurement of the filtered leachates (Figure 43). Copper recovery was the highest (53%) after 3 h of leaching, after which a plateau value was reached. Sulphur recovery (59%) seemed to reach a plateau at 2 h already, however, due to the large error it is probably safe to fix it closer to 3 h as well. Zinc recovery (62%) also peaked after 3 h of leaching after which it decreased slightly. Lead and Iron recovery decreased with increased leaching time, both reached a minimum at 3 h of leaching (3.49% and 1.54% respectively). Lower Pb leaching was due to the formation of $PbSO_4$ during longer leaching time, which is insoluble. The decrease in iron recovery could be an indirect effect. Iron oxide particles are very small and can pass through the 0.45 µm filter into the filtered leachate. However, upon longer leaching times nucleation of these particles takes place such that they increased in size and will be more easily retained in the residue or during filtration. This was true for subsequent leaching samples, which can be seen due to the yellow color that fades as well as the iron precipitates that were less prominent. Therefore, a decrease in iron recovery was observed and to be expected.

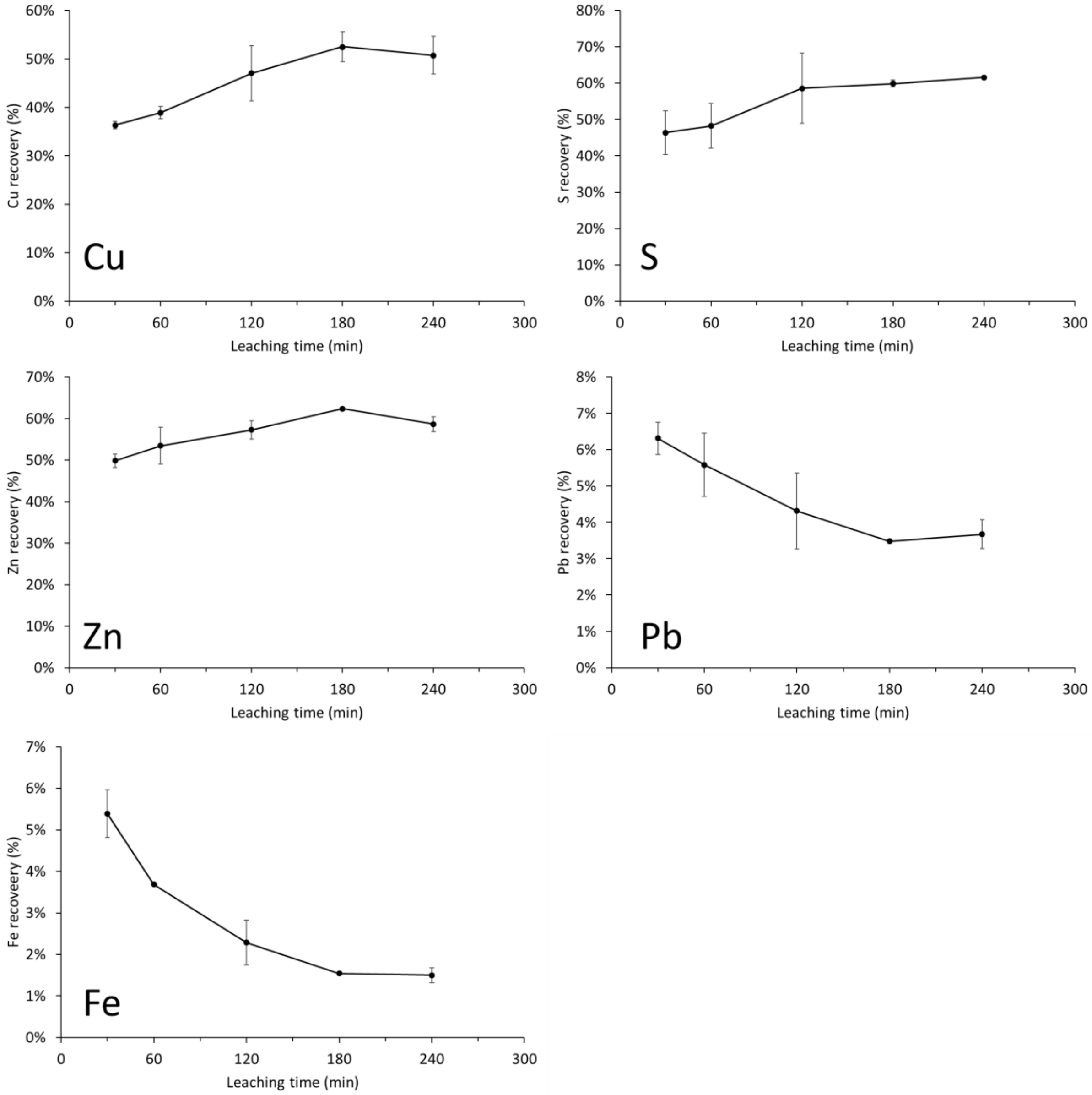

Figure 43: Elemental recovery (%) in function of the leaching time

5 Conclusion

The main objective of this work was to combine sulphidic tailing with carbonate rich waste rock (marl) in a roasting step to simultaneously oxidize sulphide minerals and capture the formed SO_2 gas as sulphates. This process was optimized in a conventional furnace (CF) by varying the roasting temperature and marl content. Initially, less mass loss and more retained sulphur was observed with increasing marl content. Q-XRD analyses showed that roasting at 500 °C was optimal because: a) nearly all FeS_2 oxidized; b) carbonates were consumed for sulphate formation with low decomposition of both and; c) the sulphate formation was the highest. The general trend was that with increasing marl content the molar amount of sulphate formed increased as more sulphur was fixated. However, with increasing marl content the amount of sulphur that was fixed per mmol of $CaCO_3$ decreased. It can be concluded that the optimal roasting temperature was 500 °C and that no optimal marl addition ratio could be determined.

Subsequently, the optimized roasting temperature (500 °C) was tested with a microwave furnace (MW) for samples of 50% tailing/50% marl. The FeS_2 oxidation of the MW-roasted sample was less completed (2.8 wt% FeS_2) in comparison with the CF-roasted sample (0.3 wt% FeS_2). This suggested that the actual sample temperature during MW roasting was situated between 400 °C and 500 °C at a set temperature of 500 °C. Subsequently, the sulphate formation as well as the carbonate consumed was less than with CF roasting. It should be noted that during CF roasting a) slower ramp up occurs and; b) more oxygen was supplied into the furnace, which both improved oxidation.

Optimization of the MW roasting with respect to roasting time (15 min, 30 min and 60 min) at 500 °C was performed. With a longer dwell time more FeS_2 oxidation was obtained, *i.e.* the contribution of the FeS_2 phase in the material decreased. As expected, the $CaCO_3$ phase decreased with increasing dwell time as it is linked to the FeS_2 oxidation becasue it contributes in the sulphate formation.

The Cu recovery from the roasted materials was assessed via ammoniacal leaching. The Cu recovery was at its highest when samples were roasted at 500 °C in a CF. By increasing the marl content in the samples, the copper recovery decreased significantly. With the addition of only 20% marl, the Cu recovery dropped from 92.5% to 67.3%. Clearly, roasting in the presence of marl caused Cu to be less accessible for leaching. At this moment, based on the available analyses data, it is unclear if the decrease in leachability was due to the physical inhibition of Cu leaching (*e.g.* Cu phases are less accessible due to deposition of inhibition layers) or due to the presence of more chemically stable Cu phases. Most likely $CuSO_4$ was the major Cu phase present in samples roasted at 500 °C.

However, for the samples roasted at 400 °C (CF) an increase in Cu recovery was obtained. This also occurred with samples roasted in the MW. Therefore, it was again concluded that the sample temperature was likely between 400 °C and 500 °C during MW roasting.

The increase in dwell time did not have a significant difference in Cu recovery. The leaching kinetics of 50% tailing/50% marl samples roasted at 500 °C in a CF showed that an optimal leaching of Cu was obtained after 3 h at 60 °C.

A few recommendations can be made for further research. Firstly, the MW roasting can be optimized. This roasting technique remains of interest because it provides fast and selective heating, and is less energy consuming than conventional roasting. The set temperature can be adjusted, so complete oxidation can be obtained. Also, the dwell times at the optimized temperature and the placement of the SiC plate are just a few options that can be considered for optimization of the MW roasting process. Secondly, Cu mineral phases present in the roasted materials can be examined with SEM-EDX to see if physical inhibition of Cu or just stable Cu phases caused the leaching behavior. Finally, an alternative carbonate waste stream can be tested as additive in the roasting of sulphidic tailings which could, besides fixation of sulphur, also result in a high Cu recovery.

Bibliography

[1] VITO, "Research," VITO, March 2019. [Online]. Available: https://vito.be/en/research. [Accessed 9 March 2019].

[2] M. Ozer, E. Acma and G. Atesok, "Sulfation roasting characteristics of copper-bearing materials," *Asia-Pacific Journal of Chemical Engineering,* no. 12, pp. 365-373, 2017.

[3] F. Krausmann, S. Gingrich, N. Eisenmenger, k. Erb, H. Haberl and M. Fischer-Kowalkski, "Growth in global materials use, GDP and population during the 20th century," *Ecological Economics,* no. 68, pp. 2696-2705, 2009.

[4] G. Calvo, G. Mudd, A. Valero and A. Valero, "Decreasing Ore Grades in Global Metallic Mining: A Theoretical Issue or a Global Reality?," *Resources,* vol. 5, no. 36, pp. 1-14, 2016.

[5] O. Levenspiel, Chemical Reaction Engineering, 3 ed., New York: John Wiley and Sons, 1999, pp. 566-588.

[6] R. Pandher, Sulphation and Sulphate Decomposition in Roasted Nickel Concentrates [Master thesis], Toronto: Applied Science Graduate Department of Materials Science and Engineering University of Toronto, 2010.

[7] H. Rezvanipour, A. Mostafavi, A. Ahmadi, M. Karimimobarakabadi and M. Khezri, "Desulfurization of Iron Ores: Processes and Challenges," *Steel research international,* vol. 89, no. 1700568, pp. 1-14, 2018.

[8] M. Shamsuddin, "Roasting of sulfide minerals," in *Physical Chemistry of Metallurgical Processes,* New Jersey, John Wiley & Sons, Incorporated, 2016, pp. 39-69.

[9] B. J. Hathaway and A. A. G. Tomlinson, "Copper(II) Ammonia Complexes," *Coordination Chemistry Reviews* , no. 5, pp. 1-43, 1970.

[10] Y. Hua, C. Cai and Y. Cui, "Microwave-enhanced roasting of copper sulfide concentrate in the presence of CaCO3," *Separation and Purification Technology,* vol. 50, no. 1, pp. 22-29, 2006.

[11] EMIS VITO, "Verkleinen deeltjesgrootte," *Belgian official journal,* pp. 1-5, 27 January 2012.

[12] K. K. Kefeni, T. A. Msagati and B. B. Mamba, "Acid mine drainage: prevention, treatment options, and resource recovery: a review," *Journal of Cleaner productions,* vol. 151, pp. 475-493, 2017.

[13] G. S. Simate and S. Ndlovu, "Acid mine drainage: Challenges and opportunities," *Journal of Environmental Chemical Engineering,* vol. 2, pp. 1785-1803, 2014.

[14] S. E. Khalafalla, J. W. Evans, C.-H. Koo, H. Y. Sohn, E. T. Turkdogan, I. B. Cutler and C. H. Pitt, "Pyrometallurgical Processes," in *Rate Processes of Extractive Metallurgy,* New York, Plenum Press, 1979, pp. 245-428.

[15] A. R. H. S. Ghosh, "Roasting," in *Principles of Extractive Metallurgy,* New Delhi, Indian Institute of Metals, 1991, p. 15.

[16] D. Yu, A. T. Utigard and M. Barati, "Fluidized bed selective oxidation-sulfation roasting of nickel sulfide concentrate: Part II. Sulfation Roasting," *Metallurgical and materials transactions B,* vol. 45, no. 2, pp. 662-674, 2014.

[17] M. Safarzadeh and S. M. Howard, "Solid state phase transformations during the oxidation of copper sulfides: Roaster diagrams for the Cu-S-O system," *Solid State Sciences,* vol. 83, p. 65–69, 2018.

[18] M. S. Safarzadeh and S. M. Howard, "Revisiting the Kellogg diagrams: roaster diagrams and their usefulness in pyrometallurgy," *Mineral processing and extracttive metallurgy review,* vol. 39, no. 3, pp. 191-197, 2017.

[19] S. Prasad and B. Pandey, "Alternative processes for treatment of chalcopyrite - a review," *Minerals Engineering,* vol. 11, no. 8, pp. 763-781, 1998.

[20] S. Prasad and B. D. Pandey, "Thermoanalytical studies on copper–iron sulphides," *Thermal Analysis and Calometry,* vol. 58, pp. 625-637, 1999.

[21] Z. D. Zivkovic, N. Mitevska and V. Savovic, "Kinetics and mechanism of the chalcopyrite-pyrite concentrate oxidation process," *Thermochimica Acta,* vol. 282/283, pp. 121-130, 1996.

[22] A. Mitovski, N. Strbac, D. Manasijevic, M. Sokic, A. Dakovic, D. Zivkovic and L. Balanovic, "Thermal analysis and kinetics of the chalcopyrite-pyrite concentrate oxidation process," *Metalurgija,* vol. 54, no. 2, pp. 311-314, 2015.

[23] Z. Yan, Z. Wang, H. Liu, Y. Tu, W. Yang, H. Zeng and J. Qiu, "Decompostion and Solid Reactions of Calcium Sulfate Doped with SIO2, Fe2O3 and Al2O3," *Journal of Analytical and Applied Pyrolysis,* vol. 113, pp. 491-498, 2015.

[24] V. M. Abzalov, A. V. Sudai and B. P. Yur'ev, "Desulfurization in roasting Iron-Ore Pellets," *Steel in Translation,* vol. 38, no. 12, pp. 1003-1007, 2008.

[25] G. Riveros, T. Marin and C. Puga, "Lime-concentrate roasting studies - effect of activated limestone," *Minerals Engineering,* vol. 17, pp. 469-471, 2004.

[26] M. Al-Harahsheh and S. W. Kingman, "Microwave-assisted leaching - a review," *Hydrometallurgy,* vol. 73, pp. 189-203, 2004.

[27] S. W. Kingman and N. A. Rowson, "Microwave treatment of minerals - a review," *Minerals Engineering,* vol. 11, no. 11, pp. 1081-1087, 1998.

[28] C. Pickles, "Microwaves in extractive metallurgy: Part 1 - Review of fundamentals," *Minerals Engineering,* vol. 22, pp. 1102-1111, 2009.

[29] Z. Moravvej, A. Mohebbi and S. Daneshpajouh, "The microwave irradiation effect on copper leaching from sulfide/oxide ores," *Materials and manufacturing processes,* vol. 33, no. 1, pp. 1-6, 2018.

[30] D. Jones, S. Kingman, D. Whittles and I. Lowndes, "Understanding microwave assited breakage," *Minerals Engineering,* vol. 18, pp. 659-669, 2015.

[31] Y. Liao, J. Zhou, F. Huang and Y. Wang, "Leaching kinetics of calcification roasting calcinate from multimetallic sulfide copper concentrate containing high content of lead and iron," *Seperation and Purification Technology,* vol. 149, pp. 190-196, 2015.

[32] H. S. Altundogan and F. Tümen, "Metal recovery from copper converter slag by roasting with ferric sulphate," *Hydrometallurgy,* vol. 44, pp. 261-267, 1997.

[33] L. You-Cai, Y. Wei, F. Jian-Gang, L. Li-Feng and Q. Dong, "Leaching kinetics of copper flotation tailings in aqueous ammonia/ammonium carbonate solution," *The canadian journal of chemical engineering,* vol. 91, no. 4, pp. 770-775, 2013.

[34] D. Bingöl, M. Canbazoglu and S. Aydogan, "Dissolution kinetics of malachite in ammonia/ammonium carbonate leaching," *Hydrometallurgy,* vol. 76, pp. 55-62, 2005.

[35] J. Han, W. Liu, K. Xue, W. Qin, F. Jiao and L. Zhu, "Influence of NH4HF2 activation on leaching of low-grade complex copper ore in NH3-NH4Cl solution," *Separation and purification technology,* vol. 181, pp. 29-36, 2017.

[36] G.-d. Zhao and Q. Liuc, "Leaching of copper from tailings using ammonia/ammonium chloride solution and its dynamics," in *International Conference on Chemistry and Chemical Engineering*, 2010.

[37] V. Radmehr, S. M. J. Koleini, M. R. Khalesi and M. R. Tavakoli Mohammadi, "Ammonia leaching in the copper industry: a review," in *International Mineral Processing Congress*, New Delhi, 2012.

[38] P. Xue, G.-q. Li, Y.-x. Yang, Q.-w. Qin and M.-x. Wei, "Recovery of valuable metals from waste diamond cutters through ammonia-ammonium sulfate leaching," *International Journal of Minerals, Metallurgy and Materials,* vol. 24, no. 12, pp. 1352-1360, 2017.

Annex

Annex A: Elemental composition via X-ray fluorescence (XRF) and ICP-OES 93

Annex A: Elemental composition via X-ray fluorescence (XRF) and ICP-OES

	Handheld XRF		ICP-OES	
Element	**Sulphidic Tailing (%)**	**Marl (%)**	**Tailing (mg/kg dm)**	**Marl (mg/kg dm)**
Ag	<dl	<dl	32	0.53
Al	1.14	4.53	3640	44800
As	0.29	<dl	2270	4.4
Au	<dl	<dl	<2	<0.1
Ba	0.06	0.02	49	486
Be	<dl	<dl	<0.5	2.2
Bi	0.03	<dl	238	0.42
Ca	2.10	13.60	8380	99400
Cd	<dl	<dl	2.9	<0.5
Ce	<dl	<dl	<dl	66
Cl	0.06	0.25	n.d.	n.d.
Co	0.07	<dl	323	13
Cr	0.05	0.03	17	107
Cu	**0.50**	<dl	**4370**	**25**
Fe	**27.72**	**3.65**	**305000**	**33900**
Ga	<dl	<dl	2.3	17
Ge	<dl	<dl	3.5	1.2
In	<dl	<dl	1.6	<0.1
K	0.20	1.67	763	18300
La	<dl	<dl	<dl	33
Mg	<dl	<dl	290	15100
Mn	0.02	0.02	102	418
Mo	<dl	<dl	8.3	<2
Na	<dl	<dl	318	6740
Ni	0.02	<dl	17	45
P	0.09	<dl	<dl	790
Pb	0.71	0.002	6700	16
Rb	<dl	0.004	n.d.	n.d.
S	**35.48**	**0.44**	**348000**	**4370**
Sb	0.03	<dl	316	<4
Sc	<dl	<dl	1.6	3.5
Se	<dl	<dl	15	<4
Si	11.54	17.26	n.d.	n.d.
Sn	0.05	<dl	58	<4
Sr	0.00	0.04	25	679
Th	<dl	<dl	1.8	7.6
Ti	0.26	0.34	1380	2190
Tl	<dl	<dl	19	<4
U	<dl	<dl	1.5	4.2
V	0.02	0.02	12	144
W	0.02	<dl	n.d.	n.d.
Y	<dl	<dl	<dl	5.7
Zn	0.11	0.01	1120	89
Zr	0.01	0.01	n.d.	n.d.
Bal*	18.34	57.77		

* Bal stands for balance. It represents x-ray energy levels that do not contribute to a particular element.

<dl: below detection limit; n.d. not determined

* Conversion from mg/kg dm to percentage is done by dividing the number by 10 000 (*e.g.* XRF – Cu = 0.50 %; ICP-OES – Cu = 0.43 %)